



HAL
open science

Photocatalytic degradation of p-hydroxyphenylacetic acid (p-HPA) and Acetaminophen (ACTP) using bismuth catalyst BiOClxIy and Fe(III)-EDDS/UV/H2O2-Na2S2O8

Xiaoning Wang

► **To cite this version:**

Xiaoning Wang. Photocatalytic degradation of p-hydroxyphenylacetic acid (p-HPA) and Acetaminophen (ACTP) using bismuth catalyst BiOClxIy and Fe(III)-EDDS/UV/H2O2-Na2S2O8. Theoretical and/or physical chemistry. Université Clermont Auvergne [2017-2020]; Université de Fudan (Shanghai, Chine), 2018. English. NNT : 2018CLFAC051 . tel-02657257

HAL Id: tel-02657257

<https://theses.hal.science/tel-02657257>

Submitted on 30 May 2020

HAL is a multi-disciplinary open access archive for the deposit and dissemination of scientific research documents, whether they are published or not. The documents may come from teaching and research institutions in France or abroad, or from public or private research centers.

L'archive ouverte pluridisciplinaire **HAL**, est destinée au dépôt et à la diffusion de documents scientifiques de niveau recherche, publiés ou non, émanant des établissements d'enseignement et de recherche français ou étrangers, des laboratoires publics ou privés.

UNIVERSITE CLERMONT AUVERGNE
ECOLE DOCTORALE DES SCIENCES FONDAMENTALES

THESE

présentée pour obtenir le grade de

DOCTEUR D'UNIVERSITE

Spécialité : Chimie théorique, physique, analytique

Par
WANG Xiaoning

Photocatalytic degradation of p-hydroxyphenylacetic acid (p-HPA) and Acetaminophen (ACTP)
using bismuth catalyst BiOCl_xI_y and Fe(III)-EDDS/UV/H₂O₂-Na₂S₂O₈

Soutenue le « 29/05/2018 », devant la commission d'examen.

Président :

Weihua SONG, PR, Université de Fudan, Chine

Examineurs :

Corinne FERRONATO, MCF, Université Claude Bernard Lyon 1, France

Feng WU, PR, Université de Wuhan, Chine

Khalil HANNA, PR, Ecole Nationale Supérieure de Chimie de Rennes, France

Wenbo DONG, PR., Université de Fudan, Chine

Marcello BRIGANTE, PR, Université Clermont Auvergne, France (Directeur de thèse)

ED SF n° d'ordre :

UNIVERSITE CLERMONT AUVERGNE
ECOLE DOCTORALE DES SCIENCES
FONDAMENTALES

THESE

présentée pour obtenir le grade de

DOCTEUR D'UNIVERSITE

Spécialité : Chimie théorique, physique, analytique

Par

WANG Xiaoning

Photocatalytic degradation of *p*-hydroxyphenylacetic acid (*p*-HPA) and Acetaminophen (ACTP) using bismuth catalyst BiOCl_xI_y and Fe(III)-EDDS/UV/ H_2O_2 - $\text{Na}_2\text{S}_2\text{O}_8$

E vue d'une soutenance le « 29/05/2018 », devant la commission d'examen.

Président :

Weihua SONG, PR, Université de Fudan, Chine

Examineur :

Corinne FERRONATO, MCF, Université Claude Bernard Lyon 1, France

Feng WU, PR, Université de Wuhan, Chine

Khalil HANNA, PR, Ecole Nationale Supérieure de Chimie de Rennes, France

Wenbo DONG, PR., Université de Fudan, Chine

Marcello BRIGANTE, PR, Université Clermont Auvergne, France

Abstract

In recent decades, pharmaceuticals and personal care products (PPCPs) have emerged as a new environmental concern. Pharmaceuticals have been widely detected in ground water, surface water and even drinking water with a concentration ranging from ng to $\mu\text{g L}^{-1}$ in wastewater effluents. Sewage treatment plants (STPs) cannot remove completely all pharmaceuticals due to their low concentration in water and resistance to biological degradation. Levels of many pharmaceutically active compounds (PhACs) are barely reduced and can be detected in wastewater-treatment plant (WWTP) effluents. In order to overcome this problem, advanced oxidation processes (AOPs) usually are adopted for the application of this wastewater treatment, which can be attributed to the strong oxidation abilities of different radicals produced.

In AOPs, the most frequently used methods include homogeneous reaction such as Fenton, Fenton like or Photo-Fenton process. Another one is heterogeneous reactions involving semiconductors to perform also called catalytic degradations. During these reactions, ultraviolet (UV) and visible lights are generally used as activation source. In this work, simulated solar light ($300\text{ nm} < \lambda < 500\text{ nm}$) was taken as radiation source to perform heterogeneous and homogeneous AOPs to efficiently degrade pharmaceutical. This result was obtained producing different kind of radicals including hydroxyl (HO^\bullet), sulfate ($\text{SO}_4^{\bullet-}$) and hydroperoxide/superoxide ($\text{HO}_2^\bullet/\text{O}_2^{\bullet-}$) radicals.

Acetaminophen (ACTP) and *p*-hydroxyphenylacetic acid (*p*-HPA) were two typical pharmaceuticals. As one kind of the most commonly detected pollutant, ACTP is extensively used globally as an analgesic and antipyretic drug, and *p*-HPA is one of the pharmaceutical intermediates, widely used in the synthesis of pesticides and commonly detected in olive oil wastewater. In this work, ACTP and *p*-HPA are taken as the representative compounds of pharmaceutical pollutant.

In the first part of my research, composite catalyst $\text{BiOCl}_{0.75}\text{I}_{0.25}$ was synthesized by precipitation method under ambient pressure and low temperature followed with a series of characterization. Catalyst showed flower-like microspheres and possessed

great surface area. Most importantly, from the detection of UV–vis diffuse reflection spectra (DRS), the band gap of $\text{BiOCl}_{0.75}\text{I}_{0.25}$ was 2.12 eV, was determined. Moreover, the adsorption and photocatalytic degradation abilities of bismuth catalyst $\text{BiOCl}_{0.75}\text{I}_{0.25}$ in water are tested under simulated solar light using *p*-HPA as chemical pollutant. On the basis of strong adsorption of *p*-HPA on the surface of catalyst, this section of my work aims at investigating the interfacial mechanism in the heterogeneous system through adsorption/desorption experiments using competition desorption with phosphate anions. Key factors affecting the degradation kinetic of *p*-HPA such as pH and dissolved oxygen are investigated. It is found that solution pH has significant effect on the adsorption and degradation rate, depending on the zeta potential of catalyst and molecular form of *p*-HPA. *p*-HPA shows a maximum adsorption at pH 4.5 and faster degradation rate at pH 3.0. Dissolved oxygen concentration is a key parameter for the pollutant removal through formation of hydroperoxide/superoxide radical anion couple ($\text{HO}_2^\bullet/\text{O}_2^{\bullet-}$). These radicals, that are the main reactive species involved in the reaction occurring after irradiation of catalyst, are detected using competition kinetic approach and selective radical probes.

In the second part, *p*-HPA was taken as representative pollutant. Our group has done a lot of work on a new complexing agent of iron, the Ethylenediamine-*N,N'*-disuccinic acid (EDDS). EDDS is a structural isomer of EDTA, and it's readily biodegradable. It has been proposed as a safe and environmentally benign replacement for EDTA for environmental remediation products. Our laboratory has studied the physicochemical properties of the Fe(III)-EDDS complex, and its application in the Fenton, Photo-Fenton and persulfate (PS) activation as iron source. While the comparison between Fe(III)-EDDS/ H_2O_2 /UV and Fe(III)-EDDS/PS/UV systems under same conditions was studied for the first time including the effects of pH, Fe(III)-EDDS concentration, H_2O_2 and PS concentrations in this part. Results showed that Fe(III)-EDDS/ H_2O_2 /UV showed higher degradation efficiency than Fe(III)-EDDS/PS/UV, especially in neutral and alkaline solutions. In Fe(III)-EDDS/ H_2O_2 /UV reaction, *p*-HPA degradation efficiency increased fast from pH 2.5 to 7.5, then it began to decrease when pH increased to 9.0. While degradation

rate ($R_{p\text{-HPA}}$) started to decrease with pH increase to 3.9 in Fe(III)-EDDS/Na₂S₂O₈/UV. The degradation rate of *p*-HPA increased using higher concentrated solution of H₂O₂ and Na₂S₂O₈. However, increasing the Fe(III)-EDDS concentration, the degradation efficiency of degradation decreases. The second order constant of *p*-HPA with HO• or SO₄•⁻ radicals under different pH were determined by laser flash photolysis (LFP) experiments for the first time. Results showed that $k_{p\text{-HPA},\text{HO}\cdot}$ was higher than $k_{p\text{-HPA},\text{SO}_4\cdot^-}$ for both anionic and molecular forms of pollutant.

Finally, different Iron-based homogeneous and heterogeneous AOPs were tested on the ACTP degradation. Moreover, reactivity of selected pollutant with HO•, SO₄•⁻ and HO₂•/O₂•⁻ that are produced by UV/H₂O₂, UV/Na₂S₂O₈, Fe(III)-EDDS/H₂O₂/UV and Fe(III)-EDDS/PS/UV system was investigated. The effects on the degradation of pH and chloride ions were studied at the same time. Results indicate that using UV/Na₂S₂O₈ system, a better removal efficiency (57%) was obtained compared to UV/H₂O₂ (11%). UV/H₂O₂ showed best degradation efficiency in neutral solution, while using UV/Na₂S₂O₈ the highest removal rate was observed in alkaline solutions. Chlorine ions (10 mM) has negligible effects in these two systems. However, the same concentrated iodine ions can accelerate the degradation in the dark (Fenton-like reaction). Fe(III)-EDDS/H₂O₂/UV and Fe(III)-EDDS/PS/UV showed a much faster degradation efficiency than UV/H₂O₂ and UV/Na₂S₂O₈ using the same irradiation source. On the contrary, Fe(III)-EDDS/H₂O₂/UV was more efficient than Fe(III)-EDDS/PS/UV, especially in neutral and basic solution. Hydroperoxide/superoxide radicals (HO₂•/O₂•⁻) are produced by the UV/BiOCl_{0.75}I_{0.25} photocatalytic process, which exhibited higher degradation rate than UV/H₂O₂ and UV/Na₂S₂O₈. ACTP can be completely removed in two hours at pH 3. Interfacial mechanism investigation showed that reaction mainly occurred on the surface of catalyst or in the bulk solution that closed to the surface of catalyst. Second order constant between ACTP and HO• or SO₄•⁻ radicals were determined by LFP and competition method, respectively.

Key words: pharmaceutical, advanced oxidation processes, photocatalytic degradation, heterogeneous, homogeneous, Photo-Fenton, $\text{BiOCl}_{0.75}\text{I}_{0.25}$, Acetaminophen, *p*-hydroxyphenylacetic acid

Content

1. Introduction.....	1
2. Bibliography	4
2-1. Pharmaceutical pollution	4
2-1-1. Source.....	4
2-1-2. Distribution and detection	5
2-1-3. Degradation	9
2-2. Model compounds	10
2-2-1. <i>p</i> -Hydroxyphenylacetic acid (<i>p</i> -HPA): presence and degradation	10
2-2-2. Acetaminophen (ACTP): presence and degradation	11
2-3. Advanced oxidation processes (AOPs).....	13
2-3-1. General description	14
2-3-2. AOPs based on heterogeneous semiconductor photo catalytic degradation.....	16
2-3-3. AOPs based on homogeneous reactions in aqueous solution.....	18
2-3-3-1. HO [•] radical.....	18
2-3-3-2. SO ₄ ^{•-} radical	20
2-3-4. Degradation of pharmaceutical pollutant by AOPs.....	22
2-4. Bismuth-based catalyst.....	25
2-4-1. Reactivity mechanism	25
2-4-2. Application	27
2-4-3. Modification and doping catalyst.....	30
2-5. Fe(III)-Ethylenediamine-N,N'-disuccinic acid (EDDS)	33
2-5-1. Iron in water	33
2-5-2. Iron complex	34
2-5-3. Ethylenediamine-N,N'-disuccinic acid (EDDS).....	36
2-5-4. Application of Fe(III)-EDDS in environment.....	38
3. Materials and Methods.....	41
3.1. Reagent	41

3.2. Synthesis of Bismuth catalyst $\text{BiOCl}_{0.75}\text{I}_{0.25}$	41
3.3. Characterization of Bismuth catalyst	42
3.4. Reaction process	43
3.4.1. Heterogeneous photocatalytic degradation of <i>p</i> -HPA by bismuth catalyst	43
3.4.2. Homogeneous degradation of <i>p</i> -HPA by Fe(III)-EDDS	44
3.4.3. Photodegradation of ACTP	45
3.5. Analytical and spectroscopic methods	45
3.5.1. <i>p</i> -HPA detection	45
3.5.2. ACTP detection	47
3.6. Laser Flash Photolysis	48
4. Bismuth catalyst mediated degradation of <i>p</i> -hydroxyphenylacetic acid (<i>p</i> -HPA): Photo-activation, interfacial mechanism and influence of some critical parameters...50	
4.1. Characterization of $\text{BiOCl}_{0.75}\text{I}_{0.25}$ composite catalyst	50
4.1.1. Phase structure	50
4.1.2. Morphology.....	51
4.1.3. XPS	52
4.1.4. Optical properties	53
4.2. Optical properties of <i>p</i> -HPA and blank experiment	56
4.3. pH effects on <i>p</i> -HPA adsorption and photocatalytic degradation	57
4.4. Reactive species generation	59
4.5. Interfacial mechanism under irradiation	63
4.6. Effects of dissolved oxygen	64
4.7. Effects of Fe^{3+} and $\text{Na}_2\text{S}_2\text{O}_8$ addition	66
4.8. TOC removal efficiency and main intermediate product.....	69
4.9. Conclusion	70
5. Comparison of hydroxyl and sulfate radical degradation efficiencies of <i>p</i> -HPA activated by Fe(III)-EDDS/UV : influence of critical parameters.....	72
5.1 Photochemistry of Fe(III)-EDDS.....	73
5.2 Evaluation of the second order rate constants.....	73

5.3 Effect of UV and Fe(III)-EDDS complex.....	76
5.4 Effects of H ₂ O ₂ and Na ₂ S ₂ O ₈ concentrations.....	80
5.5. Effects of Fe(III)-EDDS concentrations	82
5.6. Effects of pH.....	85
5.7. Identification of active species at pH 3.9.....	89
5.8. Conclusion: comparison of H ₂ O ₂ and S ₂ O ₈ ²⁻ efficiency	92
6. Degradation of Acetaminophen by UV-induced advanced oxidation processes (AOPs): different degradation abilities of HO•, SO ₄ ^{•-} and HO ₂ •/O ₂ ^{•-}	93
6.1. Blank experiment of ACTP mixed with H ₂ O ₂ and Na ₂ S ₂ O ₈ in the dark.....	93
6.2. ACTP degradation in UV/H ₂ O ₂ and UV/Na ₂ S ₂ O ₈ systems under different pH values	95
6.3. Halide ions (chloride and iodide) effects on ACTP degradation in UV/H ₂ O ₂ and UV/Na ₂ S ₂ O ₈ systems	98
6.4. Photo-degradation of ACTP in UV/H ₂ O ₂ /Fe(III)-EDDS and UV/Na ₂ S ₂ O ₈ /Fe(III)-EDDS system	102
6.5. pH effects in UV/H ₂ O ₂ /Fe(III)-EDDS and UV/Na ₂ S ₂ O ₈ /Fe(III)-EDDS system	103
6.6. Photo-catalytic degradation of ACTP by BiOCl _{0.75} I _{0.25} catalyst under different pH.....	104
6.7. Heterogeneous reaction mechanism	106
6.8. Second order reaction constant between ACTP and HO•, SO ₄ ^{•-} radicals ...	107
6.9. Conclusion	109
7. Conclusion	111
Reference	114
Published papers	139
Acknowledgement	141

1. Introduction

Pharmaceuticals in water have emerged as one of the most urgent issues due to their massive use and potential chronic health effects. Pharmaceutically active compounds (PhACs) have been detected in sewage treatment plant, surface water and even drinking water at a concentration of ng to μg per litre. Traditional wastewater treatment plant cannot remove all the pollutant compound due to its trace concentration and resistance to micro-biology degradation. So advanced oxidation processes (AOPs) can be successfully used in the field of wastewater, underground water and gas treatment, to convert toxic and bio-recalcitrant contaminants into biodegradable by-products, to remove color or to reach the complete mineralization of organic pollutants. Based on the high oxidation abilities of radicals generated in AOPs, AOPs showed a promising potential in practical use. Usually, radicals originated from the activation of H_2O_2 , $\text{Na}_2\text{S}_2\text{O}_8$ or O_3 etc. by ultraviolet (UV)-visible light but also using ferrous, ferric ions, ultrasonic or semiconductor catalyst.

Nowadays, the most commonly used AOPs are homogeneous reactions using iron as activation species (Fenton, Photo-Fenton, Fenton-like). Between the heterogeneous processes photo-degradation processes involving semiconductor catalysts are widely adopted. Numerous research papers focus on the synthesization, characterization and pollutants degradation using different catalyst. Among these catalyst, TiO_2 has attracted the most attention due to its stable physico-chemical properties, non-toxicity and high degradation efficiency. However, the large band gap (3.2 eV) of TiO_2 restricts its use under a small range of solar light; therefore, a semiconductor photocatalyst which could make full use of solar light would be a major progression. Bismuth-based compounds such as Bi_2O_3 , $\text{Bi}_2\text{O}_2\text{CO}_3$, Bi_2S_3 and BiOX ($\text{X} = \text{Cl}, \text{Br}, \text{I}$) have received wide attention due to their characteristic hierarchical structures and high photocatalytic activities. In particular, BiOX with a layered structure has been reported to have internal electric fields between $[\text{Bi}_2\text{O}_2]$ and $[\text{Cl}_2]$, which are favourable for the efficient photo-induced electron-hole

separation. Nowadays, majority of BiOX researches focused on the synthesization, modification, composite or doping method to increase its photo-catalytic activities. While mechanism of the interfacial system such as chemical reactions, adsorption kinetics and influence of solution factors are not deeply investigated.

In homogeneous AOPs, Fenton, Photo-Fenton and activation of sulfate radicals are research hot topics. Most of these reactions are based on the activation of Fe(II)/Fe(III) using UV irradiation. However, under neutral pH conditions a low efficiency of pollutant degradation system is observed. This low efficiency is mainly due to the presence of insoluble forms of Fe(III) under neutral pH conditions. So, in our group, we investigated the properties of new complexing agent Ethylenediamine-*N,N'*-disuccinic acid (EDDS), which is a structural isomer of Ethylenediaminetetraacetic acid (EDTA). It has been proposed as a safe and environmentally benign replacement for EDTA for environmental remediation products as it is also a strong complexing agent. Fe(III) is complexed by EDDS with a ratio 1:1, the physicochemical properties of Fe(III)-EDDS complex have been studied in detail. Fe(III)-EDDS complex has higher quantum yield of $\bullet\text{OH}$ radical formation at higher pH values. Furthermore, Fe(III)-EDDS complex showed an excellent activation efficiency in Photo-Fenton, Fenton and $\text{Na}_2\text{S}_2\text{O}_8$ process as iron source in our previous research. However, comparison between activation of H_2O_2 and $\text{Na}_2\text{S}_2\text{O}_8$ under same conditions has not been studied before.

Acetaminophen (ACTP) is a pharmaceutical with a heavy use and frequent detection in global. *p*-hydroxyphenylacetic acid (*p*-HPA) a pharmaceutical intermediate for the synthesis such as Atenolol, and it was also commonly detected in olive oil wastewater. ACTP and *p*-HPA are taken as the representative compounds of pharmaceutical pollution.

The aim of my thesis is to investigate the degradation of ACTP and *p*-HPA by different AOPs under simulated solar light, including homogeneous and heterogeneous reactions. In heterogeneous reactions, $\text{BiOCl}_{0.75}\text{I}_{0.25}$ was taken as the catalyst ascribing to its good response to solar light. The most important attention will focus on the interfacial mechanism of the catalyst induced reactions. In homogeneous

reactions, Fe(III)-EDDS complex is taken as iron source to activate H_2O_2 and $\text{Na}_2\text{S}_2\text{O}_8$ under same conditions. Laser flash photolysis was adopted to check the second order constant between compound with HO^\bullet and $\text{SO}_4^{\bullet-}$. Simulated solar light ($300\text{ nm} < \lambda < 500\text{ nm}$) was taken as irradiation during the whole research.

In the first part, *p*-HPA was taken as model compound, because *p*-HPA showed a much stronger adsorption on the surface of catalyst $\text{BiOCl}_{0.75}\text{I}_{0.25}$ than ACTP. Composite catalyst $\text{BiOCl}_{0.75}\text{I}_{0.25}$ was synthesized in EG- H_2O mixed solvent by precipitation method, and our previous studies has proved that $\text{BiOCl}_{0.75}\text{I}_{0.25}$ was a promising candidate in the solar-light driven photo-degradation. In this part, followed with the synthesis and characterization of $\text{BiOCl}_{0.75}\text{I}_{0.25}$, research about active species identification, pH effects, interfacial mechanism, oxygen effects, synergistic reaction with $\text{Na}_2\text{S}_2\text{O}_8$ and mineralization in the photo-catalytic degradation of *p*-HPA were investigated in detail.

In the second part, *p*-HPA was also taken as the representative compound. Compare of *p*-HPA degradation rate ($R_{p\text{-HPA}}$) in Fe(III)-EDDS/ H_2O_2 /UV and Fe(III)-EDDS/ $\text{Na}_2\text{S}_2\text{O}_8$ /UV systems was evaluated under same conditions for the first time. The effects of UV, H_2O_2 and $\text{Na}_2\text{S}_2\text{O}_8$ concentration, Fe(III)-EDDS concentration and pH were studied seriously. Furthermore, using laser flash photolysis (LFP), second order constants between *p*-HPA and HO^\bullet , $\text{SO}_4^{\bullet-}$ were determined under different pH.

Finally, ACTP was taken as the representative compound. We compared the degradation efficiency by different AOPs. ACTP degradation in UV/ H_2O_2 , UV/ $\text{Na}_2\text{S}_2\text{O}_8$, Fe(III)-EDDS/ H_2O_2 /UV, Fe(III)-EDDS/ $\text{Na}_2\text{S}_2\text{O}_8$ /UV and UV/ $\text{BiOCl}_{0.75}\text{I}_{0.25}$ were investigated. Effects of pH, halogen ions and interfacial mechanism were studied at the same time. Second order constant between ACTP and HO^\bullet , $\text{SO}_4^{\bullet-}$ was determined by LFP and competition method, respectively.

2. Bibliography

2-1. Pharmaceutical pollution

With the fast economic development, a better living condition leads to longer life expectancy, which increased the total population, in particular the elderly group. It may result in increase in the demand of pharmaceutical for people in domestic use or in hospital¹. In recent decades, pharmaceuticals and personal care products (PPCPs) have emerged as a new environmental concern due to its wide spread, huge amount and undetectable biotoxicity. Pharmaceuticals have been widely detected in ground water, surface water and even drinking water. These kinds of pollutants include analgesics, anti-inflammatory drugs, antibiotics, lipid regulators, psychiatric drugs and β -blockers, detected in concentrations ranging from nanograms per litre to micrograms per litre in wastewater influent. Sewage treatment plants (STPs) cannot remove all kinds of pharmaceuticals completely due to their trace concentration in water and resistance to biological degradation. Levels of many pharmaceutically active compounds (PhACs) are barely reduced and can be detected in wastewater-treatment plant (WWTP) effluents. Although the amount of these pharmaceuticals in the aquatic environment is low, its continuous input may constitute in the long-term a potential risk for aquatic and terrestrial organism. Therefore, over the past few years they are considered to be an emerging environmental problem²⁻⁶.

2-1-1. Source

Normally, the source of pharmaceuticals presented in water can be divided into two ways: point source pollution and diffuse source pollution. Point source pollutant is a single identifiable source which originates from separate locations and can be calculated in mathematical modeling like pharmaceutical industrials or hospitals. On the contrary, diffuse source pollutant is hard to be identified the discrete location which occurs over board geographical scales like rivers in countryside. **Fig.2-1** reports the sources and receiving media of pharmaceutical pollution. There are six

major sources namely, landfill, animal waste, freshwater aquaculture waste, hospital waste, industrial waste and domestic waste which is summarized and simplified by several review literatures. The receptors of pharmaceuticals can be divided as three major bodied in the natural environment, for instance, soil zone, groundwater and surface water^{1,7}.

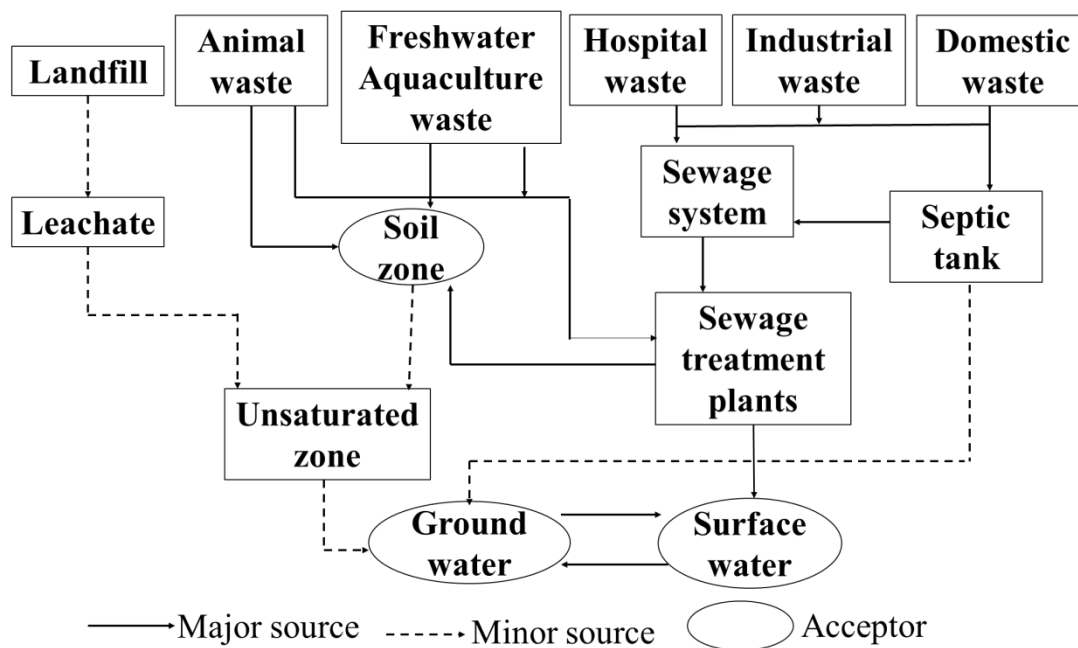


Fig.2-1 Potential sources and pathways of pharmaceutical pollution in soil and water

2-1-2. Distribution and detection

In addition to the pharmaceutical industry, the effluent from the wastewater treatment plant also contains a large number of pharmaceutical compounds. Aleksandra Jelic et al.⁸ collected 72 samples in two years to study the residues of medical materials in the influent, effluent and sediment of three traditional sewage treatment plants. These samples belong to different kinds of medicine, including non-steroidal anti-inflammatory drugs, lipid regulators (fibrates and statins), psychotropic drugs (benzodiazepines and antiepileptic drugs), histamine H₂- receptor antagonist, systemic use of antibacterial agents, β -blockers, β -agonists, diuretics, angiotensin angiotensin converting enzyme (ACE) inhibitors and anti-diabetic drugs. The results showed that in the influent and effluent 32 kinds and 29 different organic

molecules were respectively detected and their concentration was in the range of $\mu\text{g}\text{-ng L}^{-1}$. 21 kinds of pharmaceuticals were detected in the sediment of the three wastewater treatment plant, with a concentration of about 100 ng g^{-1} . These pollutants show different removal efficiencies, even if they belong to the same type of drug.

Jelena et al.^{9,10} studied the concentration of 31 active substances in sewage and solid phase after treated by traditional activated sludge process (CASs) and membrane bioreactor (MBRs). These drugs belong to different species and have different physical and chemical properties. In these two kinds of treatment methods, the most commonly detected pollutants are analgesic and anti-inflammatory drugs, including ibuprofen ($14.6\text{-}31.3 \mu\text{g L}^{-1}$) and acetaminophen ($7.1\text{-}11.4 \mu\text{g L}^{-1}$), antibiotic ofloxacin ($0.89\text{-}31.7 \mu\text{g L}^{-1}$), lipid regulators gemfibrozil ($2.0\text{-}5.9 \mu\text{g L}^{-1}$) and bezafibrate ($1.9\text{-}29.8 \mu\text{g L}^{-1}$) β -blocker atenolol ($0.84\text{-}2.8 \mu\text{g L}^{-1}$), hypoglycemic agent glibenclamide ($0.12\text{-}15.9 \mu\text{g L}^{-1}$) and diuretic hydrochlorothiazide ($2.3\text{-}4.8 \mu\text{g L}^{-1}$). In addition, several drugs such as ibuprofen, ketoprofen, diclofenac, ofloxacin and azithromycin were detected in the sludge, at concentration of 741.1, 336.3, 380.7, 454.7 and 299.6 ng g^{-1} dry weight, respectively.

According to literature data, the most commonly detected drugs in soil include species reported in **Table 2-1**. Generally, the concentration of drugs in soil is lower than that in water. Studies have shown that in China five kinds of the six most common drugs are regularly detected. However, the detection of antibiotics is the world's highest concentration, followed by Kuwait and the United States.⁴

The detection of drugs and active substances in water is shown in **Table 2-2**, which listed several frequently detected pollutants in plant effluent, surface water and groundwater. The drug concentration was higher in the sewage treatment plant, followed by the surface water and fresh water, mainly because of natural causes in the water, for example by biotransformation, photolysis, dispersion, adsorption and volatilization etc¹⁶. In Asia, the most commonly detected pollutants in effluent and fresh water are antibiotics, such as trimethoprim and sulfamethoxazole¹⁷.

Table 2-1 Concentration of pharmaceuticals found in soil in different countries

Country/region	Range of concentration ($\mu\text{g kg}^{-1}$)	Number of samples	references
Carbamazepine			
Mexico	2.6-7.5	4	Gibson et al 2010 ¹¹
Hebei, China	0.02-0.06	18	Chen et al 2011 ¹²
USA (a)	n.d ^a	3	Kinney et al 2008 ¹³
USA (b)	0.7-1.4	1	Wu et al 2010 ¹⁴
Trimethoprim			
USA (a)	n.d-0.64	3	Kinney et al 2008 ¹³
Hebei, China	0.64-2.15	18	Chen et al 2011 ¹²
Malaysia	3.1-60.1	10	Ho et al 2012 ¹⁵
Ibuprofen			
Mexico	n.d-0.1	4	Gibson et al 2010 ¹¹
Hebei, China	1.51-5.03	18	Chen et al 2011 ¹²
Diclofenac			
Mexico	n.d	4	Gibson et al 2010 ¹¹
Hebei, China	0.35-1.16	18	Chen et al 2011 ¹²
Sulfadiazine			
Hebei, China	1.15-3.82	18	Chen et al 2011 ¹²
Malaysia	n.d	10	Ho et al 2012 ¹⁵
Triclosan			
USA (b)	n.d	1	Wu et al 2010 ¹⁴
Mexico	n.d-16.7	4	Gibson et al 2010 ¹¹

a: undetectable

Table 2-2 Occurrence and concentration of pharmaceuticals found in effluent, freshwater and groundwater from America, Europe and Asia.

Source	Range of concentration (ng L ⁻¹)								
	America			Europe			Asia		
	Effluent WWTP /STP	Freshwater-rivers, canals	Groundwater	Effluent WWTP /STP	Freshwater-rivers, canals	Groundwater	Effluent WWTP /STP	Freshwater-rivers, canals	Groundwater
Location	New Mexico, Balkan	New Jersey, Canada	California, Canada	Spain, Italy	Spain	Pan-European	Taiwan, Korea	Taiwan, Vietnam	
Compound									
Antibiotics									
Trimethoprim	2550	145	18	39	59.9		2000	1808	
Ciprofloxacin		77	0.28	499	n.d ^a		2050		40
Sulfamethoxazole	310	170	458	185	33	38	397	4330	3
Analgesics									
Naproxen	1550	555			80.5				
Ibuprofen	11900	203	3.97	8000	468	395	1660	30	
Acetaminophen			1890		40				
Ketoprofen		16		940	293	2886	128	620	
Diclofenac	4200			740	794	24	1760	62	
Salicylic acid				3170	184				
Antiepileptic									
Carbamazepine	1550	735	420	150	366	3600	21000	120	
Stimulants									
Caffeine			290	300	568	4500	3180		
Reference	Brown et al, 2006 ¹⁸ Terzic et al, 2008 ⁷	Gibs et al, 2013 ³ , Kleywegt et al, 2011 ¹⁹	Van Stempvoort et al, 2013 ²⁰ , Fram and	Martin et al, 2012 ²¹ , Al Aukidy et al, 2012	Calderon-Preciado et al, 2011 ²³ , Lopez-Serna et	Loos et al, 2010 ²⁵	Sim et al, 2011 ²⁶ , Fang et al, 2012 ²⁷	Zhang et al, 2017 ¹ , Hoa et al, 2011 ¹⁷	

a: undetectable

2-1-3. Degradation

Recently, the degradation of pharmaceutical pollutant included various physical, chemical and microbiology methods^{5, 28-44}, and it can be divided into these classifications:

1) *Microbiological degradation*, which is used in many domestic and foreign wastewater treatment plants, including activated sludge process and membrane bioreactor method⁴⁵. The treatment of pharmaceutical wastewater by microbiological treatment is characterized by low cost and avoiding the second pollution. At the same time, there are also some disadvantages such as leaving residue in effluent and sludge. Jelena et al.⁴⁵ studied the degradation of different classes of pharmaceuticals, such as analgesics, anti-inflammatory agents, lipid modulators and antibiotics in a laboratory membrane bioreactor, and compared with the traditional activated sludge process. The membrane bioreactor showed a stronger removal efficiency of medical pollutants than the activated sludge process. For most of the drugs, the removal rate can achieve 80%, and the drug concentration in the effluent is also more stable than the activated sludge process. For Carbamazepine, which is the most resistant biodegradable compound, it cannot be removed or transformed by membrane bioreactor and activated sludge method, because the COD, TOC and ammonia nitrogen of effluent have not been greatly improved.

2) *Adsorption*, representing the treatment of wastewater by adsorption method predominantly depended on the physical or chemical adsorption actions between the compounds and adsorbent such as activated carbon, and the characterizations showed below⁴⁶⁻⁴⁸:

(1) Active carbon has strong adsorption on organic matter in water and possessed low cost. (2) Active carbon has a strong adaptability to the change of water quality, water temperature and water amount. At the same time, it doesn't need to adjust the

water pH and concentration. For the same kind of organic pollutants in sewage, activated carbon has similar removal effect whatever in high concentration or low concentration; (3) Activated carbon wastewater treatment plant just needs small area, simple operation, management and it's easy to control; (4) Activated carbon has strong adsorption capacity for some heavy metal compound, such as mercury, lead, iron, copper, nickel, chromium, zinc, cobalt; (5) The saturated carbon can be reused after regeneration, avoiding the second pollution. A lot of research and practice have proved that activated carbon is a kind of excellent adsorbent. It has special treatment effect in the treatment of industrial wastewater.

2-2. Model compounds

2-2-1. *p*-Hydroxyphenylacetic acid (*p*-HPA): presence and degradation

p-hydroxyphenylacetic acid is one a phenolic pollutant, mainly from the agricultural industrial plant, such as olive oil wastewater and distilleries, and so on⁴⁹. Its chemical structure is shown in **Fig.2-2**, and physical chemical properties are reported in **Table 2-3**. In addition, as one kind of organic intermediates for the synthesis of the production of β -blocker atenolol, 4,7- two hydroxy isoflavone and pesticide, it is currently regarded as one popular intermediate favored by the majority of medical experts. While with a large amount of *p*-hydroxyphenylacetic acid discharging into the water, this phenolic compound will cause a series of damage to the water environment. Although the environmental harm of *p*-hydroxyphenylacetic acid is not reported, a lot of discharge will result in unknown dangers in the future.

Benitez et al⁴⁹ investigated the reaction between *p*-HPA and hydroxyl radical (HO \bullet), which was produced by UV/H₂O₂ and Fenton process. Comparing with the direct photolysis under UV irradiation, the presence of H₂O₂ accelerates the degradation efficiency. At the same time, the effects of Fe²⁺ concentration H₂O₂ concentration and pH of solution were discussed in detail. Finally, the second order constant between *p*-HPA and HO \bullet was determined to be $7.02 \times 10^8 \text{ M}^{-1} \text{ s}^{-1}$. Miguel A. Miranda⁵⁰ et al investigated the photocatalytic degradation of *p*-HPA by pyrylium

salt. At pH 3.0 and the addition of 5% pyrylium salt, the remove percentage can achieve 50% in 350 min. The researchers also studied the degradation of *p*-HPA by ozone and UV. Irama Sanche et al.⁵¹ studied the catalytic degradation of *p*-HPA by zero valance iron, and the degradation efficiency was checked by the detection of COD and TOC of the wastewater. Minh, D. Pham et al.⁵² investigated the degradation of *p*-HPA and *p*-hydroxybenzoic acid, which were two most commonly detected pollutants in olive oil industrial wastewater. The authors studied the catalytic oxidation in a batch reactor using platinum and ruthenium catalysts supported on titanium and zirconium oxides at 140 °C and 50 bar of total air pressure. Furthermore, the degradation pathway and intermediates of these two compound were elucidated showing the formation of different aromatic compound and short chain organic acid through hydroxylation and decarboxylation. Electro chemical oxidation methods were adopted by Flores et al.⁵³ to investigate the degradation of *p*-HPA. In this work, mineralization, kinetic reaction and photoproducts were reported. The TOC removal and degradation of *p*-HPA both followed the pseudo first order kinetic reactions. Finally, *p*-hydroxybenzaldehyde, *p*-hydroxybenzyl alcohol and acetic acid were the main intermediates during the process. However no significant decrease of TOC was reported. Flores et al.⁵⁴ investigated the degradation of *p*-HPA by HO• produced by H₂O₂, electro-Fenton and photo-electro-Fenton, and excellent mineralization was achieved.

2-2-2. Acetaminophen (ACTP): presence and degradation

Acetaminophen (ACTP), that is a drug and personal care product (PPCPs), is used as an alternative to aspirin, which mainly plays a role in relieving pain. Its chemical structure is shown in **Fig.2-3**, and physical chemical properties are reported in **Table 2-3**. The global consumption of ACTP is estimated to be about 70 thousand tons, and estimated the existing production capacity of 90 thousand tons. As for the huge quantity of production and consumption, acetaminophen has become an important object in environmental treatment studies. Younghee Kim⁵⁵ investigated the

toxicity of ACTP on one kind of Marine bacteria, freshwater invertebrates, and Japanese green fish. Results showed that ACTP presents a risk for these organisms when its concentration increased beyond $1.8 \mu\text{g L}^{-1}$. In Spain although the removal efficiency of ACTP in wastewater treatment plants can achieve 90%, it also can be detected in surface water with a concentration $0.033 \mu\text{g L}^{-1}$, and $0.22 \mu\text{g L}^{-1}$ in effluent of sewage treatment plant (STP)⁵⁶. In South Korea, ACTP was detected with a concentration 0.071 and $6.8 \mu\text{g L}^{-1}$ in surface water and effluent of STP, respectively. Moreover, in the process of chlorine disinfection, ACTP can be transformed to more toxic substances. So acetaminophen has been regarded as a potential environmental pollutant by environmental scientists.

Recently, numerous researches focus on the degradation of ACTP by advanced oxidation processes (AOPs). Zhang et al.⁵⁷ investigated the photocatalytic degradation of ACTP by TiO_2 under irradiation. TiO_2 based photocatalytic degradation can efficiently remove ACTP from water. Under pH 3, with the addition of TiO_2 0.5 g L^{-1} , the degradation of ACTP can obtain 59.1% with an initial concentration $30 \mu\text{mol L}^{-1}$ after 60 min. Andreozzi et al.⁵⁸ degraded ACTP by using ozone and H_2O_2 in aqueous solution. These two methods both can attack the benzene rings and the mineralization can achieve 30% and 40% respectively under the current conditions. Furthermore, the intermediates of ACTP were identified by GC-MS. Mark Daniel G. de Luna et al.^{59, 60} investigated the decomposition of ACTP by Fenton process regarding the dosage of ferrous and influences of $[\text{Fe}^{2+}]/[\text{H}_2\text{O}_2]$ ratio. Main intermediates were identified by SPME/GC-MS. Chia-Chi Su et al.⁶¹ discussed on the degradation of ACTP by aeration Fenton. Solution pH, concentration of Fe^{2+} and H_2O_2 were studied on the effects on the removal efficiency and mineralization was reported. Alam et al.⁶² studied the degradation of ACTP in photo-Fenton processes by taking FeSO_4 and iron complex as different iron source under solar light irradiation. Results demonstrate a significant degradation in the presence of FeSO_4 and same intermediates (with two different sources of iron) were identified. Meanwhile, the toxicity assessment using vibrio fischeri and water flea showed that these two different photo-Fenton processes can decrease the toxicity of solution to 40% representing a safe and effective method

for the degradation of ACTP.

Table 2-3 Physical-chemical properties of *p*-hydroxyphenylacetic acid and acetaminophen

English Name	<i>p</i> -hydroxyphenylacetic acid
Abbreviation	p-HPA
CAS number	156-38-7
Molecular formula	C ₈ H ₈ O ₃
Molecular weight	152.15
Melting point(°C)	149-150
pKa	4.5, 10.5
Solubility	Slightly soluble in water
English Name	acetaminophen
Abbreviation	ACTP
CASnumber	103-90-2
Molecular formula	C ₈ H ₉ NO ₂
Molecular weight	151.16
Solubility(20 °C)	14 g/L
LogKow	0.46
pKa	9.38

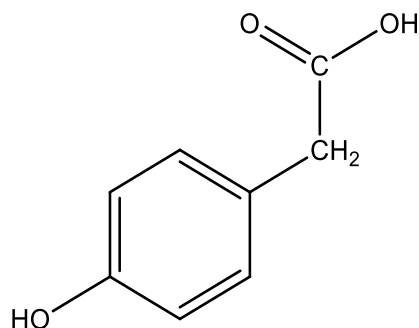


Fig.2-2 Structure of *p*-hydroxyphenylacetic acid (*p*-HPA)

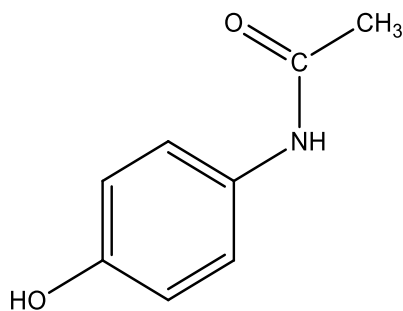


Fig.2-3 Structure of acetaminophen (ACTP)

2-3. Advanced oxidation processes (AOPs)

2-3-1. General description

In the last few decades, the development of modern industry has produced strong negative impacts on the natural environment. The pollutants presence in water exhibit major changes, emerging pollutants attract great attention, which lead to fast evolution of the research activities devoted to wastewater treatments. Compare with traditional physical, chemical and biology wastewater treatment technics, advanced oxidation processes (AOPs) present particular advantages for the degradation of persistent organic pollutant (POPs) up to the trace level concentration.^{63, 64} As one new and effective pollutant control technics, AOPs emerged in history from 1980s. AOPs efficiency are based on the formation of various radicals by semiconductor catalyst, irradiation, electricity, ultrasonic and activation of H₂O₂, Na₂S₂O₈, and ozone.

H₂O₂ alone is a weak oxidation with E^0 (H₂O₂/H₂O) = 1.763 V/SHE in acidic solution and E^0 (H₂O₂/OH⁻) = 0.88 V/SHE in alkaline medium. It's only effective for attacking reduced sulfur compound, cyanides and certain organics such as aldehydes, formic acid and some nitro-organic and sulfo-organic compound. Its oxidation power can be notably improved by combination with ozone, UV radiation and transition metals such as iron ions. The latter technology is the so-called Fenton chemistry explained in the section below. Among the reactive species involved in AOPs, the most commonly researched radicals include HO[•] ($E^0=2.80V$)^{65, 66}, SO₄^{•-} (2.6-3.2

V)⁶⁷⁻⁷⁰. All of the radicals formed by AOPs possess high oxidation abilities, and standard reduction potential in aqueous medium of the most commonly reported oxidizing agents was showed in the following **Table2-4**.

For the source of •OH radical in AOPs, a combination of conventional strong oxidants such as ozone, oxygen or hydrogen peroxide and catalysts (e.g., transition metal, iron and copper), semiconductor solid (e.g., TiO₂ and Fe₂O₃) together with energy sources of UV-visible irradiation, ultrasound, electricity or ionizing radiation was used. Once the radicals are formed, it will induce a series of free radical chain reactions, which can make most of the organic compounds mineralized or decomposed into low toxic or non-toxic small molecules, and even directly degrade to carbon dioxide and water. The pharmaceutical pollutant in water cannot be completely removed by microbiological method. It can be treated by advanced oxidation process for the second time, so as to reduce its toxicity and achieve discharge standard⁷².

Among the activation methods in AOPs, light is a kind of green and sustainable energy, the application of light irradiation into wastewater treatment is of great interest in related research field. The basic and popular systems of this kind, excluding the application of iron, include UV/H₂O₂⁷³, UV/Na₂S₂O₈⁷⁴, UV/O₃^{75, 76}, UV/semiconductor⁷⁷⁻⁷⁹ and photoelectrochemical^{80, 81} processes. For one example, the UV/H₂O₂ oxidizing ability can be attributed to the formation of •OH, O₂• and HO₂•, the reaction process is shown as following⁸²:

Initiation:



Propagation:



Termination:



Table 2-4 Standard Reduction Potentials in Aqueous Medium of the Most Commonly Reported Oxidizing Agents⁷¹

NO.	Oxidizing agent	Standard reduction potential (E^0/V)
1	F ₂	3.05
2	HO•	2.80
3	SO ₄ • ⁻	2.60-3.20
4	Cl•	2.40
5	FeO ₄ ²⁻	2.20
6	O ₃	2.08
7	S ₂ O ₈ ²⁻	2.01
8	H ₂ O ₂ /H ₂ O	1.76
9	H ₂ O ₂ /OH ⁻	0.88
10	MnO ₄ ⁻ (I)	1.67
11	HO ₂ ⁻ (I)	1.65
12	HCO ₃ ⁻ or CO ₃ ⁻	1.59-1.63
13	MnO ₄ ⁻ (II)	1.51
14	HOCl	1.48
15	HO ₂ ⁻ (II)	1.65-1.44
16	Cr ₂ O ₇ ²⁻	1.36
17	Cl ₂ ⁻	1.36
18	Cl ₂	1.36
19	MnO ₂	1.23
20	O ₂	1.23
21	Br ₂	1.07

2-3-2. AOPs based on heterogeneous semiconductor photo catalytic degradation

Compared with traditional homogeneous AOPs, the formation of radicals need the addition of H₂O₂, Na₂S₂O₈ or iron ions, will easily make the second pollutant. So

heterogeneous photocatalytic degradation technics based on semiconductors have the advantages of low cost and recycle use. In 1972, Fujishima and Honda⁸³ carried out the reaction of photocatalytic cracking water on the n type semiconductor TiO₂ electrode, which made the photocatalytic technology emerged on the historical stage. Photocatalysis technology, as a new pollution control method, uses semiconductor materials to convert light energy into chemical energy and electric energy. Because of its advantages of high efficiency, low cost, complete oxidation and no second pollution, it has attracted wide attention from researchers.

Recently, the commonly researched semiconductors included TiO₂⁸⁴, ZnS/Ag⁸⁵, WO₃⁸⁶, BiOX⁸⁷, CdS⁸⁸, V₂O₅⁸⁹, Ag₃PO₄^{90,91} and so on. Under a certain wavelength of light excitation, valence band electrons can be excited into the conduction band, and photogenerated electron hole pairs can be generated, following the reaction with water, hydroxide, and oxygen, which can generate radicals after (see **R7-11, Fig 2-4**). With strong oxidation abilities, the free radicals can transform most organic pollutants degradation into biodegradable compound, or even directly oxidize them to carbon dioxide and water in aqueous solution. Because the position of the valence band and the conduction band is different, the photocatalytic activity of different semiconductors is different, and the degradation effect of the specific organic matter is also obviously different. Among them, TiO₂ has the characteristics of high chemical stability, light resistant corrosion, harmless to human body, low cost, and deep valence band level. It is widely used in the field of pollutants degradation, air purification, decomposition of water, solar energy conversion and storage and other fields⁹². However, TiO₂ photocatalytic technology has some shortcomings, which restrict its wide application. First of all, TiO₂ possesses large band gap (rutile type TiO₂ band gap is 3.0 eV, anatase type TiO₂ band gap is 3.2 eV), the rutile type TiO₂ only can be irradiated by the light less than 413 nm wavelength, and excitation wavelength of anatase TiO₂ response is shorter than 387.5 nm, which both belongs to the ultraviolet (UV) light region. The light utilization rate of solar light is only 5%⁹³. Secondly, the recombination rate of photogenerated carriers is very high, resulting in low light quantum efficiency. In addition, the photocatalyst is powdery, difficult to

recover and reuse. It is also one of the important factors that restrict its development. Therefore, in order to improve the energy utilization and quantum efficiency of TiO₂, the problem of recovery has become a hot topic in the field of photocatalysis.

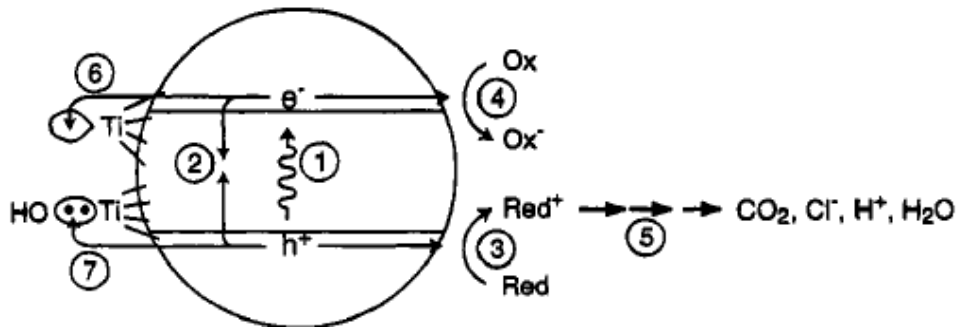
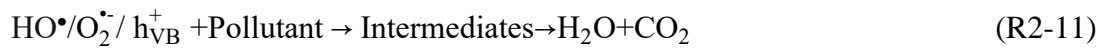


Figure 2-4 basic mechanism of TiO₂ photocatalytic process

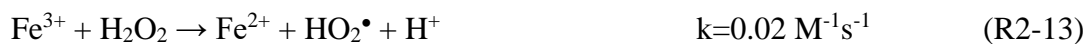
2-3-3. AOPs based on homogeneous reactions in aqueous solution

2-3-3-1. HO[•] radical

As it is known from previous research that iron species are photosensitive and can enhance the cycling and transformation of reactive radicals in the environment, hence it could obviously be expected that iron species can be used in AOPs to participate in wastewater treatment. The processes including photochemical process employing Fe(III)/Fe(II) species, photocatalytic processes in the presence of iron oxides, Fenton and photo-Fenton processes have already been widely investigated and proved to be efficient to produce HO[•]. Among all these processes, Fenton and photo-Fenton processes are the most promising and attracting methods, since this kind

of process is proved to be green, efficient, easy to operate and low-cost, leaving water and carbon dioxide as byproduct. The reaction between H₂O₂ and Fe(III)/Fe(II) is a well-known method for the generation of the hydroxyl radical (HO•), including Fenton (Fe(II)/H₂O₂)^{65, 72}, Fenton-like (Fe(III)/H₂O₂)⁹⁴ and photo-Fenton (UV/Fe(III)/H₂O₂) reactions^{66, 95-98}, the reaction equation and second order constant was shown below (R12-25). As it is known to all, Fenton process was found more than 100 years ago, and application to destroy the structure of toxic organic compounds was started from late 1960s. It is found that the Fenton reaction could be very efficient in the removal of many hazardous organic pollutants which were resistant to biological treatment from water in a short time and could completely remove the contaminants to harmless compounds such as CO₂, H₂O and inorganic salts. With high oxidation abilities, HO• (E⁰=2.8 V) has a wide application in removing environment contaminates like endocrine disrupter, chlorophenol, dye wastewater, heavy metals, pharmaceuticals, pesticide and landfill leachate due to its nonselectivity to organic chemicals.^{58, 65, 99, 100, 101}

In recent decades, the mechanism of Fenton process has been widely used in inclusive number of wastewater treatments research such as (1) homogeneous Fenton and Fenton-like systems using different kinds of Fe(II) and/or Fe(III) salt and peroxide in acidic medium; (2) homogeneous photo-Fenton system by using UV irradiation to reduce Fe(III) to Fe(II)¹⁰²; (3) heterogeneous Fenton and Fenton-like system using clay, zero valent iron or iron oxides; (4) electro-Fenton or photo-electro-Fenton system. The effect of variables such as temperature, pH value, initial concentration and inorganic ions was also determined in these related researches^{101, 103-108}.





2-3-3-2. $\text{SO}_4^{\bullet-}$ radical

While in recent years, studies on sulfate radical ($\text{SO}_4^{\bullet-}$) have proved that it's very effective in degrading recalcitrant organic pollutants due to its higher oxidation-reduction potential ($E^0=2.6-3.2 \text{ V}$)⁶⁷, longer half-life period and more selective abilities than $\text{HO}\bullet$. Although the research on $\text{SO}_4^{\bullet-}$ has been studied long time ago, the application of AOPs based on $\text{SO}_4^{\bullet-}$ to environmental treatment was started in recent years. In wastewater treatment, peroxydisulphate only adopted as the source of sulfate radical. Peroxydisulphate mainly includes two classes, one is persulfate (PS), and the other one is peroxymonosulfate (PMS). The representative compound are $\text{Na}_2\text{S}_2\text{O}_8$, $\text{K}_2\text{S}_2\text{O}_8$, $(\text{NH}_4)_2\text{S}_2\text{O}_8$ and KHSO_5 , respectively. As shown in **Fig.2-5**, similar to H_2O_2 , PS and PMS are both strong oxidizing agent, possessing "O-O" persad in structure. Compared with H_2O_2 and O_3 , PS and PMS are more stable in low temperature, they can be existed for several weeks in underground environment. The utilization of PMS was not so much in the previous literatures, so normally, peroxydisulphate usually indicating PS. $(\text{NH}_4)_2\text{S}_2\text{O}_8$ can release ammonia gas during the application process. The solubility of $\text{K}_2\text{S}_2\text{O}_8$ is relatively low in water. So with a solubility 549 g L^{-1} , low-cost $\text{Na}_2\text{S}_2\text{O}_8$ has obtained the maximum use.

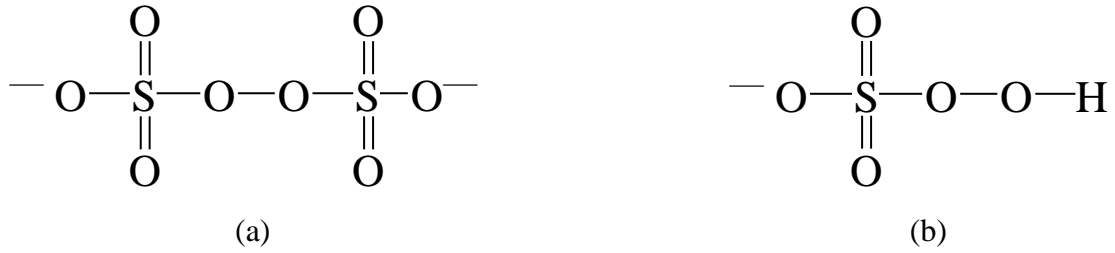
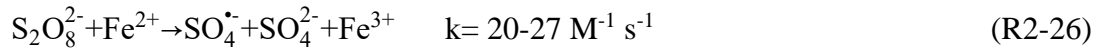


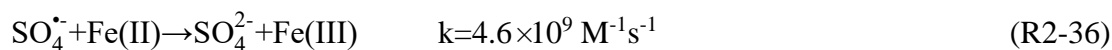
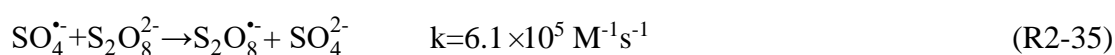
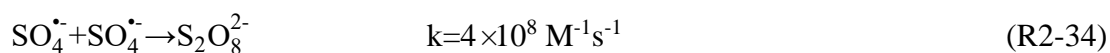
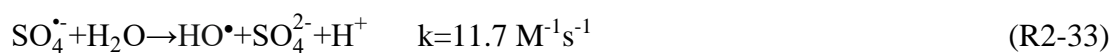
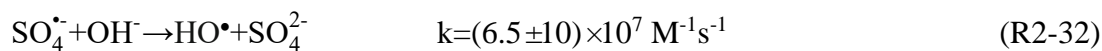
Fig.2-5 Structure of persulfate and peroxymonopersulfate

The generation of $\text{SO}_4^{\bullet-}$ usually derives from the activation of persulfate (PS) by heat⁷⁰, UV and transition metals^{69, 109, 110}. Among these activation processes, $\text{Fe}^0/\text{Fe}^{2+}/\text{Fe}^{3+}/\text{UV-PS}$ methods are efficient, energy-saving and relatively nontoxicity⁶⁹. The main formation of HO^{\bullet} and $\text{SO}_4^{\bullet-}$ from iron activation route is shown below^{69, 111}:



When $\text{S}_2\text{O}_8^{2-}$ is activated, it will produce $\text{SO}_4^{\bullet-}$, which will undergo a series of free radical chain reaction (**R2-32**, **2-33**) in aqueous solution, and eventually $\text{SO}_4^{\bullet-}$ and HO^{\bullet} will coexist in water. The amount of existence of the two radicals is determined by the pH value of the solution. Guo-Dong Fang et al.¹¹² used Electron Paramagnetic Resonance (EPR) to study the types of radicals existing in the solution of $\text{S}_2\text{O}_8^{2-}$ under different pH conditions. The results show that, in acidic and neutral conditions (pH = 2-7), is mainly $\text{SO}_4^{\bullet-}$ exist; in weak alkaline condition (pH = 8-10), $\text{SO}_4^{\bullet-}$ and HO^{\bullet} co-existed; in strong alkaline conditions (pH > 11), HO^{\bullet} has become the main oxidative species solution. However, because of the weak oxidation of HO^{\bullet} under alkaline conditions, the effect of $\text{SO}_4^{\bullet-}$ oxidation system on alkaline wastewater treatment is lower than that under acidic or neutral conditions. Same with H_2O_2 , in the

application $\text{SO}_4^{\bullet-}$, attention should be paid to the addition amount of persulfate to avoid the self-quenching effects. Furthermore, in the activation by iron ions, the molar ratio between iron ions and persulfate also is very important because of the high reaction rate between ferrous ions and sulfate radical (see **R2-34**, **2-35** and **2-36**)



2-3-4. Degradation of pharmaceutical pollutant by AOPs

In recent years, advanced oxidation processes (AOPs) have been proposed as alternative methods to remove persistent organic pollutants (POPs) in different environmental media¹¹³⁻¹¹⁵. Generally, AOPs can achieve the recalcitrant pollutant destruction when biological treatments are unfeasible, such as for endocrine disrupting chemicals (EDCs)^{116, 117}, pharmaceuticals and personal care products (PPCPs)^{118, 119}. Main oxidation processes are usually based on the *in situ* production high reactive species such as hydroxyl (HO^{\bullet}) and sulfate radical ($\text{SO}_4^{\bullet-}$) which are able to oxidize organic pollutants in aqueous solutions^{113, 114}. In the last two decades different AOPs based on iron activation under dark^{120, 121}, UV light¹²² and/or in the presence of radical precursors¹²³ have been proposed demonstrating their efficiency for organic pollutants abatement. On the other hand, heterogeneous semiconductor photocatalysis is also one of the most promising oxidation process. Under irradiation, electron (e^-) and hole (h^+) pairs are produced in conduction and valence band, leading to the formation of reactive oxygen species (ROS) such as HO^{\bullet} or hydroperoxyde/superoxide radical anion ($\text{HO}_2^{\bullet}/\text{O}_2^{\bullet-}$, $\text{pka } 4.88$)¹²⁴. Nowadays, the degradation of pharmaceuticals by AOPs included these methods as follows, and commonly used AOPs in degrading high detected pharmaceutical pollutants are listed

in **Table 2-5**.

1) *Photocatalytic degradation*. In the presence of catalyst, organic compound in wastewater can be decomposed by strong oxidant species. Some organic compound can be directly mineralized into CO₂ and H₂O. Some refractory organics can also be converted into biodegradable molecules, or molecules can be direct photolyzed. This process can significantly decrease COD, while BOD/COD increase, increasing the biodegradability of wastewater, and making it suitable to be discharged. The treatment of pharmaceutical industry wastewater by catalytic oxidation can overcome the insignificant effect of traditional biochemical treatment of pharmaceutical wastewater, and effectively attack the conjugated bonds of organic molecules, so as to achieve the goal of removing COD and improving biodegradability¹²⁵. In the photocatalytic degradation processes, the choice of catalyst is the most important step. So, in recent years, more and more researchers concentrate on the modification, enhancement and optimization of photocatalysts. It's well known that carbamazepine is one of the most difficult removal pharmaceutical in traditional microbiological technics such as STP or MBR⁴⁵. While, it can be removed effectively by photocatalytic methods.^{81, 126} Hongche et al.¹²⁷ proposed the degradation of carbamazepine by BiOCl/Fe₃O₄ under simulated solar light irradiation. Results showed that 90.3% of carbamazepine can be removed after 60 min reaction with an initial concentration of 2 mg L⁻¹. Stapleton et al.¹²⁸ investigated the degradation of 2- chlorpyridine and 2- fluorine pyridine by 254 nm photolysis, and the remove of COD_{Cr} only achieved 40%. In 2010, Stapleton et al investigated the same pollutant by TiO₂ photocatalytic degradation processes, and TOC can be removed 80%¹²⁹.

However, this kind of application should have few limitations if suspended particles are present in wastewater. In fact, particles can partially absorb the UV and visible light decreasing the photoactivation of catalyst reducing, as consequence, the degradation efficiency of pollutants in the wastewater. Moreover, the above chemical methods have not been fully utilized under solar irradiation in the environment. In order to reduce the cost of sewage treatment as much as possible, the use of solar light to treat sewage will become a trend in the future of photocatalytic development.

2) *Fenton and photo-Fenton*. Most organic compound can react with HO• formed in Fenton and photo-Fenton processes with a second order constant of $\sim 10^9 - 10^{10} \text{ M}^{-1} \text{ s}^{-1}$ and can be finally transformed into CO₂, H₂O and other inorganic compound. The combination of Fenton and microbiological treatment can increase the biodegradability. Huseyin et al.¹²⁵ used Fenton process to increase the biodegradability of wastewater discharged from pharmaceutical industry with a COD 900-7000 mg L⁻¹. Results showed that through the treatment of Fenton and aerobic bioreactor, COD can be removed up to the 98%. Photo-Fenton oxidation processes are a new kind of AOPs developed from Fenton. Compared with traditional Fenton and photolysis, this method utilizes oxidations O₃ or H₂O₂ activated by UV or visible light with the assistant of Fe²⁺, Fe³⁺ or iron complex, to finally produce HO•. Hilla et al.¹³⁰ investigated the degradation of metronidazole by UV, Fenton and Photo-Fenton. Results showed that, the efficiency of UV/H₂O₂ was higher than direct photolysis, and the remove efficiency can increase with the increased addition of H₂O₂. While under the same conditions, Photo-Fenton can increase the efficiency by 20% compared with Fenton.

Table 2-5 Representative studies dealing with the top 5 pharmaceuticals most commonly treated by AOPs. na: not available

Reference	Initial concentration	Water matrix	AOPs	Removal percentage (%)
Diclofenac				
Perz-Estrada et al.,2005 ⁷⁹	50 mg L ⁻¹	Freshwater	Photofenton under solar irradiation 200 mg L ⁻¹ TiO ₂	Completely removed in 100 min
Calza et al.,2006 ¹³¹	15 mg L ⁻¹	Distilled water	photocatalytic degradation under solar irradiation	Completely removed in 60 min
Hartmann et al.,2008 ¹³²	50 mg L ⁻¹	Distilled water	Ultrasonic degradation with 100 mg L ⁻¹ TiO ₂	85% removed in 30 min
Carbamazepine				
Doll et al., 2005 ⁷⁸	4.2 mg L ⁻¹	Lake water with 0.5 mg L ⁻¹ NOM	100 mg L ⁻¹ TiO ₂ photocatalytic degradation under solar irradiation	75% removed in 9 min

Hua et al., 2006 ⁷⁶	0.3-3.8 ng L ⁻¹	Raw river water	1.5-2 mg L ⁻¹ ozone	Completely removed in 20 min
Pereira 2007 ¹³³	240-710 µg L ⁻¹	Surface water	10 mg L ⁻¹ H ₂ O ₂ /UV (200-300 nm)	90% removed with 835 mJ/cm ²
Sulfamethoxazole				
Abellan et al.,2007 ¹³⁴	100 mg L ⁻¹	Distilled water	100 mg L ⁻¹ TiO ₂ photocatalytic degradation under solar irradiation	88% removed in 360 min
Gonzalez et al.,2007 ¹³⁵	200 mg L ⁻¹	Distilled water	Photo-Fenton	Completely removed
Dantas et al.,2008 ¹³⁶	200 mg L ⁻¹	Distilled water	0.4 g/L ozone	99% removed in 60 min
Chlorobainic acid				
Andreozzi et al.,2003 ⁷⁵	215-320 mg L ⁻¹	Distilled water	1M H ₂ O ₂ /UVC	90% removed in 60 min
Molinari et al.,2006 ¹³⁷	10 mg L ⁻¹	Distilled water	1 g/L TiO ₂ /UV	Completely removed in 20min
17β estradiol				
Coleman et al.2005 ¹³⁸ ,	0.8 mg L ⁻¹	Acetonitrile, water	TiO ₂ /UV	50% removed in 2 min
Murugananthan et al., 2007 ¹³⁹	0.5 mg L ⁻¹	Distilled water	Electrolysis	Completely removed in 8 min

2-4. Bismuth-based catalyst

2-4-1. Reactivity mechanism

In order to make catalyst more available to the application of wastewater treatment, many researchers focused on the catalyst ability to absorb solar light. As reported, the ultraviolet light ($\lambda < 400$ nm) in the solar light is about 3%-5%, and the visible light ($400 < \lambda < 800$ nm) can account for 47%, and the rest is the infrared radiation¹⁴⁰. Many catalysts can be only activated by UV and their application is limited for the practical wastewater treatment. Nowadays different researches focused on the new types of photocatalyst, which mainly concentrated on some layered compounds and structural compounds. The representative catalyst is Bi-based materials, such as Bi₂O₃^{141, 142}, BiOX¹⁴³, Bi₂O₂CO₃¹⁴⁴, Bi₂WO₆¹⁴⁵, Bi₂₅VO₄₀¹⁴⁶. The feature of these semiconductors concludes special layered structure and suitable

bad-gap that be responsible to visible light. Bismuth based oxide has good responsibilities to visible light and relatively high strong oxidation abilities. For example, semiconductor Bi_2O_3 with a band gap 2.8 eV ¹⁴⁷ can adsorb visible light. Furthermore, Bi_2O_3 is non-toxicity and stable, which deciding that it's a promising catalyst in the future. On the other hand, Zhang and his group¹⁴⁸ synthesized BiOX (X=Cl, Br, I) catalyst by solve thermal method, and this was the first halogen oxide that regarded as photocatalyst. Results exhibited that this catalyst efficiently absorbs the sun-simulated radiation, so it became a new topic in the photocatalytic field.

As the most typical photocatalyst in bismuth based materials, BiOX ¹⁴⁹ is one kind of new-fashioned semiconductors. It possesses special electricity structure, good optical and catalytic properties. Its characteristics are layered structure, enough space to polarize the corresponding atoms and their tracks, resulting in the induced dipole moment. BiOX belongs to indirect transition semiconductor, and the excited electrons must pass through some K layers to migrate to the valence band. The recombination rate of photogenerated electron hole pairs is an important factor affecting photocatalytic performance. The above two characteristics can effectively reduce the recombination rate of photoelectron hole pair of bismuth oxide¹⁵⁰. Bismuth halide is a highly anisotropic layered structure semiconductor. The crystal structure of bismuth halide is PbFCl type, which belongs to the tetragonal system. X^- and O^{2-} distribution around Bi^{3+} , the two inverse square columns coordination, Cl- layer is Affirmative coordination, the next layer is O^{2-} layer, Bi^{3+} layer sandwiched in the middle, the crystal structure of BiOCl as shown in **Figure 2-6**¹⁴³, the three-dimensional lattice model, each ion independent occupy a level. As "the five layer Cl-Bi-O-Bi-Cl structure", with van Edward, the large molecules tend to laminated structure. The crystal structure of BiOX can also be seen as the double X^- ion layer and Bi_2O_2 layer alternately arranged along the c axis. The halogen atoms are bonded by halide atoms through non chemical bond force, and the binding force is relatively small, so it is easy to dissociate.

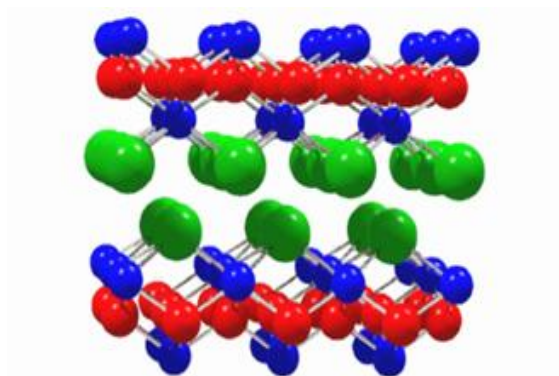


Figure 2-6 Structure diagram of BiOCl (small ball-Bi³⁺, middle ball- O²⁻, big ball- Cl⁻)

2-4-2. Application

Due to the characteristic structure and properties of BiOX, it has attracted there is a lot of attention during the recent years.¹⁵¹ Zhang and co-workers¹⁴⁸ determined the band gap of different BiOX catalyst as following: BiOCl (3.22 eV), BiOBr (2.64 eV) and BiOI (1.77 eV). As consequence, the photo-activation of BiOX can be prolonged from ultraviolet region to visible light region. BiOCl^{150, 152-155} possesses relatively wide band-gap, but the photo-induced holes and following formed hydroxyl radicals presented very strong oxidation abilities, showing excellent removal efficiency of organic dye, endocrine disruptor, pharmaceuticals and persistent organic pollutants in aqueous solution. BiOBr^{156, 157} and BiOI have narrow band-gap and, as consequence, they can be activated by visible light. They have promising wide applications in the practical treatment compared with wide band gap TiO₂ in the future. Towards the different photo-sensitization to Riboflavin (RhB) between BiOCl and P25, Hu et al.¹⁵⁸ investigated in details the mechanisms. Through the characterization of Mott-Schottky, it showed that both BiOCl and P25 belonged to n-type semiconductors. Furthermore, P25 possessed higher surface area 50 m² g⁻¹ compared with BiOCl 16 m² g⁻¹. BiOCl and P25 these two kind of catalyst had similar adsorption of RhB in the dark and similar degradation efficiency under ultraviolet irradiation. However, the most different phenomenon located at the different degradation efficiency under visible light irradiation, and BiOCl showed a much

higher efficiency compared with P25. So BiOCl and P25 have significantly different responsibilities to photo-sensitization. Scanning of FT-IR found that, P25 catalyst showed no different before and after adsorption of RhB, indicating that this adsorption was only physical adsorption, and RhB was just adsorbed on the surface of catalyst. However, the scanning of BiOCl showed that there were some typical peaks of RhB locating at 1619 cm^{-1} . Although BiOCl and P25 have the similar band structure, the chemical adsorption favored the migration of electrons from activated RhB molecules to the conduction band of BiOCl, therefore helping the formation of superoxide radicals. Meanwhile, from the fluorescence analysis of RhB after adsorptions by BiOCl and P25, it was shown that the fluorescence maximum at 580 nm was evidently weaker after BiOCl treated compared with P25. Although the adsorption removal percentage was similar in these two catalysts, this difference indicated that the excited state of RhB is easier to transfer electrons to the BiOCl conduction band.

Nowadays, the synthesis of BiOX include solve-thermal, precipitation at room temperature¹⁵⁹, sol-gel¹⁶⁰ and hydrolysis¹⁶¹. During the process of synthesis, various solvent are adopted such as water, ethanol, methanol, isopropanol, ethylene glycol, diglycol, glycerol^{154, 162, 163}. In order to increase the surface area of catalyst and form oriented space structure, some surface active agent such as polyvinylpyrrolidone (PVP)¹⁶⁴, polyacrylamide (PAM)¹⁶⁵ and cetyltrimethylammonium bromide (CATB)¹⁶⁶. The synthesized BiOX possessed great surface area, and pore volume, enhancing the adsorption and degradation abilities of pollutant. The morphology of catalyst showed different if they were synthesized by different method, such as three dimensional (3D) microspheres¹⁶⁷, flower-like¹⁵⁹, two dimensional plants (2D)¹⁶⁸, one dimensional (1D) fibers¹⁶⁹. In fact, in comparison with 1D and 2D nanostructures, 3D hierarchical nanostructures are more efficient for solar energy storage and conversion. These structures can improve light harvesting and result in faster interfacial charge separations by supplying more reactive sites, thus enhancing photocatalytic efficiencies. According to previous experiences, the 3D structure has an absolute advantage in the adsorption of pollutants and the utilization of photons. Various

efforts have been focused on optimizing the surface feature of 3D structured BiOX materials to fully develop their unique properties. In a previous paper, Xiao et al. transferred random BiOI platelets to hierarchical microspheres by replacing only water with ethanol in the reaction media via precipitation¹⁴⁹. Wang et al. successfully synthesized microflower-constructed BiOCl in a glycerol–H₂O mixed solvents and nanoplate-constructed BiOCl in sole water by solvothermal method¹⁷⁰. Kim et al. also used the solvothermal method to form 3D flower-like and 2D plate-like microstructured BiOCl_xI_{1-x} in ethylene glycol and water solvents respectively¹⁷¹. As mentioned above, all the 3D BiOX catalysts exhibited considerably superior photocatalytic abilities than the 2D materials. Solvents evidently performed important functions as structure-directing agents in the catalyst synthesis process because of their special physical and chemical properties. The majority of solvents involved in the reaction media included certain types of alcohols, especially polyols like ethylene glycol, diethylene glycol, and glycerol.

The production of reactive species under light excitation are also different, including the photo-induced holes, hydroxyl and superoxide radicals. The use of semiconductors on the degradation of pollutants mainly relates to dyes, pharmaceutical wastewater, phenols, and heavy metals and so on. Synthesis and degradation of BiOX material are summarized as shown in **Table 2-6**.

Table 2-6 Synthesis of BiOX catalyst and degradation of pollutant

Reference	Synthesis method	Irradiation light	Pollutant
BOCl			
Yu et al. ¹⁶⁵	Low temperature wet chemical	UV	Methyl orange and phenol
Wang et al. ¹⁷⁰	Solve thermal	Visible	Rhodamine B
Gao et al. ¹⁷²	Solve thermal	Xenon lamp	Carbamazepine
Zhang et al., ¹⁷³	Precipitation	UV	Rhodamine B
Zhang et al., ¹⁶¹	Hydrolysis	High pressure mercury	Methyl orange

Xiong et al., ¹⁷⁴	Solve thermal	Visible	Rhodamine B
Tian et al., ¹⁷⁵	Combination of wet etching and liquid crystal growing	/	/
Hu et al., ¹⁵⁸	Solve thermal	Visible	Rhodamine B
BiOBr			
Zhang et al. ¹⁷⁶	Ion thermal	Fluorescent lamp	Heavy metal Cr and organic dye Methylene blue
Feng et al., ¹⁷⁷	Solve thermal	UV and UV-Vis	Toluene
Tian et al. ¹⁶⁷	Solve thermal	Solar light	Bisphenol A
Shang et al., ¹⁷⁸	Solve thermal	Visible	Methyl orange
Zhang et al., ¹⁵⁷	Hydrolysis	Visible	Methylene blue, Methyl orange and Rhodamine B
Xu et al., ¹⁵⁶	Solve thermal	Solar light	Four brominated bisphenol A
BiOI			
Li et al. ¹⁷⁹	Precipitation and Solve thermal	Visible	Methyl orange and phenol
Xia et al., ¹⁸⁰	Solve thermal	Visible	Methyl orange
Shi et al., ¹⁶⁴	Solve thermal	Visible	Methyl orange
Lei et al., ¹⁸¹	Precipitation	Visible	Methyl orange, Methylene blue and Rhodamine B
Hao et al., ¹⁸²	Precipitation	Visible	Tetracycline hydrochloride
Xiao et al., ¹⁴⁹	Precipitation	Visible	Phenol

2-4-3. Modification and doping catalyst

While BiOX also have some disadvantages, as described above, BiOCl only can be responsible to ultraviolet light, but it possesses high oxidation abilities. BiOBr and BiOI can be activated by visible light, but the oxidation abilities are relatively weak. From the previous studies, BiOCl and BiOBr belong to n type semiconductor^{158, 183}, and BiOI belongs to p type semiconductor¹⁸⁴. So the modification and optimization of BiOX mainly concentrated on the composite catalyst, especially p-n types. Now the

representative modification is described as follows:

(1) BiOCl/BiOI, Dong¹⁵⁹ et al synthesized BiOCl/BiOI catalyst with different chlorine and iodine molar ratio by precipitation methods at room temperature. The morphology of the catalyst showed flower-like. From the characterization of X-ray powder diffraction (XRD), solid solution was formed between these two catalysts. Under the irradiation of visible light, composite catalyst showed better removal efficiency in degrading NO compared with single catalyst. When the molar ratio of chlorine and iodine was 3:1, it showed the fastest removal rate. Xiao¹⁸⁵ et al also synthesized BiOCl/BiOI composite catalyst by solve-thermal method. Under the irradiation of visible light, removal rate of Biphenol A (BPA) was much better when treated by composite catalyst, and it was 40 times higher than P25. When the molar ratio of chlorine and iodine was 1:9, it showed the best removal efficiency. This phenomenon mainly can be attributed to the heterojunction which was formed in the composite catalyst that can decrease the combination rate of electron-hole pairs. Wang¹⁸⁶ et al and Kim¹⁷¹ et al synthesized the similar BiOCl/BiOI composite catalyst, all showing better photocatalytic properties ascribing to its special band structure and great surface area.

(2) BiOX/Bi₂O₃, Chai¹⁸⁷ et al synthesized BiOCl/Bi₂O₃ composite catalyst, under the visible light irradiation, both BiOCl and Bi₂O₃ showed very low catalytic efficiency. While, the removal of organic matter has been improved by the composite catalyst, and the organic matter can be completely mineralized and no intermediate products are produced. Among the composite catalyst, BiOCl plays a major role, and the holes produced on the valence band is the main active species, and the main function of Bi₂O₃ is the photosensitizer that absorbs visible light. Li et al.¹⁸⁸ synthesized BiOI/Bi₂O₃ catalyst, under visible light, it has good degradation effect on phenol and four chlorophenol. By studying the two kinds of catalysts, we can find that the good catalytic efficiency is mainly due to the effective separation of electrons and holes and reduction of recombination by composite catalysts

(3) BiOX/TiO₂, Li et al.¹⁸⁹ synthesized BiOCl/TiO₂ catalysts by solvothermal treatment, the reason for better catalytic properties mainly can be attributed to the

heterojunction formation that can effectively separate the photogenerated electron hole pairs and promote the formation of free radicals. Duo et al.¹⁹⁰ also synthesized BiOCl/TiO₂ catalyst by hydrolysis at low temperature. Under simulated solar light, the removal efficiency was highly improved towards the degradation of phenol. Composite catalyst can broaden the adsorb range of light, and the heterojunctions can effectively decrease the combination rate of electron hole pairs.

(4) BiOX/Bi₂S₃, Jiang et al.¹⁹¹ synthesized BiOCl by precipitation methods first, then BiOCl was taken as precursor, BiOCl/Bi₂S₃ was fabricated by ion-exchange methods. The as-prepared composite catalyst still exhibited 3D flower-like hierarchical structure and great surface area. Under visible light irradiation, the degradation efficiency of RhBs higher by this 3D flower-like crystal than the 2D plate like BiOCl/ Bi₂S₃, which can be attributed to its greater surface area and higher separation rate of photo-induced hole and electron pairs. By the same ion-exchange method, Cao et al.¹⁹² synthesized BiOI/Bi₂S₃, under visible light activation, it showed excellent degradation of methyl orange, and 4% Bi₂S₃/BiOI showed the best efficiency among these prepared catalyst due to its same reason with the above description. However, this kind of catalyst did little work to the colorless pollutant like phenol or four chlorophenol.

(5) BiOX/Bi₂O₂CO₃, Zhang et al.¹⁴⁴ obtained BiOCl, BiOCl/Bi₂O₂CO₃ and Bi₂O₂CO₃ catalysts by adding different amount to the bismuth nitrate solution. Under simulated solar light, composite catalyst showed better degradation abilities than single catalyst, and it can remove 95% COD of methyl orange solution in 8 hours. Solve thermal method was adopted by Yu et al.¹⁹³ to synthesize BiOCl/Bi₂O₂CO₃, it showed better catalytic abilities under visible light than P25 under ultraviolet light irradiation in removing RhB.

(6) BiOX/Fe, BiOI/Fe₃O₄ was prepared by Li et al.¹⁹⁴ at 85 °C by using precipitation method. This catalyst showed favorable magnetic properties. When visible light was taken as irradiation source, RhB can be removed up to the 90.1% in 40 min. While single BiOI only can remove 50.3% of RhB during the same period. After recycle for five times, there was no obvious decrease in degradation abilities.

The main active species were hole and superoxide radicals determined by radicals quenching experiments. This magnetic material can be easily removed from water by magnet, opening a new word, opening a new chapter for the recovery and utilization of the Bi catalyst. Xu et al.¹⁹⁵ synthesized a 3D-structured Bi₂WO₆- Fe₃O₄, it showed better degradation abilities than single Bi₂WO₆ and P25 in removing RhB under the irradiation of visible light. 98.6% of RhB disappeared in 150 min irradiation. By the same way, it also can be recovered effectively from water by external magnet.

(7) BiOX/Ag. The deposit of noble metals has always been a big direction in the improvement of the catalyst, and BiOX/Ag/AgX has been widely studied¹⁹⁶⁻²⁰⁵. Cheng et al.²⁰³ synthesized AgI/BiOI by precipitation method at low temperature. The fluorescence of composite catalyst was weaker than the single catalyst, indicating its lower recombination rate of photo-induced hole-electron pairs. Under irradiation with visible light, composite catalyst activated better than the single catalyst in removing methyl orange and phenol. Furthermore, the addition amount of AgI played significant roles, and when the addition achieved 20%, it exhibited the best. It was found that AgI stayed stable in the recycle use of AgI/BiOI, showing promising abilities in the practical use of wastewater treatment under visible light.

2-5. Fe(III)-Ethylenediamine-N,N'-disuccinic acid (EDDS)

2-5-1. Iron in water

Iron is a natural element present in different phases of the earth. In the Earth crust, iron is the second abundant metal following aluminum; iron also exists in living creature, and exhibits as one of the most important trace elements in human body which is essential for health; after all, iron is also one of the common compositions in natural aqueous phase, including rain, cloud water, fog, other atmospheric water and surface water. There were a lot of related reports about the iron detection in natural aqueous phase. In fact, iron is present under a variety of forms in water ranging from soluble to colloidal and particulate species. But, most of the iron in natural waters exists in the form of insoluble ferric oxides and (hydr)oxides. The concentration of

dissolved iron is very low and most of the dissolved iron is associated with strong organic ligands in natural waters. It has been known that the iron species including Fe^{3+} , $\text{Fe}(\text{OH})^{2+}$, $\text{Fe}(\text{OH})_2^+$ and $\text{Fe}_2(\text{OH})_2^{4+}/\text{Fe}_2\text{O}^{4+}$ exist in aqueous Fe(III) salt solution, however, actual species in natural water depend on different conditions. In the aqueous solutions at $\text{pH} < 5$, there are at least four kinds of Fe(III) complexes with different forms, including Fe^{3+} , $\text{Fe}(\text{OH})^{2+}$, $\text{Fe}(\text{OH})_2^+$ and $\text{Fe}_2(\text{OH})_2^{4+}$. The distribution of these complex forms is described by the following equilibria^{71, 206}:



Iron can also absorb sun radiation and effect on the environmental chemistry through photoinduced process is of great relevance. The different products from hydrolysis of iron salts have different photochemical property. At pH around 3, $[\text{Fe}(\text{H}_2\text{O})_5(\text{OH})]^{2+}$ is the predominant species, which exhibits significant photoactivity in the UV and visible region of solar radiation. It can generate HO^\bullet through photolysis, and the quantum yield of the reaction is determined to be 0.075 at 360 nm²⁰⁶, whereas the photochemical reduction could be shown as following (R2-40). And Fe(II), photoreduced from Fe(III), can be oxidized again to Fe(III). Except the most reactive $\text{Fe}(\text{OH})^{2+}$, other Fe(III)-OH complexes are also photosensitive.



2-5-2. Iron complex

As reported above, the generation of HO^\bullet and $\text{SO}_4^{\bullet-}$ species using iron sources, mainly combined with UV irradiation, has played predominant roles in advanced oxidation processes. However, there are several key parameters in these activation methods. The most predominant drawback is the fact that Fe^{3+} ions precipitate at pH higher than 4.0 and usually under these conditions Fe^{2+} is naturally oxidized into Fe^{3+} . Therefore, most of the iron species presenting in natural and slightly basic solution, exist in the form of insoluble ferric oxides and (hydr)oxides^{96, 207}. Due to these

physicochemical properties of iron in water, the activation of persulfate by $\text{Fe}^{2+}/\text{Fe}^0$ is more favorable in acidic solution than in neutral and alkaline pH⁶⁹. So the development of Fe(II)/Fe(III) organic complexes is essential to improve the removal efficiencies in higher pH solutions.

Polycarboxylate acids like citrate, oxalate and aminopolycarboxylic acids like ethylenediaminetetraacetic acid (EDTA) can form stable water soluble complexes with iron in neutral and slightly basic pH solutions, enhancing the dissolution of iron in natural water. Moreover, these complexes are photochemically active and efficient leading by photoredox process to the production of oxidative species like hydroxyl radicals^{100, 208, 209}. Among the complexes formed between EDTA and metals, Fe(III)-EDTA is obviously proved to be the most photosensitive. Different researches revealed that the decay of Fe(III)-EDTA under UV irradiation depends strongly on the wavelength of irradiation and the pH value of environment, as it is reported that the half-life of Fe(III)-EDTA in surface waters ranges from 11.3 min to more than 100 h, which depend on the different light conditions employed. And the intermediate and decay pathways of photodegradation of Fe(III)-EDTA complex depends significantly on the oxygen of the system.

Zhao et al.²¹⁰ studied the degradation process of iron oxalate (Fe(III)-oxalate) complex under ultraviolet light and visible light. Unlike most advanced oxidation processes, Fe(III)-oxalate/ H_2O_2 /photochemical system can initiate to both reductive and oxidative degradation processes. Zhou et al.²¹¹ compared the degradation of diethylstilbestrol in water by Fe (III)/UV and Fe (III)-oxalate/UV system. The results showed that the degradation efficiency of Fe (III)-oxalate/UV system was much higher. Hug et al.²¹² studied the oxidation removal effect of various oxidants on arsenic trivalent As (III) under the neutral condition (pH=6.5-8), UVA ultraviolet was taken as radiation source. The results showed that As (III) could not be oxidized under the condition of only Fe (III) or H_2O_2 . When citrate was added to the system, the removal efficiency of As (III) was greatly improved due to the formation of the complex of iron citrate (Fe (III)-citrate).

2-5-3. Ethylenediamine-N,N'-disuccinic acid (EDDS)

Very recently different research groups started to work with a new complexing agent of iron EDDS, its physical and chemical properties are shown in **Table 2-7**. EDDS is a structural isomer of EDTA, has two chiral centers and exists as three stereoisomers, namely [S,S]-EDDS (25%), [R,R]-EDDS (25%) and [R,S/S,R]-EDDS (50%), see **Fig.2-7**. As it is reported in the previous research, [S,S]-EDDS is readily biodegradable, while the [R,S/S,R] and [R,R] stereoisomers are less biodegradable^{213, 214}.

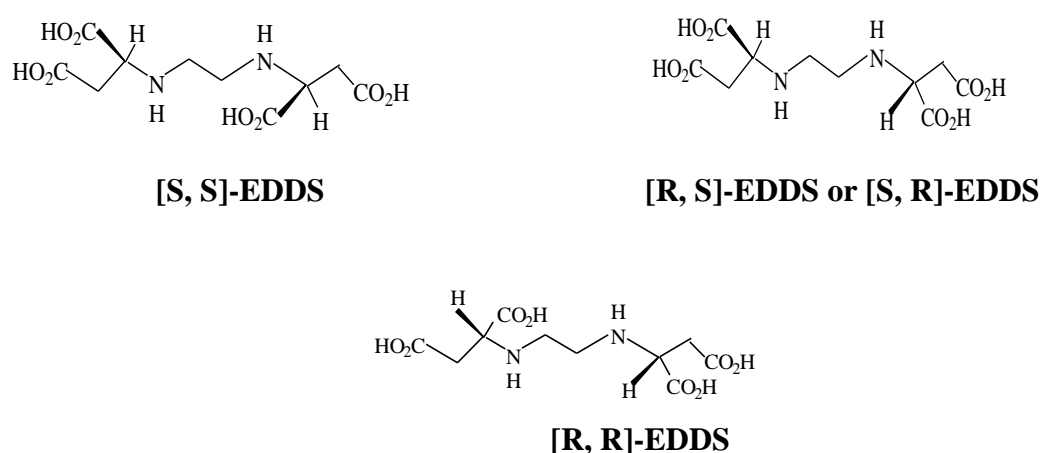


Fig. 2-7 Chemical structures of three different stereoisomers of EDDS

Currently, S,S-EDDS is used as laundry detergent (the tri-sodium salt) to replace phosphorous containing chelant, in hair products to stabilize peroxide solutions and as enhancer of biocides, for the metal removal in wastewater and soil washing treatment. The use of the S,S-EDDS as chelant for Ca^{2+} , Sn^{2+} , Cu^{2+} , Fe^{3+} and Zn^{2+} was widely investigated in previous literatures. In 2002, total production of EDDS achieved 10000 tons. Nowadays, EDDS is a chelating reagent available in Europe on a large scale, and the demand for S,S-EDDS acid has been growing at the rate of 15% per year²¹⁴.

Our group has studied the physiochemical properties of the Fe(III)-EDDS complex with a ratio of 1:1. Under irradiation, Fe(III)-EDDS was easily photolyzed leading to the formation of HO^\bullet in the wide pH range between 3 and 9. As shown in **Fig. 2-7**, the molecule of EDDS contains four carboxyl functional groups, consequently, EDDS ionization equilibrium in the solutions is described in following

reactions (R41)-(R44). For simplification, EDDS molecules were represented as H_4L ^{215, 216}.

The physicochemical properties of the Fe(III)-EDDS complex are also investigated. When Fe (III) is complexed with EDDS, the generated Fe(III)-EDDS can be presents as four main forms FeL^- , $Fe(OH)L^{2-}$, $Fe(OH)_2L^{3-}$ and $Fe(OH)_4^-$ under different pH conditions. Through the theoretical calculation of software Gaussian09, the distribution of four main forms at different pH values is obtained by Wu et al.²¹⁷, as shown in **Fig. 2-8**. From the chemical calculation results show that when the pH value is less than 6, all the complexes exist in the form of FeL^- ; with the increase of pH, the gradual emergence of $Fe(OH)L^{2-}$, $Fe(OH)_2L^{3-}$ and $Fe(OH)_4^-$, and the proportion of FeL^- decreased gradually; at the same time, with the increase of pH, $Fe(OH)_3$ is also gradually formed, so the total amount of soluble Fe (III) decreased gradually.

The work of Li et al.²¹⁸ gave evidence of the potential role of Fe(III)-EDDS as a photoactive species in natural water. For the first time, the quantum yield of HO^\bullet was detected by photolysis of Fe(III)-EDDS under UV irradiation. The quantum yield of HO^\bullet was independent of the concentration of Fe(III)-EDDS. The effects of oxygen and irradiation wavelength on the quantum yield of HO^\bullet were very well known and are the same as for any other iron species. On the contrary, the quantum yield of HO^\bullet radical formation was higher at higher pHs between 3.0 and 9.0. This result is particularly interesting in terms of the natural environment.



Table 2-7 Chemical and physical properties of EDDS

ethylenediamine-N,N'-disuccinic acid	
CAS number	20846-91-7
Molecular formula	C ₁₀ H ₁₆ N ₂ O ₈
Molecular weight	292.24 g/mol
Melting point	516.68 °C at 760 mmHg
Boiling point	220-222 °C
λ_{\max}	none
Intensity	1.44 g/cm ³ (25°C)
logK _{ow}	-5.44 (KowWin est.)
Solubility in water	slightly soluble
Flash point	38 °C

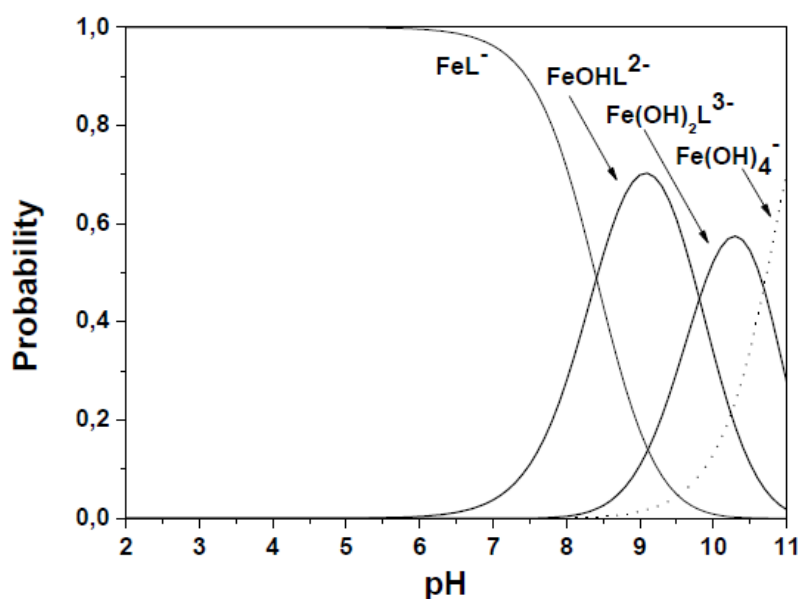


Figure. 2-8 The proposed theoretical model distribution of the predominant species for the Fe(III)-EDDS complex as a function of pH

2-5-4. Application of Fe(III)-EDDS in environment

Due to the photochemical properties, Fe(III)-EDDS was widely used in the environment treatment especially in AOPs. As reported, most of the use of Fe(III)-EDDS based on the activating H₂O₂ to produce HO• and PS to produce SO₄^{•-}.

Photo-generation of HO^\bullet and $\text{SO}_4^{\bullet-}$ based on Fe(II)/Fe(III)-EDDS complexes has been widely studied in recent years, showing excellent efficiency in removing organic pollutants and heavy metals in water and soil near neutral pH^{95, 96, 111, 217, 219-223}. In the previous study of our group, Huang et al (2013) demonstrated that in homogeneous Fenton process (Fe(III)-EDDS/ H_2O_2), Fe(III)-EDDS (molar ration 1:1) showed better removal efficiency of bisphenol A (BPA) in alkaline solution than in acidic one¹¹¹. At the same time, Wu et al (2014) demonstrated that under UV, photo-Fenton process (Fe(III)-EDDS/ H_2O_2 /UV) has much higher efficiency in removing 4-tert-Butylphenol (4-tBP) than Fenton process. This result can be explained with the fast generation of Fe(II) under irradiation⁹⁶. In the presence of PS with Fe(III)-EDDS/UV, efficient oxidation of 4-terbutylphenol (4-tBP) was observed due to the formation of $\text{SO}_4^{\bullet-}$. In neutral and basic pH conditions, the efficiency of 4tBP degradation was much higher with Fe(III)-EDDS than with Fe(III) aqua complexes⁶⁷. So the use of Fe(III)-EDDS complexes leads to efficient oxidations whatever the sources of radical species (HO^\bullet or $\text{SO}_4^{\bullet-}$).

Miralles-Cuevas et al.⁹⁹ demonstrated that mild solar photo-Fenton combined with EDDS (low starting concentration of iron, no pH modification and low consumption of H_2O_2), could be a good option for the tertiary treatment of nan filtration concentrates from municipal wastewater treatment plants containing low concentrations of pharmaceuticals. Photo-Fenton-like Fe(III)-EDDS complex makes it possible to work at pH over 6. Papoutsakis et al.²²³ verified that the treatment of micro-contaminants with the use of EDDS as a n iron-complexing agent is possible in real wastewater effluent at a pH range between 5 and 8. Yan et al.²⁰⁹ investigated the effectiveness and mechanisms of naphthalene and metal removal from artificially contaminated soil by FeEDTA/FeEDDS-activated persulfate through batch experiments. Using FeEDTA-activated persulfate, higher naphthalene removal from the soil at 7 hours was achieved 89%, compared with Fe(III)EDDS-activated persulfate (75%). Although EDDS is advantageous over EDTA in terms of biodegradability, it is not preferable for iron chelate-activated persulfate oxidation since persulfate was consumed to oxidize EDDS. Zhang et al.²¹⁹ assessed the

application of calcium peroxide activated with Fe(II)-EDDS to enhance trichloroethylene degradation in aqueous solution. And the results indicated that EDDS prevented soluble iron from precipitation, and the optimum molar ratio of Fe(II)/EDDS to accelerate pollutant degradation was 1:1.

3. Materials and Methods

3.1. Reagent

S, S'-Ethylenediamine-N, N'-disuccinic acid trisodium salt solution, (EDDS), 35% in water, Sigma-Aldrich.

Ferric perchlorate ($\text{Fe}(\text{ClO}_4)_3 \cdot x\text{H}_2\text{O}$), $\geq 97\%$, Fluka.

p-HPA, analytical degree, Aladdin

ACTP, analytical degree, Sinopharm Chemical Reagent Co., Ltd

Hydrogen peroxide (H_2O_2), 30% in water, Fluka.

2-propanol (IPA), 99.9%, Sigma-Aldrich.

Sodium hydroxide (NaOH), $> 97\%$, Prolabo.

Sodium chloride (NaCl) $\geq 99\%$, Sigma-Aldrich

Perchloric acid (HClO_4), $> 97\%$, Merck.

Sodium persulfate ($\text{Na}_2\text{S}_2\text{O}_8$), $\geq 99\%$, Sigma-Aldrich

Bisphenol A (BPA), $\geq 99\%$, Sigma-Aldrich

Benzoquinone (BQ), $\geq 99\%$, Sigma-Aldrich

Phosphoric acid (H_3PO_4), $\geq 99\%$, Sigma-Aldrich

Sodium dihydrogen phosphate ($\text{NaH}_2\text{PO}_4 \cdot \text{H}_2\text{O}$), $\geq 99\%$, Sigma-Aldrich

Tert-butyl alcohol (TBA), $\geq 99\%$, Aldrich

Methnaol (MeOH), for HPLC, $\geq 99\%$, Sigma-Aldrich

Potassium iodide (KI), $\geq 99\%$, Sigma-Aldrich

Bismuth nitrate ($\text{Bi}(\text{NO}_3)_3 \cdot 5\text{H}_2\text{O}$), analytical degree, Sinopharm Chemical Reagent Co., Ltd

Ethylene glycol (EG), analytical degree, Sinopharm Chemical Reagent Co., Ltd

Ammonium thiocyanate (NH_4SCN), $\geq 99\%$, Fluka

3.2. Synthesis of Bismuth catalyst $\text{BiOCl}_{0.75}\text{I}_{0.25}$

Firstly, 12 mM $\text{Bi}(\text{NO}_3)_3 \cdot 5\text{H}_2\text{O}$ was dissolved in 24 mL EG and kept stirring at 80 °C for 20 minutes. KCl and KI at molar ratios 3:1 were dissolved in 96 mL

deionized water, maintaining their total molar amount equal to the molar amount of $\text{Bi}(\text{NO}_3)_3 \cdot 5\text{H}_2\text{O}$. The aqueous solution was added dropwise into the previous EG solution, and the pH of this mixture was adjusted to 9.0 with NH_3 . Thereafter, the solution was continually stirred at 80 °C for 3 hours. Finally, the mixture was separated by centrifugation, washed several times with deionized water and ethanol, dried at 60 °C for 12 hours. To improve the repeatability of the experiment, samples were calcined at 200 °C for 2 h to remove the residual EG. The synthesised materials could be regarded as $\text{BiOCl}_{0.75}\text{I}_{0.25}$.

3.3. Characterization of Bismuth catalyst

The crystal phase structure was characterized by X-ray diffraction (XRD, Bruker D8 Advance) using $\text{Cu K}\alpha$ radiation (40 kV and 40 mA) as X-ray source ($\lambda = 0.154056$ nm) with a 2θ scope of 10–90°. The morphology of the photocatalyst was observed through field emission scanning electron microscopy (FESEM, Ultra 55, Germany). Surface area and pore distribution of the catalysts was determined by N_2 adsorption and desorption, using the multipoint Brunauer–Emmett–Teller (BET) analysis methods by an AUTOSORB-1 N_2 adsorption apparatus (Quantachrome, USA). The UV–vis diffuse reflection spectra (DRS) were obtained for the samples using a Scan UV–vis spectrophotometer (Thermo Nicolet Evolution 500 UV-vis), equipped with an integrating sphere assembly, and BaSO_4 was used as reflectance sample. X-ray photoelectron spectroscopy (XPS) spectra are recorded with a PerkinElmer PHI 5000C ESCA system equipped with a hemispherical electron energy analyzer. The $\text{Mg K}\alpha$ ($h\nu = 1253.6$ eV) anode was operated at 14 kV and 20 mA. The carbonaceous C 1s line (284.6 eV) was used as the reference to calibrate the binding energies (BEs).

3.4. Reaction process

3.4.1. Heterogeneous photocatalytic degradation of *p*-HPA by bismuth catalyst

Photocatalytic degradation experiments were performed in a homemade photoreactor placed in a cylindrical stainless steel container. Four fluorescent bulb lamps (Philips TL D15W/05) were separately placed in the four different axes while the photoreactor, a water-jacketed Pyrex tube of 2.8 cm internal diameter, was placed in the center of the setup, as shown in **Fig.3-1**. Irradiation with the predominant wavelength between 300 to 500 nm was used to simulate solar light, and the emission spectrum is shown in **Fig. 3-2**. The emission spectrum (Figure S1) reaching the solution was determined using an optical fiber coupled with a CCD spectrophotometer (Ocean Optics USD 2000+UV-VIS) calibrated using a DH-2000-CAL Deuterium Tungsten Halogen Reference Lamp. Energy has been normalized to actinometry results by using paranitroanisole/pyridine actinometer²²⁴. At the wavelength range of 300–500 nm, a total flux of 1451 W m⁻² reaching the solution was determined.

Solutions were magnetically stirred with a magnetic bar during irradiation, and the total volume of the solution was 100 mL. *p*-HPA adsorption on bismuth catalyst was investigated in the dark with continuous magnetic stirring. All the experiments were carried out at room temperature (293 ± 2 K) using a circulating cooling water system. An aliquot of solution (1 mL) was withdrawn from the reactor at fixed interval times and the catalyst solid was removed by 0.2 μm PTFE filters before analysis. Prior to the use of PTFE filter, control experiments were performed, showing that no adsorption of *p*-HPA was observed on these filters. Experiments are performed using a *p*-HPA concentration of 50 μM and BiOCl_{0.75}I_{0.25} catalyst of 0.3 g L⁻¹. The effect of dissolved oxygen on the *p*-HPA degradation and radical species involvement are carried out bubbling N₂ or O₂ for 20 min before catalyst addition and during all the time of the experiment (with and without light).

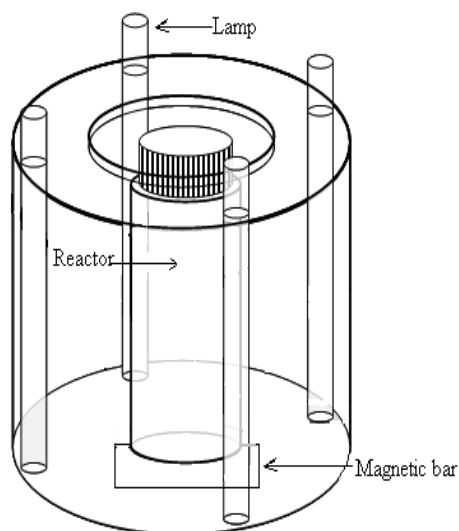


Fig. 3-1 Home-made photoreactor with four tubes

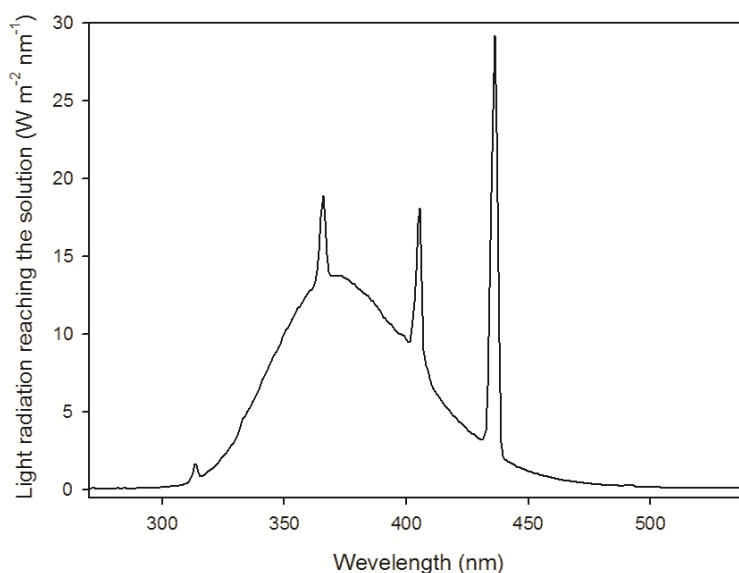


Fig. 3-2 Emission spectrum reaching the solution

3.4.2. Homogeneous degradation of *p*-HPA by Fe(III)-EDDS

As for the control experiment in the dark, reaction was performed in a brown bottle with continuous magnetic stirring at room temperature. The reaction started from the addition of H₂O₂ or Na₂S₂O₈. For the degradation of *p*-HPA under irradiation, the experiments were performed in a same home-made photoreactor as shown in **Fig. 3-1**. The total volume of reaction solution was 100 mL. All the experiments were carried out at room temperature (293 ± 2 K), supported by a circulating cooling water system. The initial concentration of *p*-HPA was 50 μM in all experiments, and

samples were taken from the reaction tube at fixed time intervals. In order to stop the Fenton reaction after the samples taken from the photoreactor, 20 μL IPA was added in each sample bottles.

3.4.3. Photodegradation of ACTP

The irradiation setup was the same for *p*-HPA. The solutions were magnetically stirred with a magnetic bar during irradiation, and the total volume of the solution was 100 mL. All the experiments were carried out at room temperature (293 ± 2 K) supported by a circulating cooling water system. Samples were taken from the reaction tube at fixed interval times and the catalyst solid was removed by 0.2 μm PTFE filters before analysis. In the experiments, the concentration of ACTP was always stayed at 50 μM , concentration of H_2O_2 and $\text{Na}_2\text{S}_2\text{O}_8$ was always 1 mM and $\text{BiOCl}_{0.75}\text{I}_{0.25}$ catalyst was kept at 0.3 g L^{-1} .

3.5. Analytical and spectroscopic methods

3.5.1. *p*-HPA detection

The concentration of the *p*-HPA remaining in the aqueous solution was determined by an Alliance high performance liquid chromatography (HPLC) equipped with a photodiode array detector (Waters 2998, USA) and Waters 2695 separations module. The flow rate was 0.15 mL min^{-1} , the injection volume was 50 μL and the mobile phase was a mixture of water (0.1% H_3PO_4 included) and methanol (65/35, v/v). The column was a Nucleodur 100–3 C18 of 150 \times 2.0 mm, particle size of 3 μm . Under these conditions *p*-HPA was detected at 274 nm and retention time was 6.7 min. Calibration of *p*-HPA was shown in **Fig.3-3**. The concentration of BQ was determined by HPLC-UV using the same column and mobile phase was a mixture of water and methanol (75/25, v/v) with a detection wavelength set at 245 nm. The retention time of BQ is 4.9 min, and for calibration see **Fig.3-4**.

UV–vis spectra were recorded with a Cary 300 UV–visible spectrophotometer.

pH values of the solutions were measured using a Cyberscan 510 pH meter. Mineralization of *p*-HPA solution was determined by total organic carbon (TOC) analysis (5050A, Shimadzu, Japan). The limit of detection and limit of quantification have been determined to be 50 and 17 $\mu\text{gC L}^{-1}$, respectively, considering the signal-to-noise ratio.

For $\text{BiOCl}_{0.75}\text{I}_{0.25}$ photocatalytic degradation process under simulated solar light, the transformation products of *p*-HPA were detected by GC-MS (7890A/5975C, Agilent, USA). Products were extracted from aqueous solution with CH_2Cl_2 by solid-phase extraction (SPE). The GC-MS was equipped with an HP-5MS polysiloxane polymer column ($30\text{ m} \times 0.25\text{ mm} \times 0.25\text{ }\mu\text{m}$) with helium as the carrier gas at a flow rate of 1.0 mL min^{-1} . Column temperature was programmed at $100\text{ }^\circ\text{C}$ (held for 2 min), increasing at a rate of $15\text{ }^\circ\text{C/min}$ until reaching $300\text{ }^\circ\text{C}$. The injector and interface temperature were both set at $280\text{ }^\circ\text{C}$. An electron impact (EI) ionization is used for MS measurement in full scan mode ($m/z = 50\text{--}600$) and the MS source settings were as follows: ionization voltage: 70 eV, electron multiplier voltage: 1 kV, source temperature: $230\text{ }^\circ\text{C}$, quadruple temperature: $150\text{ }^\circ\text{C}$, vacuum degree: 6.0×10^{-6} Torr.

Total *p*-HPA ($[\textit{p}\text{-HPA}]_{\text{tot}}$) was determined as the sum of *p*-HPA presents in aqueous solution ($[\textit{p}\text{-HPA}]_{\text{aq}}$) and adsorbed on the catalyst surface which is determined after desorption experiments. Desorption of *p*-HPA is performed by adding 500 μL of sodium diphosphate solution (1 mM) to 500 μL of sample. Solution is filtered after 5 min to remove catalyst particles and analyzed by HPLC-UV.

$[\textit{p}\text{-HPA}]_0$ and $[\textit{p}\text{-HPA}]_t$ are the initial and remaining concentrations of *p*-HPA at time t , k_{app} is the pseudo-first-order apparent rate constant (s^{-1}). The initial degradation rate of *p*-HPA is $R_{\textit{p}\text{-HPA}} (\text{M s}^{-1}) = k_{\text{app}} \times [\textit{p}\text{-HPA}]_0$. Each value is the average of 3 consecutive detection and the reported error is $\pm 3\sigma$, obtained from the scattering of the experimental data.

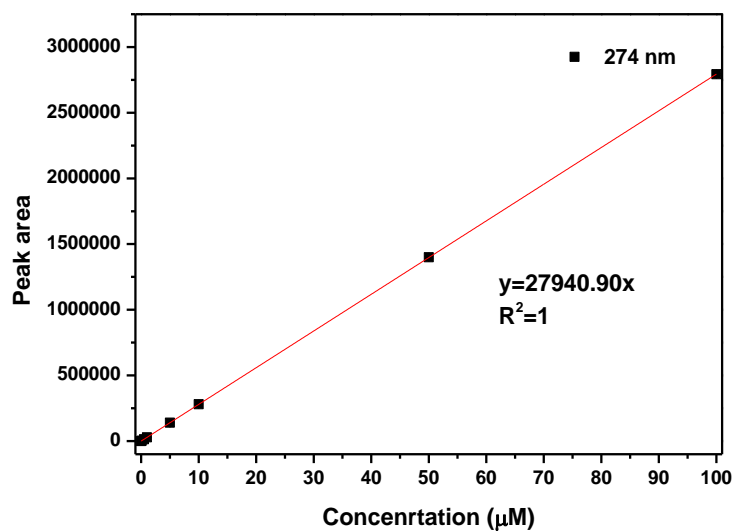


Fig. 3-3 The standard curve of *p*-HPA

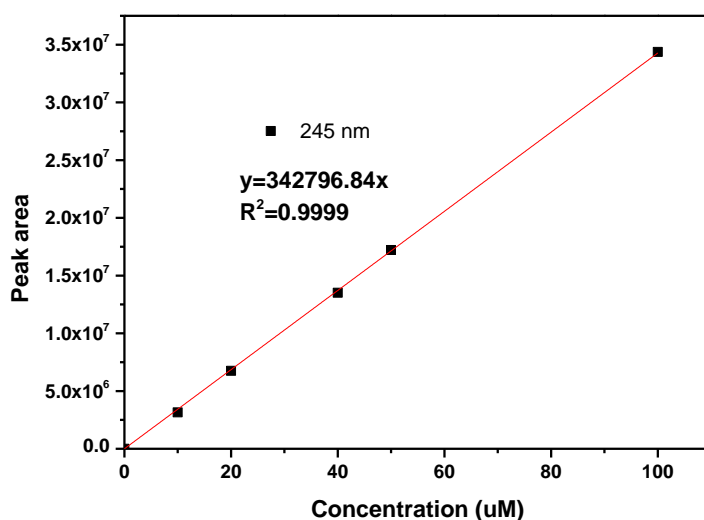


Fig. 3-4 The standard curve of BQ

3.5.2. ACTP detection

The concentration of the ACTP remaining in the aqueous solution was determined by high performance liquid chromatography (HPLC) (Alliance, Waters, 2695, USA) equipped with a photodiode array detector (Waters 2998). A Nucleodur 100-3 C18 reverse column (150×2.0 mm, 3.0 µm) was used to separate the compound in the solution. The flow rate was 0.15 mL min⁻¹ with a mobile phase mixture of methanol

and 0.1% H₃PO₄ contained water (30/70, v/v). The UV detection of ACTP was set at 244 nm wavelength, and the retention time was 4.9 min, and for calibration see **Fig.3-5**.

UV-vis spectra were recorded with a Cary 300 UV-visible spectrophotometer. pH values of the solutions were measured using a Cyberscan 510 pH meter.

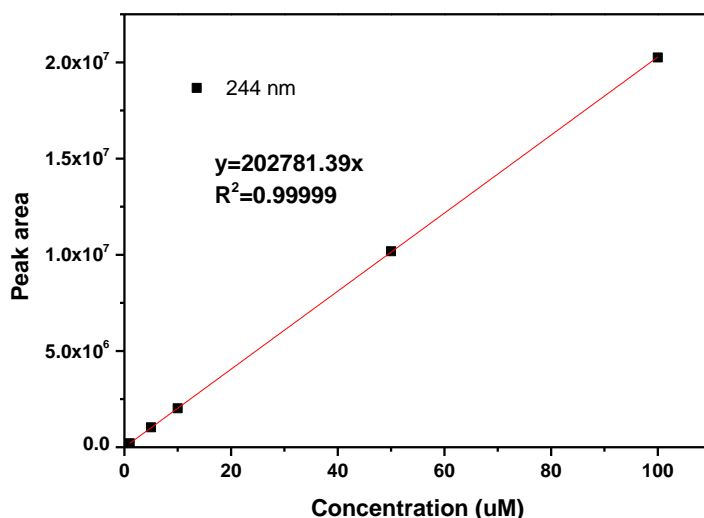


Fig. 3-5 The standard curve of ACTP

3.6. Laser Flash Photolysis

Experiments were carried out using the fourth harmonic ($\lambda_{\text{exc}} = 266 \text{ nm}$) of a Quanta Ray GCR 130-01 Nd:YAG laser system instrument and the energy was set at 45 mJ/pulse. Other conditions are kept the same to those described in previous articles^{67, 225}. Two different solution were prepared at pH 2.5 and 8.5 (milli-Q water adjusted with HClO₄ and NaOH). High concentrated stock solutions (*p*-HPA, ACTP, Na₂S₂O₈, H₂O₂ and SCN⁻) were mixed just before each experiment and diluted with Mili-Q water to obtain the desired mixtures and concentrations in a 3 mL quartz cuvette. For the detection of second order rate constant between *p*-HPA, ACTP and HO[•], SCN⁻ (0.1 mM), H₂O₂ (5.5 mM) and different concentrated *p*-HPA and ACTP were mixed in the quartz cell. The detection wavelength was set at 475 nm to detect maximum absorbance of SCN[•]. For second order rate constant between *p*-HPA and SO₄^{•-}, 10

mM $\text{Na}_2\text{S}_2\text{O}_8$ and different concentrated *p*-HPA solutions were set under pulse irradiation. Sulfate radical decay was followed at 450 nm corresponding to the maximum absorption of this species.

4. Bismuth catalyst mediated degradation of *p*-hydroxyphenylacetic acid (*p*-HPA): Photo-activation, interfacial mechanism and influence of some critical parameters

In the current study, hierarchical $\text{BiOCl}_{0.75}\text{I}_{0.25}$ composite materials have been synthesised in ethylene glycol (EG)-water (H_2O) mixed solvent by precipitation method at a relatively low temperature ($80\text{ }^\circ\text{C}$) and ambient pressure. The synthesised solids have been characterised in detail by XRD, FESEM, DRS, XPS and N_2 sorption. *p*-hydroxyphenylacetic acid (*p*-HPA), one of pharmaceutical and pesticides intermediates widely detected in olive oil extraction and wine distillery processes was chosen as a model pollutant. In this paper, $\text{BiOCl}_{0.75}\text{I}_{0.25}$ was used to remove *p*-HPA in solution under simulated solar light. Particular attention was paid to the interfacial mechanisms and role of adsorption on the photo-induced *p*-HPA degradation in the presence of catalyst. Moreover, the effect of solution pH and dissolved oxygen were elucidated using chemical competition approach.

4.1. Characterization of $\text{BiOCl}_{0.75}\text{I}_{0.25}$ composite catalyst

4.1.1. Phase structure

Fig.4-1 shows the XRD patterns of the as-prepared $\text{BiOCl}_{0.75}\text{I}_{0.25}$ samples synthesized in EG– H_2O media. All the samples can be indexed to a tetragonal phase BiOCl (JCPDS card NO. 06-0249), diffraction peaks of BiOI can be found hardly because of its relatively low content, and no other impurities can be observed. It can be deduced that solid solution has been formed in this composite catalyst because the similar diffraction peaks between BiOCl and BiOI , and it's not just a mixture between these two crystals.^{159, 226}

4.1.2. Morphology

The FESEM images of $\text{BiOCl}_{0.75}\text{I}_{0.25}$ made in EG- H_2O solvent with different magnifications are shown in **Fig. 4-2**. It can be seen that all the samples exhibited 3D flower-like hierarchical structures consisting of numerous nanosheets. The morphology $\text{BiOCl}_{0.75}\text{I}_{0.25}$ displayed irregular globular hierarchical structures of about 0.5 μm in size, and the nanospheres had a wide distribution. Compared with the same BiOX catalyst synthesized in water in previous literatures²²⁷, by the precipitation method, smaller particle size solids were formed in this study just by changing the reaction solvent to EG- H_2O . It is generally accepted that controlling the size of materials could induce the emergence of new physical and chemical properties. Small particle sizes lead to large surface area and high surface-to-volume ratios, increasing the adsorption of micro pollutants in water and supplying more active sites.

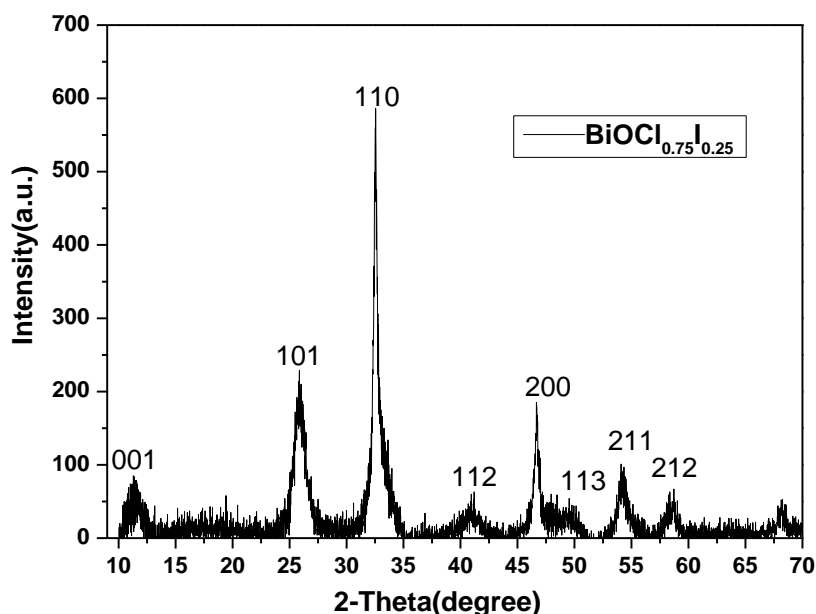


Fig.4-1 XRD patterns of $\text{BiOCl}_{0.75}\text{I}_{0.25}$ samples synthesized in EG- H_2O media

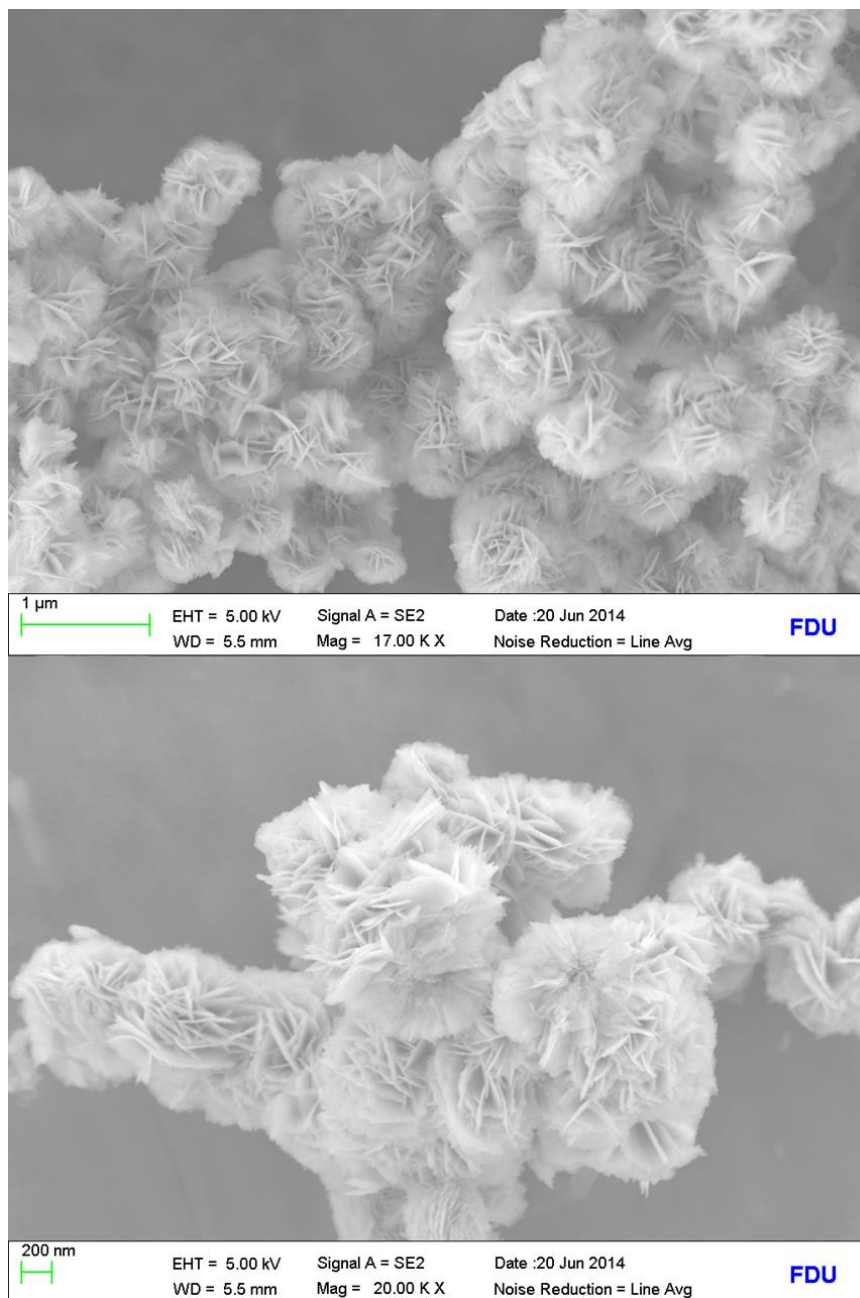


Fig.4-2 FESEM images of $\text{BiOCl}_{0.75}\text{I}_{0.25}$ samples with different magnifications

4.1.3. XPS

To further investigate the surface chemical compositions of $\text{BiOCl}_{0.75}\text{I}_{0.25}$ samples, XPS studies are conducted, and the spectra are illustrated in **Fig. 4-3**. As shown in **Fig. 4-3A**, $\text{BiOCl}_{0.75}\text{I}_{0.25}$ sample is composed of C, Bi, O, Cl and I peaks. Their corresponding high-resolution XPS spectra are further displayed in **Figs. 1B to 1F**, respectively. **Fig 4-3B** displayed the carbon peak fixed at 284.6 eV and 281.39 eV,

which can be attributed to the adventitious carbon on the surface of sample from solvent and XPS instrument^{156, 159}. **Fig 4-3C** shows that two strong peaks with binding energies of 164.42 eV and 159.11 eV corresponded to the Bi 4f_{5/2} and Bi 4f_{7/2}, indicating that the main chemical state of Bi element is trivalent²²⁸. The O 1s spectrum is shown in **Fig. 4-3D**, which can be fitted by three peaks at binding energies of 530.61, 531.85 and 532.83 eV, respectively. The peak at 530.61 eV is characteristic of Bi-O binding energy, and the left two peaks with higher binding energies can be assigned to adsorbed H₂O (or surface hydroxyl groups) on the surface of sample¹⁹³. Cl 2p_{3/2} and Cl 2p_{1/2} peaks at 197.95 and 199.6 eV binding energies, indicate that the valence state of chlorine element is -1 in the sample (**Fig 4-3E**)¹⁸³. As shown in **Fig 4-3F**, the iodine 3d peaks are divided into two peaks at around 630.63 and 619.21 eV, corresponding to I 3d_{3/2} and I 3d_{5/2}, indicating that the valence state of iodine was -1¹⁸³. Finally, we can argue that BiOCl_{0.75}I_{0.25} sample was well constructed with correct chemical composition and valence state.

4.1.4. Optical properties

The optical properties of BiOCl_{0.75}I_{0.25} catalyst were measured by UV-vis DRS, as shown in **Fig.4-4**, which were important factors in determining the photocatalytic performance of semiconductors. It can be seen that the absorbance edge of BiOCl_{0.75}I_{0.25} were located at about 550 nm, the addition of iodine prolonged the adsorption to visible light region. The band-gap is also one of the important factors in photocatalysis processes. For a crystalline semiconductor, the optical absorption near the band edge follows the equation (**Eq.4-1**):^{143, 148, 227}

$$\alpha h\nu = A(h\nu - E_g)^{n/2} \quad (\text{R4-1})$$

where α , ν , E_g and A are absorption coefficient, light frequency, band gap energy, and a constant, respectively. Among them, n is determined by the type of optical transition of a semiconductor ($n = 1$ for direct transition and $n = 4$ for indirect transition), and for BiOCl and BiOI, $n = 4$. Therefore, the E_g of different BiOCl_{0.75}I_{0.25} samples can be calculated from a plot of $(\alpha h\nu)^{1/2}$ versus $(h\nu)$, as shown in **Fig.4-4b**, and the band-gap

was 2.12 eV.

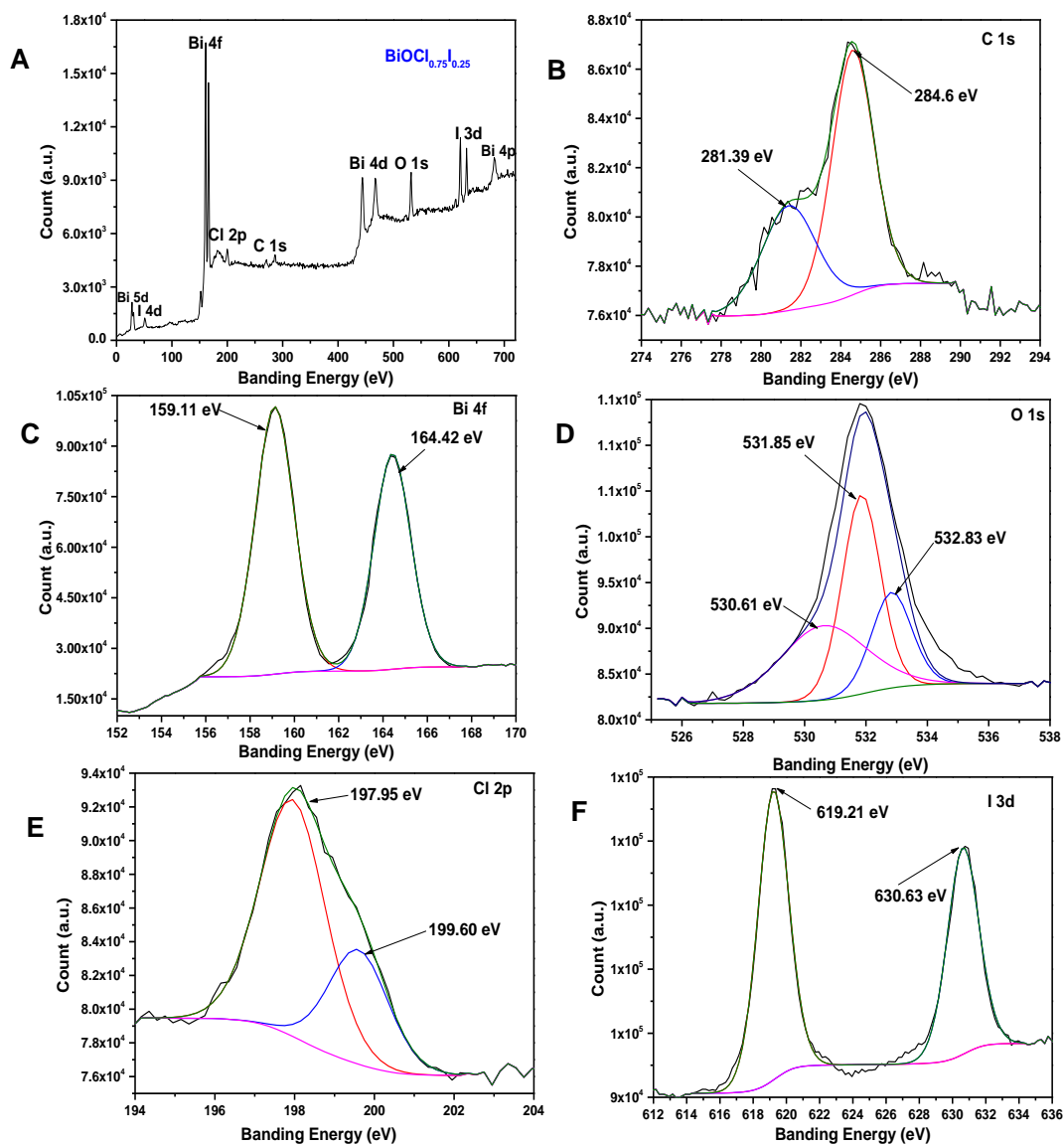


Fig.4-3 XPS spectra of $\text{BiOCl}_{0.75}\text{I}_{0.25}$ sample: (A) survey spectra, (B) C 1s, (C) Bi 4f, (D) O 1s, (E) Cl 2p and (F) I 3d.

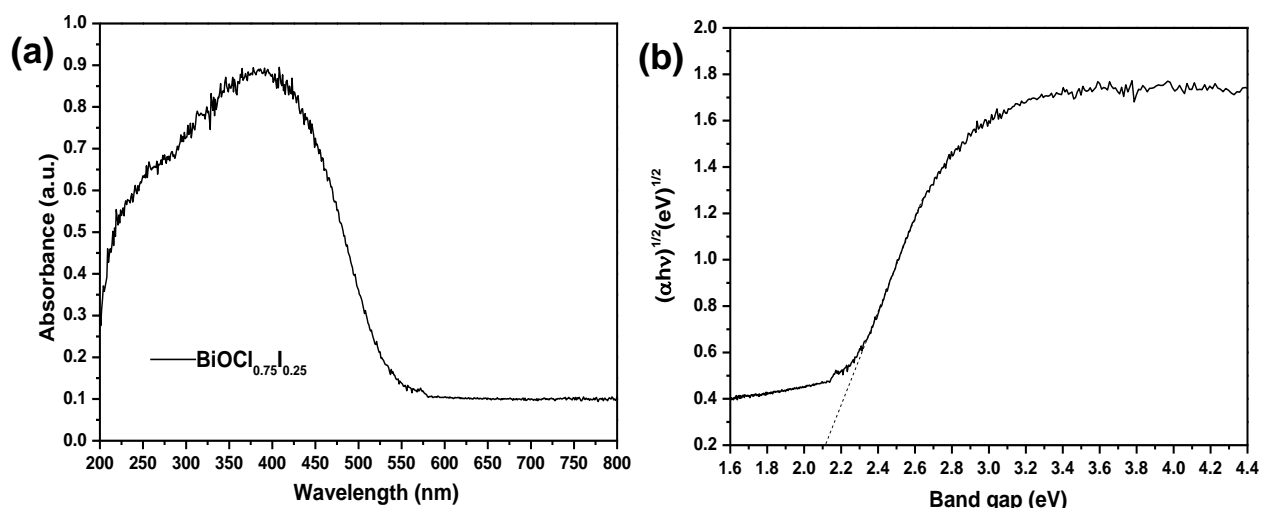


Fig. 4-4. (a) UV-vis DRS of the as-prepared BiOCl_{0.75}I_{0.25} sample, (b) the band gaps (E_g) of BiOCl_{0.75}I_{0.25} samples.

Physicochemical properties of BiOCl_{0.75}I_{0.25} catalyst are summarized in **Table 4-1**. The catalyst was synthesized through a precipitation method in ambient pressure in EG-H₂O mixed solvent²²⁶, BiOCl_{0.75}I_{0.25} crystals showed flower-like morphologies. Compared with BiOX catalyst researched before, BiOCl_{0.75}I_{0.25} possessed greater surface area and total pore volume determined by N₂ sorption^{159, 229}, facilitating the adsorption of *p*-HPA molecules on the surface and supplying abundant active sites for the oxidation ability. Introduction of iodine to BiOCl crystalline lattices induces the formation of heterojunction, and decreases the recombination rate of hole-electron pairs. Different to BiOCl alone, the band-gap of BiOCl_{0.75}I_{0.25} was adjusted to 2.12 eV, which is suitable for the utilization of simulated solar light ($\lambda > 300$ nm).

Table 4-1 physicochemical parameters of BiOCl_{0.75}I_{0.25} catalyst

Parameters	BET surface area (m ² g ⁻¹)	Average pore diameter (nm)	Total pore density (cm ³ g ⁻¹)	Morphology	Band-gap (eV)
	34.93	16.99	0.1483	Flower-like	2.12

4.2. Optical properties of *p*-HPA and blank experiment

The UV-vis spectra of *p*-HPA (500 μM) at different pH conditions are shown in **Fig.4-5**, in which can be seen that *p*-HPA has a maximum absorb at 274 nm. When pH was lower than 9, the absorb edge located at 300 nm, indicating that it can't absorb visible light. While, when pH of the solution was changed to 10.4 and 11.1, it showed an obvious red shift, prolonging the absorb edge to longer wavelength. From the literature, *p*-HPA has two pKa, one is 4.5, coming from carboxyl, and the other one is 10.5, from hydroxyl. **Fig.4-6** shown the direct photolysis of *p*-HPA for 24 hours at pH 3 and pH 9.4. It can be seen that it was very stable at pH 9.4 and slight degradation at pH 3. While at the first three hours, there was negligible degradation due to the negligible absorption of *p*-HPA solution.

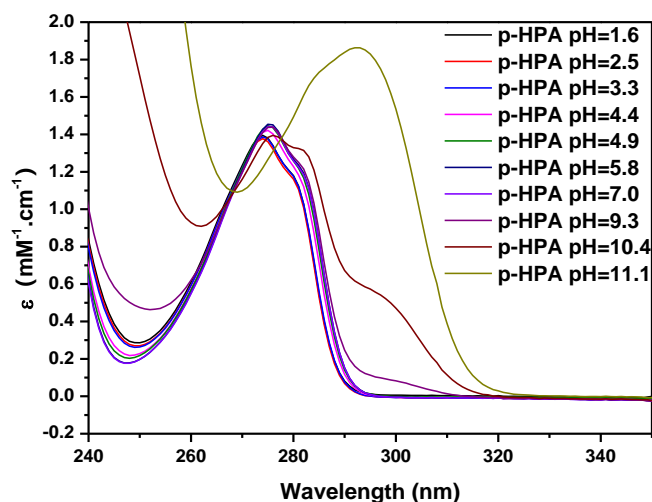


Fig.4-5 The UV-vis spectra of *p*-HPA (500 μM) at different pH conditions

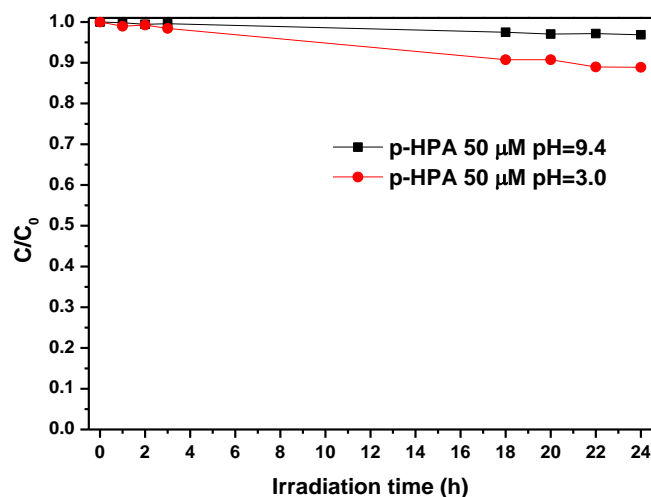


Fig.4-6 The direct photolysis degradation of *p*-HPA

4.3. pH effects on *p*-HPA adsorption and photocatalytic degradation

p-HPA adsorption on the surface of catalyst and photocatalytic degradation in aqueous solution are investigated at different pH values (**Fig.4-7**). The adsorption of *p*-HPA is strongly related to the molecular form of *p*-HPA ($pK_{a1}=4.5$ and $pK_{a2}=10.5$) and the surface zeta potential of $\text{BiOCl}_{0.75}\text{I}_{0.25}$ catalyst²³⁰. Moreover, the zeta potential of $\text{BiOCl}_{0.75}\text{I}_{0.25}$ is tested as function of pH, as shown in **Fig.4-8**. It can be seen that the point of zero charge of $\text{BiOCl}_{0.75}\text{I}_{0.25}$ is located at pH 1.6, meaning that within our experimental pH range, the zeta potential of $\text{BiOCl}_{0.75}\text{I}_{0.25}$ is always negative. In previous reports, K. Li et al.²³¹ and G. Li et al.⁸⁷ obtained similar results. This means that in solutions, electrostatic attraction occurred between the positively charged *p*-HPA and negatively charged $\text{BiOCl}_{0.75}\text{I}_{0.25}$, inducing a strong adsorption of *p*-HPA on the surface of catalyst²³². Similar trend is observed for Rhodamine B, which presents one carboxyl group^{157, 232}. **Table 4-2** summarizes the pseudo-first order decay of *p*-HPA at different pH as well as zeta potential of $\text{BiOCl}_{0.75}\text{I}_{0.25}$. At pH 3.0, *p*-HPA is under molecular form, and zeta potential of $\text{BiOCl}_{0.75}\text{I}_{0.25}$ was -8 mV. In fact, solution pH decrease and presence of H^+ compete with *p*-HPA molecules to the adsorption onto the negatively charged catalyst surface. At natural pH (4.5), *p*-HPA is 50% under molecular and anionic form, and adsorption is not modified by the

presence of other external ions. The zeta potential of $\text{BiOCl}_{0.75}\text{I}_{0.25}$ at pH 4.5 is more negative compared to the value at pH 3.0 and adsorption is higher (~45 %). When the pH increases to 7.5 and 9.5, *p*-HPA is under anionic form, and zeta potential of $\text{BiOCl}_{0.75}\text{I}_{0.25}$ is more negative with value lower than -38 mV. At these two pH values, the more negative surface charge would cause electrostatic repulsion and thus a decrease of *p*-HPA adsorption is observed. As reported in **Fig. 4-7**, the faster degradation observed at pH 3.0 under irradiation is consistent with previously reported works showing that under acidic solutions the photodegradation of pollutant in aqueous solution by BiOX catalyst is also faster^{172, 233}. Several factors could induce this result, one is the different form of main active species $\text{HO}_2^\bullet/\text{O}_2^{\bullet-}$ ($\text{pK}_a=4.88$), the other one is the form of *p*-HPA (pK_a 4.5) present in solution, both are tightly related to the pH. Zeta-potential of $\text{BiOCl}_{0.75}\text{I}_{0.25}$ was more negative with pH increased, so less photo-induced electrons can transferred to the surface of the catalyst. While, as discussed above, electrons were crucial to form $\text{HO}_2^\bullet/\text{O}_2^{\bullet-}$, which were main active species involved in the degradation processes. So, combined with our previous studies, conclusion we can argue that *p*-HPA has higher reactivity with the radicals HO_2^\bullet under its molecular form.

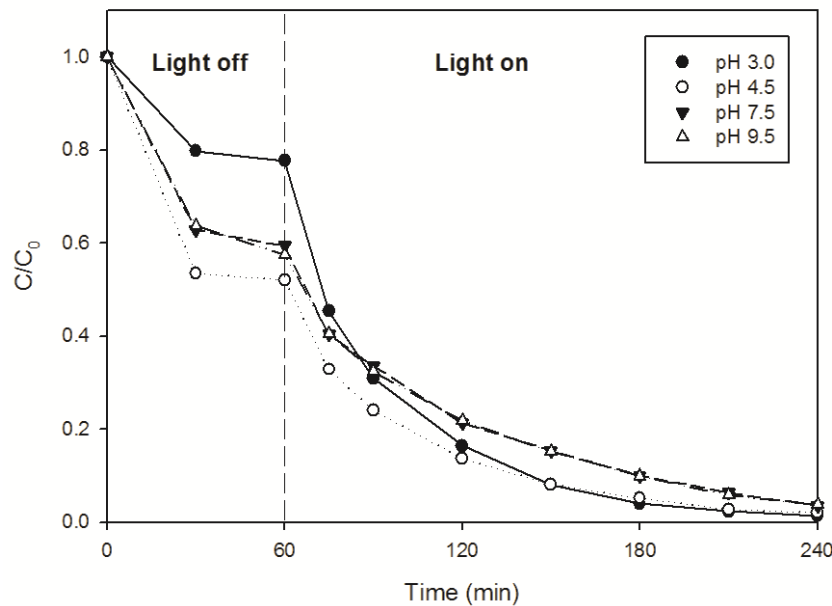


Fig. 4-7: Time evolution of *p*-HPA concentration under dark and light experiments at

different pH. Conditions were: [*p*-HPA] = 50 μM, [BiOCl_{0.75}I_{0.25}] = 0.3 g L⁻¹.

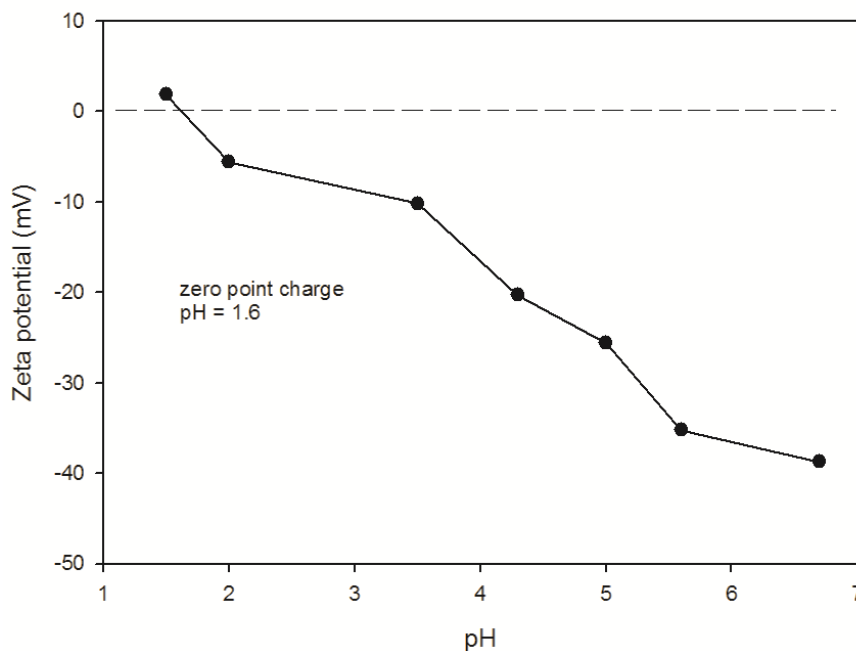


Fig.4-8 Zeta-Potential of BiOCl_{0.75}I_{0.25} catalyst determined at different pH

Table 4-2 Zeta potential of BiOCl_{0.75}I_{0.25} catalyst, *p*-HPA molecule form and pseudo first-order reaction constant under different pH

pH	Zeta potential	<i>p</i> -HPA	Pseudo first-order reaction constant (min ⁻¹)
3.0	≈ - 8 mV	molecular form	2.24 × 10 ⁻²
4.5 (natural pH)	≈ - 21 mV	50/50 molecular and anionic forms	1.80 × 10 ⁻²
7.5	< - 38 mV	anionic form	1.47 × 10 ⁻²
9.5	< - 38 mV	anionic form	1.47 × 10 ⁻²

4.4. Reactive species generation

Reactive species generated under irradiation of BiOCl_{0.75}I_{0.25} catalyst are determined using competition kinetic approach with specific scavengers in solution. Isoproponal (IPA), potassium iodide (KI) and benzoquinone (BQ) are taken as HO[•]

$(k_{IPA,HO^\bullet} = 1.9 \times 10^9 \text{ M}^{-1} \text{ s}^{-1})^{234}$, hole (h^+)²³⁵ and $HO_2^\bullet/O_2^{\bullet-}$ ($k_{BQ,O_2^{\bullet-}} = 9.0 \times 10^8 \text{ M}^{-1} \text{ s}^{-1}$)²³⁶ scavengers respectively. Addition of 1 mM of IPA using 0.3 g L^{-1} of catalyst does not modify the degradation rate of *p*-HPA under irradiation at pH 3.0 (**Fig.4-9**) indicating that HO^\bullet is not generated during irradiation of $BiOCl_{0.75}I_{0.25}$ catalyst. The effect of KI addition is investigated at pH 4.5 due to the anion-exchange with Cl^- and consequent modification of catalyst occurring at pH 3.0²³⁷. The presence of 1 mM of KI (**Fig.4-10**) strongly inhibits the adsorption of *p*-HPA due to the electrolyte changed surface charge of $BiOCl_{0.75}I_{0.25}$ catalyst. As a matter of fact, if we compare the concentration of remaining *p*-HPA in the solution in the presence and absence of KI (85% and 58%, respectively, as shown in **Fig 4-10**), then we can argue that the difference (approximately 27%) corresponds to the *p*-HPA adsorbed on the catalyst surface after 60 min in the dark. Under irradiation, a similar value for the pseudo first order kinetic constant of *p*-HPA degradation (k_{app}) is determined without and with KI (respectively 0.020 and 0.019 min^{-1}), indicating that valance band holes are not the main active species responsible for *p*-HPA removal. When 1 mM of BQ ($HO_2^\bullet/O_2^{\bullet-}$ scavenger) was added in solution, *p*-HPA adsorption (first 60 min) is not modified and no degradation is observed under irradiation (**Fig.4-11**). This experiment indicates that generated $HO_2^\bullet/O_2^{\bullet-}$ ($pK_a = 4.88$) under catalyst irradiation, drive the *p*-HPA degradation in agreement of previously reported works²²⁶. To further investigate the degradation mechanism and catalyst surface implication, the concentration of BQ is followed during adsorption and photo-degradation steps (**Fig.4-12**). Despite no adsorption observed for the first 60 min in the dark, BQ disappeared under irradiation indicating the formation of $HO_2^\bullet/O_2^{\bullet-}$ species in solution. Adsorption experiments were always in the dark. For the photocatalytic degradation experiments, first 60 min were in the dark, then under irradiation.

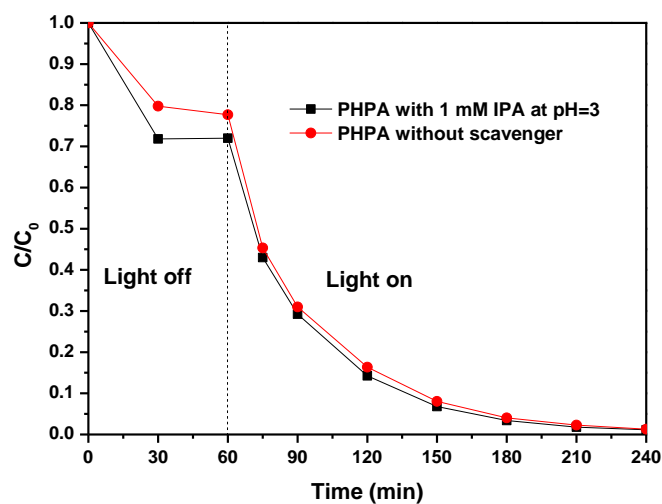


Fig.4-9 *p*-HPA degradation with and without IPA. Conditions: [*p*-HPA] = 50 μM, [BiOCl_{0.75}I_{0.25}] = 0.3 g L⁻¹, [IPA] = 1 mM and pH = 3.0.

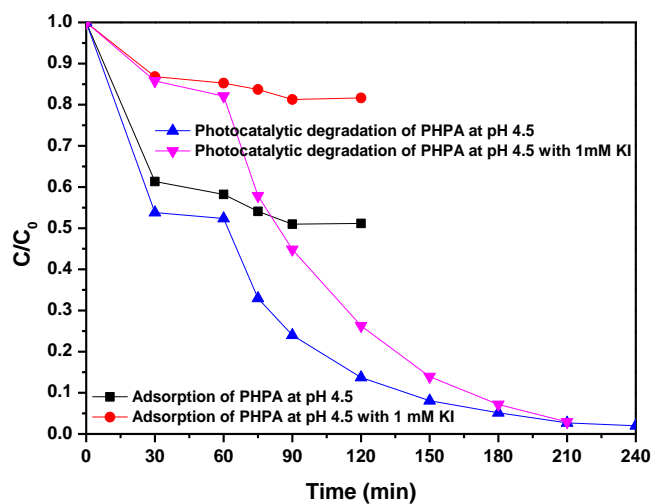


Fig.4-10 Photocatalytic and adsorption experiments of *p*-HPA degradation with and without KI. Conditions: [*p*-HPA] = 50 μM, [BiOCl_{0.75}I_{0.25}] = 0.3 g L⁻¹, [KI] = 1 mM and pH = 4.5.

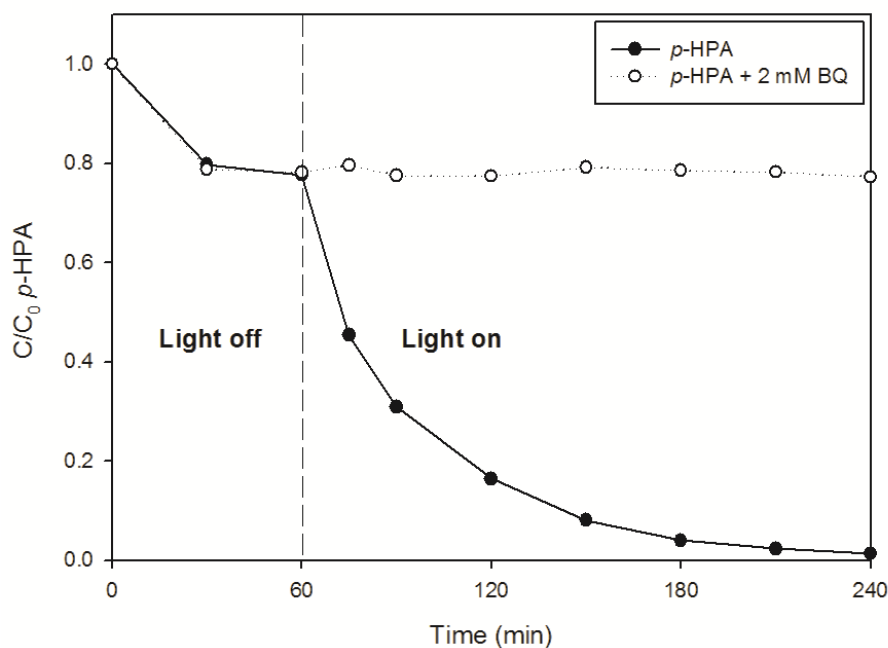


Fig.4-11: *p*-HPA concentration decrease with (○) and without (●) BQ addition. Adsorption experiments were performed in the dark. Conditions: [*p*-HPA] = 50 μM, [BiOCl_{0.75}I_{0.25}] = 0.3 g L⁻¹, [BQ] = 2 mM and pH = 3.0.

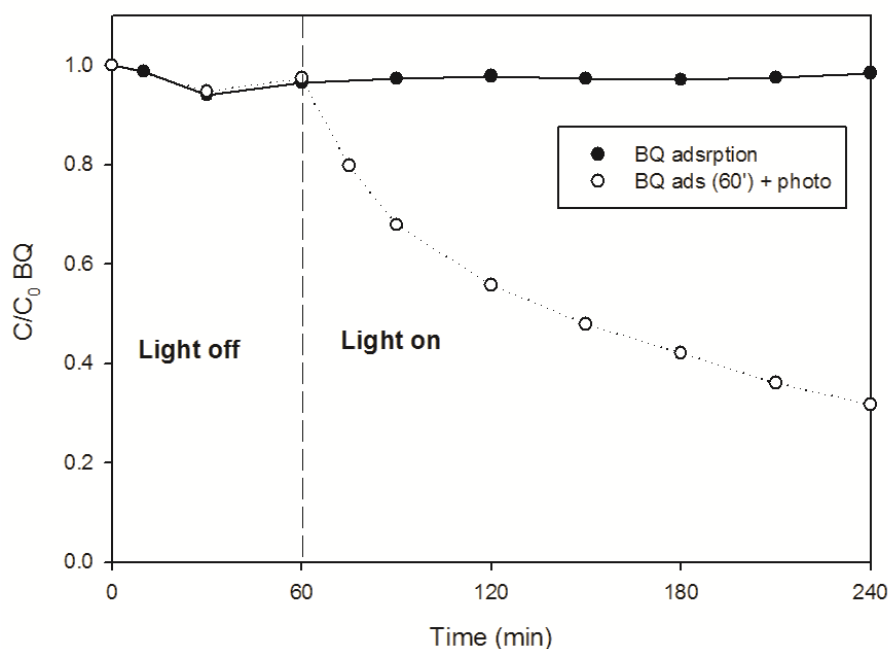


Fig.4-12 BQ concentration as function of time for adsorption (●) and photocatalytic (○) experiments after 60 min of adsorption on BiOCl_{0.75}I_{0.25}. Adsorption experiments were performed in the dark. Conditions: [*p*-HPA] = 50 μM, [BiOCl_{0.75}I_{0.25}] = 0.3 g L⁻¹,

[BQ] = 2 mM and pH = 3.0.

4.5. Interfacial mechanism under irradiation

In order to investigate the role of catalyst surface on the *p*-HPA degradation under irradiation, different experiments are performed in the presence of diphosphate ions which can compete with *p*-HPA for adsorption on the catalyst surface. In the presence of 2 mM sodium diphosphate in solution, quite no adsorption of *p*-HPA is observed in the dark (during 1 h) and degradation under irradiation was strongly inhibited (**Fig.4-13A**). This effect suggests that degradation of *p*-HPA occurs mainly on the catalyst surface. Experiments to assess the role of catalyst surface on the possible adsorption of *p*-HPA are reported in **Fig.4-13B** in which BQ (used as HO₂•/O₂•⁻ scavenger) was added in solution. BQ does not affect the *p*-HPA adsorption on the catalyst surface. In fact, for the first 30 min in the dark, about 15% of *p*-HPA are adsorbed on the catalyst surface with and without BQ. However, when light is turned on, quite no degradation can be observed in the presence of BQ. The inhibition of degradation suggests that adsorption on the catalyst surface and generation of reactive species such as HO₂•/O₂•⁻ which are formed by dissolved oxygen with the electron generated in the valence band, are the main processes responsible for the degradation of *p*-HPA in solution. At the same time, this figure indicated that the adsorbed *p*-HPA molecules are gradually degraded to some by-products. Possible implication of H₂PO₄⁻ on hydroxyl radical quenching is negligible under adopted experimental conditions. As a matter of fact, considering the low second-order rate constant between H₂PO₄⁻ and HO• in the solution ($\sim 2 \times 10^4 \text{ M}^{-1} \text{ s}^{-1}$)²³⁸ and concentration adopted for the desorption experiment (2 mM), we can find that this reaction is few orders of magnitude lower than the reaction between HO• and *p*-HPA in the solution.

4.6. Effects of dissolved oxygen

Effects of dissolved oxygen on *p*-HPA degradation during the photocatalytic degradation process is investigated by supplying proper gas (oxygen and nitrogen) to the reaction solutions before (for 20 min) and during experiments. Despite no significant differences in the adsorption of pollutants on the catalyst, the degradation of *p*-HPA is accelerated with the increasing of oxygen concentration (**Fig.4-14**). In fact, the pseudo-first order degradation constant is found to increase from $(2.4 \pm 0.5) \times 10^{-3} \text{ min}^{-1}$ in N_2 saturated to $(2.4 \pm 0.2) \times 10^{-2} \text{ min}^{-1}$ in O_2 saturated solutions. This trend indicates that oxygen plays a key role in the photocatalytic degradation process through the formation of $\text{HO}_2^\bullet/\text{O}_2^{\bullet-}$ species.

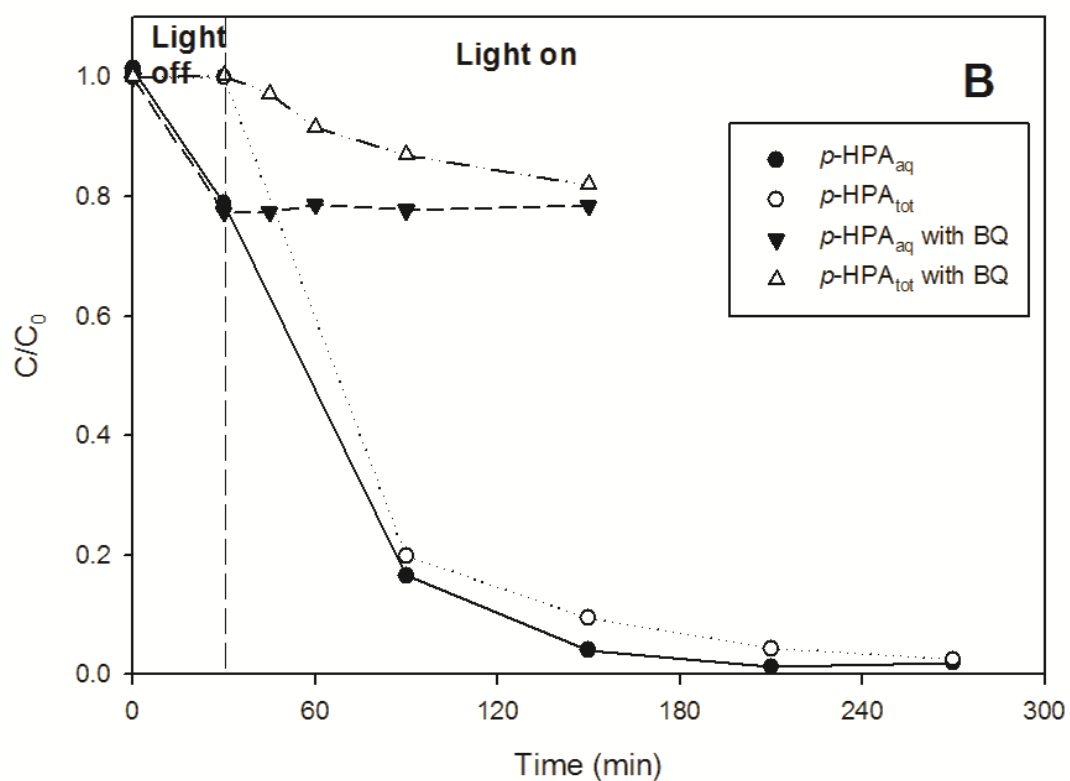
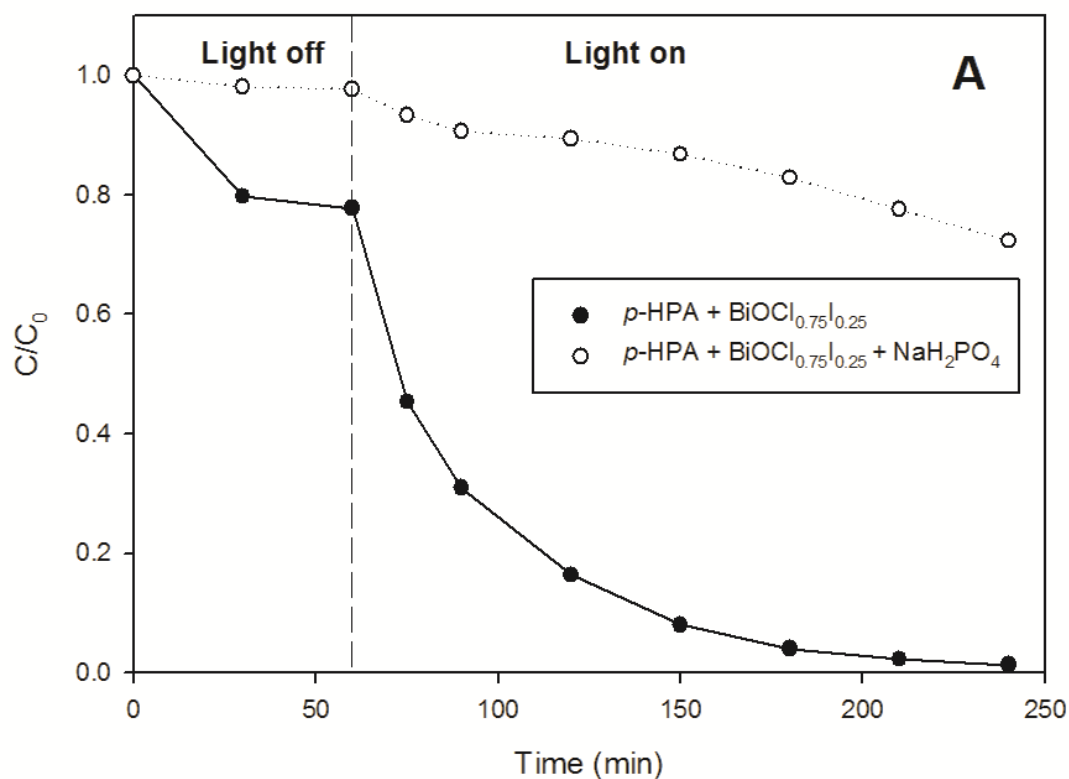


Figure 4-13: (A) Effect of NaH₂PO₄ addition on the *p*-HPA adsorption (first 60 min in the dark) and on *p*-HPA concentration in solution after photocatalytic experiment. (B)

p-HPA concentration in solution in the presence and absence of BQ before and after desorption experiments performed with NaH₂PO₄. Conditions: [*p*-HPA] = 50 μM, [BiOCl_{0.75}I_{0.25}] = 0.3 g L⁻¹, [BQ] = 1 mM, [NaH₂PO₄] = 2 mM and pH = 3.0. Total *p*-HPA concentration (*p*-HPA_{tot}) corresponds to the sum of *p*-HPA in solution (*p*-HPA_{aq}) + concentration of *p*-HPA adsorbed on the surface of the catalyst.

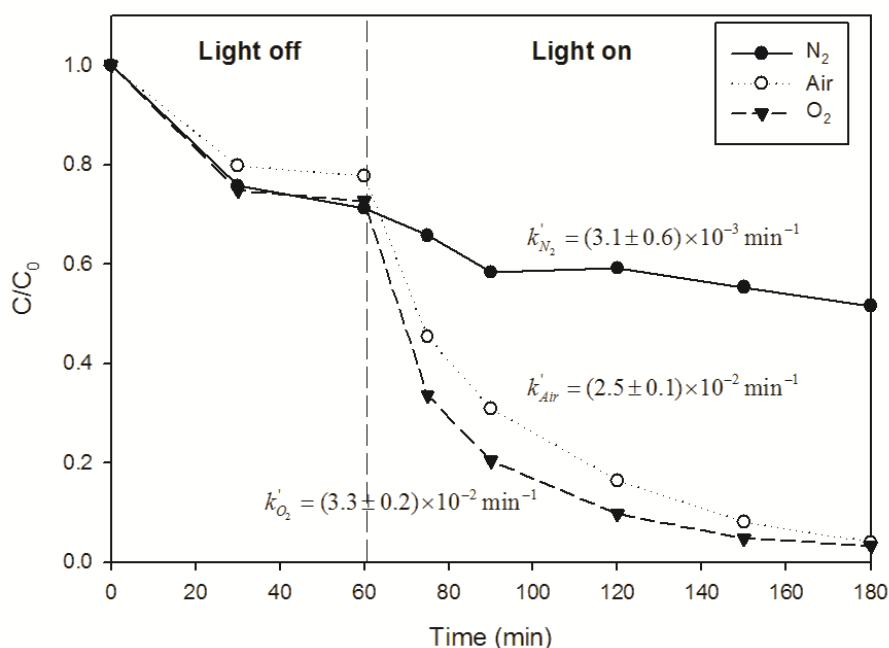
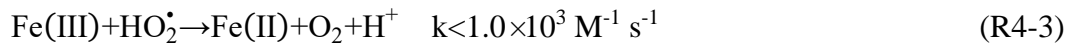


Figure 4-14: Effects of dissolved oxygen in the photocatalytic degradation of *p*-HPA by BiOCl_{0.75}I_{0.25}. Conditions were: [*p*-HPA] = 50 μM, [BiOCl_{0.75}I_{0.25}] = 0.3 g L⁻¹, pH = 3.0

4.7. Effects of Fe³⁺ and Na₂S₂O₈ addition

In traditional AOPs methods, Fe³⁺⁹⁸ and S₂O₈²⁻¹²³ were widely studied in the removal of organic pollutant through the generation of HO• and SO₄^{•-} with high oxidation abilities. While research on the combination effects of BiOX with Fe³⁺ and S₂O₈²⁻ was rare up to now. In this paper, the degradation of *p*-HPA by Fe³⁺ alone and combined with BiOCl_{0.75}I_{0.25} catalyst were investigated at pH 3.0 to avoid precipitation (Fig.4-15). Under irradiation, Fe³⁺ can produce HO• through a series of chain

reactions (**R4-2**), which would oxidize *p*-HPA fast in the first 15 min followed with a very slow degradation because of the consumption of Fe³⁺. When Fe³⁺ and BiOCl_{0.75}I_{0.25} both existed in the solution, the adsorption was similar, while the degradation rate of *p*-HPA unexpectedly decreased compared with catalyst alone. The pseudo first order constant supplied in **Table 4-3**. To explain this problem, reactions between Fe³⁺ and HO₂[•]/O₂^{•-} radicals must be taken into consideration (**R4-3 and R4-4**)¹²². Although Fe³⁺ donated the generation of HO[•], which possessed higher oxidation potential than HO₂[•]/O₂^{•-}, while in current conditions the quantum yield of HO[•] was limited and HO₂[•]/O₂^{•-} was consumed a lot to the transformation between Fe²⁺ and Fe³⁺, thus competing with *p*-HPA molecules and decreasing the removal efficiency.



To explore the possible synergic effects on the *p*-HPA removal using the Na₂S₂O₈/BiOCl_{0.75}I_{0.25}/UV system, UV/ Na₂S₂O₈ efficiency was firstly investigated, as shown in **Fig.4-16**. Approximately 30% of *p*-HPA can be removed in two hours when pH changed from 3.0 to 9.8, indicating activation of S₂O₈²⁻ by UV is not directly correlated to the pH. However, when BiOCl_{0.75}I_{0.25} catalyst was added, the degradation efficiency increased compared with catalyst alone (see **Table 4-3**), especially in neutral and alkaline solutions. This result was totally different to the pH effects in **Fig.4-7**. The increased degradation can be ascribed to the following reasons. Firstly, the direct photolysis of S₂O₈²⁻ generating SO₄^{•-} (E⁰=2.6-3.2 V) contributed to the oxidation of *p*-HPA. Secondly, S₂O₈²⁻ also can trap the photogenerated conduction band electron results in the formation of SO₄^{•-} (**R4-5**)²³⁹. For the third reason, G. Fang et al. has demonstrated the reaction of O₂^{•-} with persulfate anion to generate SO₄^{•-} proceeds according to Eq. (**R4-6**)²⁴⁰. This reaction can explain why the degradation efficiency was faster in neutral and alkaline solutions.

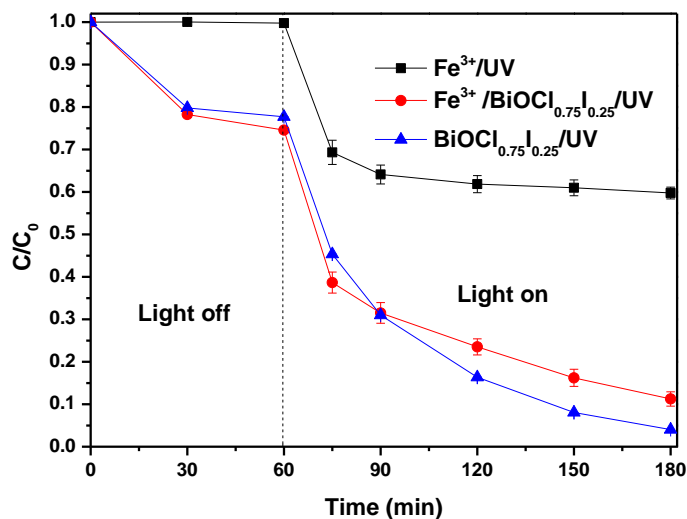
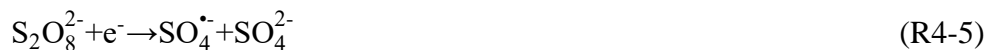


Fig.4-15 The degradation of *p*-HPA in the UV/Fe³⁺/ BiOCl_{0.75}I_{0.25} system, Conditions: [p-HPA]= 50 μM, [BiOCl_{0.75}I_{0.25}] = 0.3 g L⁻¹, pH = 3.0, [Fe³⁺]= 1mM

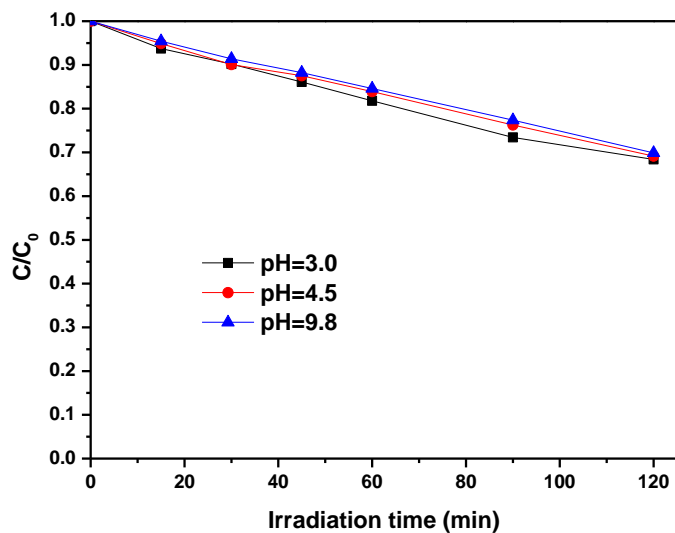


Fig.4-16 The degradation of *p*-HPA in the UV/ Na₂S₂O₈ (1 mM) system

Table 4-3 The pseudo first-order kinetic constant (k_{app} , min^{-1}) of *p*-HPA photocatalytic degradation with Fe^{3+} and $\text{Na}_2\text{S}_2\text{O}_8$ (1 mM) addition under different pH

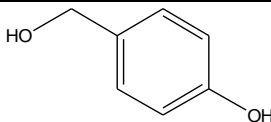
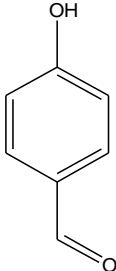
	pH = 3.0	pH = 4.5	pH = 9.8
With Fe^{3+}	0.01399	/	/
With $\text{Na}_2\text{S}_2\text{O}_8$	0.02448	0.02937	0.03053

4.8. TOC removal efficiency and main intermediate product

One of the most important parameters indicating the complete mineralization of organic pollutants is the total organic carbon (TOC) quantification. So, in addition to the degradation of *p*-HPA, mineralization is another important factor to estimate the removal ability of catalyst. During irradiation in the presence of $\text{BiOCl}_{0.75}\text{I}_{0.25}$ catalyst, the TOC change in solution and after desorption are shown in **Fig.4-17**. TOC trend in solution and after desorption of samples from the catalyst, suggested that *p*-HPA and its by-product can be adsorbed on the catalyst surface.

These results also suggest that $\text{BiOCl}_{0.75}\text{I}_{0.25}$ catalyst is able to decompose the by-products of *p*-HPA to CO_2 and H_2O . After 2 hours of irradiation TOC removal percentage is around 45% and do not significantly change after 3 more hours, suggesting that some by-product can be adsorbed on the surface of catalyst, occupying the adsorption site. However, after 5 hours of irradiation, complete degradation of *p*-HPA is observed. $\text{HO}_2^\bullet/\text{O}_2^{\bullet-}$ couple seems to be less reactive on the by-products than on *p*-HPA. *p*-HPA by-product generated during the photocatalytic process were detected by GC-MS after solvent extraction. 4-hydroxybenzyl alcohol and *p*-hydroxybenzaldehyde are identified as main intermediates (**Table 4-4**) on the basis of molecular mass and literature data^{50, 52}.

Table 4-4 The intermediate products of *p*-HPA and their proposed structures

Products	Tret (min) ^a	Main fragment ions	Structure
1	6.415	124; 95, 77	
2	6.540	122; 93, 65	

^a Retention time.

4.9. Conclusion

In this work, $\text{BiOCl}_{0.75}\text{I}_{0.25}$ has been prepared by precipitation method in EG- H_2O mixed solvent. The as-prepared samples showed 3D flower-like morphology, possessing great surface area $34.93 \text{ m}^2 \text{ g}^{-1}$ and narrow band-gap 2.12 eV. Furthermore, adsorption and photocatalytic degradation of *p*-HPA by $\text{BiOCl}_{0.75}\text{I}_{0.25}$ in water have been investigated. Interfacial mechanism experiments reveal that photocatalytic degradation of *p*-HPA occurred mainly on the catalyst surface. pH strongly affects the adsorption percentage and degradation rate through changing the surface charge of catalyst and molecular form of *p*-HPA. *p*-HPA showed the maximum adsorption at pH 4.5 (Natural pH) which can be ascribed to the electrostatic attraction occurred between the positively charged *p*-HPA and negatively charged $\text{BiOCl}_{0.75}\text{I}_{0.25}$. While, *p*-HPA exhibited the faster degradation rate at pH 3. Dissolved oxygen concentration is a key parameter necessary to generate $\text{HO}_2^\bullet/\text{O}_2^{\bullet-}$, the main active species responsible for the pollutant degradation, which was identified by quenching experiment. $\text{Na}_2\text{S}_2\text{O}_8$ showed synergistic effect with $\text{BiOCl}_{0.75}\text{I}_{0.25}$ under UV irradiation by supplying $\text{SO}_4^{\bullet-}$ radicals. $\text{BiOCl}_{0.75}\text{I}_{0.25}$ shows promising *p*-HPA removal abilities but some photo-generated by-products still adsorbed on the surface of catalyst, seems not degraded. This photocatalyst, generating mainly $\text{HO}_2^\bullet/\text{O}_2^{\bullet-}$, is

very promising and can have strong implication in the treatment of polluted media in which hydroxyl radical should be strongly scavenged by organic matter or inorganic constituents.

5. Comparison of hydroxyl and sulfate radical degradation efficiencies of *p*-HPA activated by Fe(III)-EDDS/UV : influence of critical parameters

The reaction between H₂O₂ and Fe(III)/Fe(II) is a well-known method for the generation of hydroxyl radicals (HO•), including Fenton (Fe(II)/H₂O₂)^{65, 72}, Fenton-like (Fe(III)/H₂O₂)⁹⁴ and photo-Fenton (UV/Fe(III)/H₂O₂) reactions^{66, 95-98}. However, in recent years, studies on sulfate radical (SO₄•⁻) have proved that this radical is outstanding in degrading recalcitrant organic pollutants ascribing to its similar oxidation-reduction potential ($E^0 = 2.6-3.2 \text{ V}$)⁶⁷, longer half-life time and more selective reactivity compared with HO•. From previous literatures, the generation of SO₄•⁻ usually derives from the activation of persulfate (PS) by heat⁷⁰, UV or transition metals^{69, 109, 110}. The generation of HO• and SO₄•⁻ based on iron source, mainly combined with UV irradiation, has played predominant roles in advanced oxidation processes. So the development of Fe(II)/Fe(III) organic complexes is essential to improve the removal efficiencies in higher pH solutions. Photo-production of HO• and SO₄•⁻ based on Fe(II)/Fe(III)-EDDS complexes has been widely studied in recent years, showing excellent efficiency in removing organic pollutants and heavy metals in water and soil near neutral pH.

Our laboratory has studied the physicochemical properties of the Fe(III)-EDDS complex. Fe(III) is complexed by EDDS with a ratio 1:1. Results showed that the use of Fe(III)-EDDS complexes leads to efficient oxidations whatever the sources of radical species (HO• or SO₄•⁻). However, the comparison between Fe(III)-EDDS/H₂O₂/UV and Fe(III)-EDDS/PS/UV systems under same conditions has never been studied before, including the effects of pH, Fe(III)-EDDS concentration, H₂O₂ and PS concentrations. The main goal of this study is to compare these two processes using *p*-HPA as a model pollutant. Kinetics degradation of *p*-HPA were investigated in detail with Fe(III)-EDDS/H₂O₂/UV and Fe(III)-EDDS/PS/UV systems. The aim of this study is to quantify the different

activation efficiency of H₂O₂ and PS by Fe(III)-EDDS under irradiation in the same experimental conditions and to correlate with the production of HO• and SO₄•⁻ radicals. Especially to reach this goal and understand well the different mechanisms.

5.1 Photochemistry of Fe(III)-EDDS

As it is known from previous research of our group the best stoichiometry between Fe(III) and EDDS in Fe(III)-EDDS complex is 1:1²¹⁷, the stock solution of Fe(III)-EDDS (5 mM) was prepared by mixing 10 mM EDDS solution with 10 mM Fe³⁺ solution together. It is observed that Fe(III)-EDDS complex in water solution is stable for at least 10 days when kept in 4 °C. The UV-visible spectrum of Fe(III)-EDDS (200 uM, pH 3.9) complex solution stayed at different days showed in **Fig.5-1**. It showed a particular absorb at about 240 nm.

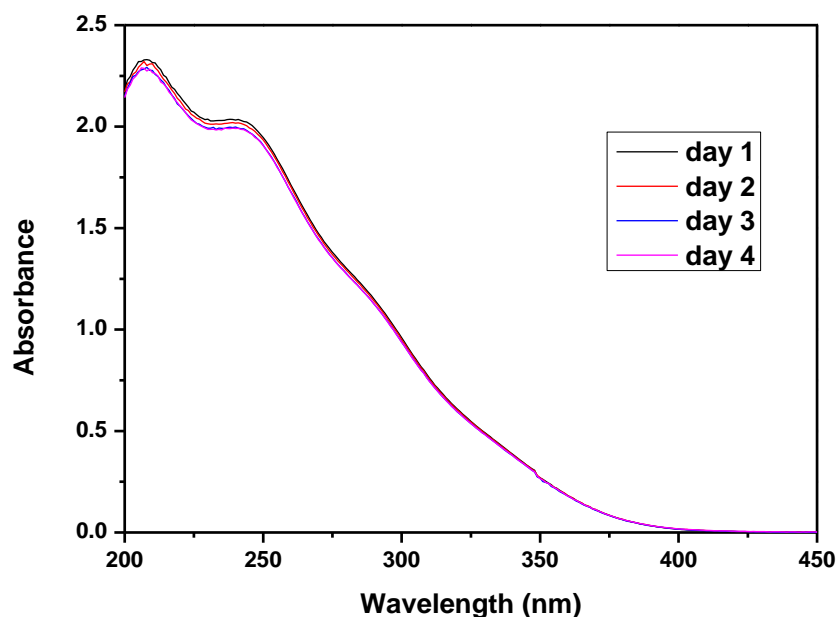


Fig.5-1. UV-Vis spectrum of Fe(III)-EDDS complex solution kept for different time

5.2 Evaluation of the second order rate constants

p-HPA has two pKa (4.5 and 10.5) but due to our experimental conditions, only pKa = 4.5 is taken into consideration in this study. In order to identify if the molecule

forms can affect the reaction constant with the different radicals, two pH's, pH 2.5 (molecular form) and pH 8.5 (anionic form), are adopted to determine the second order rate constant. Under 266 nm laser excitation of *p*-HPA alone, there is no detected transition species in the solution between 300-600 nm (Δ 20 nm). The determination of the second order rate constant between *p*-HPA and HO• ($k_{p\text{-HPA},\text{HO}\cdot}$) is determined by using chemical competition kinetics with thiocyanate anions (SCN⁻) and di-thyociante radical anions (SCN₂^{•-}) specie, as shown in equations R5-1-R5-4 and Scheme 5-1. $k_{p\text{-HPA},\text{HO}\cdot}$ is obtained by following the absorbance of SCN• at 475 nm with different concentration of *p*-HPA added. The absorbance decreases when *p*-HPA concentration increases because *p*-HPA compete with SCN⁻ for the reaction of HO•. The slope “a” can be obtained from the linear regression of Abs₀/Abs versus different *p*-HPA concentrations and thus the second order rate constant $k_{p\text{-HPA},\text{HO}\cdot}$ under two different pH's 2.5 and 8.5 can be evaluated (**Table 5-1**). Details concerning the second order rate constant determinations are reported in **Fig. 5-2**.

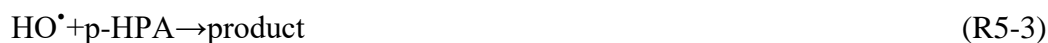


Table 5-1 Second order constant $k_{p\text{-HPA},\text{HO}\cdot}$ and $k_{p\text{-HPA},\text{SO}_4^{\cdot-}}$ at two different pH

	pH 2.5	pH 8.5
$k_{p\text{-HPA},\text{HO}\cdot} (\text{M}^{-1} \text{s}^{-1})$	$(2.2 \pm 0.12) \times 10^{10}$	$(7.27 \pm 0.30) \times 10^9$
$k_{p\text{-HPA},\text{SO}_4^{\cdot-}} (\text{M}^{-1} \text{s}^{-1})$	$(4.77 \pm 0.09) \times 10^9$	$(3.51 \pm 0.12) \times 10^9$

$$\frac{1}{Abs} = \frac{1}{Abs_0} \left(1 + \frac{k_{HO^\bullet, P}[P]}{k_{HO^\bullet, SCN^-}[SCN^-]} \right)$$

$$\frac{Abs_0}{Abs} = 1 + \frac{k_{HO^\bullet, P}[P]}{k_{HO^\bullet, SCN^-}[SCN^-]}$$

$$y = b + ax$$

$$y = \frac{Abs_0}{Abs}, \quad b = 1, \quad x = [P]$$

$$a = \frac{k_{HO^\bullet, P}}{k_{HO^\bullet, SCN^-}[SCN^-]} \Rightarrow k_{HO^\bullet, P} = a k_{HO^\bullet, SCN^-}[SCN^-]$$

Scheme 5-1: second order constant calculation process, where Abs is the absorbance at 475 nm with different concentrated *p*-HPA, Abs₀ is the absorbance in the absence of *p*-HPA. $k_{HO^\bullet, SCN^-} = 1.2 \times 10^{10} \text{ M}^{-1} \text{ s}^{-1}$ ²⁴¹. [P] is the concentration of *p*-HPA.

To obtain $k_{p\text{-HPA}\cdot\text{SO}_4^{\bullet-}}$, transient absorption spectra of $\text{SO}_4^{\bullet-}$ obtained are recorded after 266 nm laser excitation of $\text{S}_2\text{O}_8^{2-}$ in the absence or presence of *p*-HPA. Maximum absorption of $\text{SO}_4^{\bullet-}$ occurred at 450 nm, and the first-order decay constants of the radical were determined as it is described in our previous paper⁶⁷. At pH 2.5, a decrease of the transient species is observed with a pseudo-first order constant $k_{\text{SO}_4^{\bullet-}}: 4.29 \times 10^4 \text{ s}^{-1}$. After the addition of *p*-HPA ($3.33 \times 10^{-4} \text{ M}$), the transient decay increases to $1.58 \times 10^6 \text{ s}^{-1}$, indicating that $\text{SO}_4^{\bullet-}$ and *p*-HPA react with each other with high yield. The second order rate constant $k_{p\text{-HPA}\cdot\text{SO}_4^{\bullet-}}$ can be calculated using a linear regression of the pseudo-first order decay constant of $\text{SO}_4^{\bullet-}$ (k' , s^{-1}) versus the *p*-HPA concentration (**Fig. 5-2B**). The same method is applied at pH 8.5 and the results are gathered in **Table 5-1**. It is clear that pH can affect $k_{p\text{-HPA}, \text{HO}^\bullet}$ and $k_{p\text{-HPA}, \text{SO}_4^{\bullet-}}$, showing faster reaction activities in acidic solution (molecular form of *p*-HPA) than alkaline solution (anionic form of *p*-HPA). This effect is more pronounced with HO^\bullet , $k_{p\text{-HPA}, \text{HO}^\bullet}$ is 3 times higher at pH 2.5 than at pH 8.5, than with $\text{SO}_4^{\bullet-}$, $k_{p\text{-HPA}, \text{SO}_4^{\bullet-}}$ is only around 1.3 times higher at pH 2.5 than at 8.5.

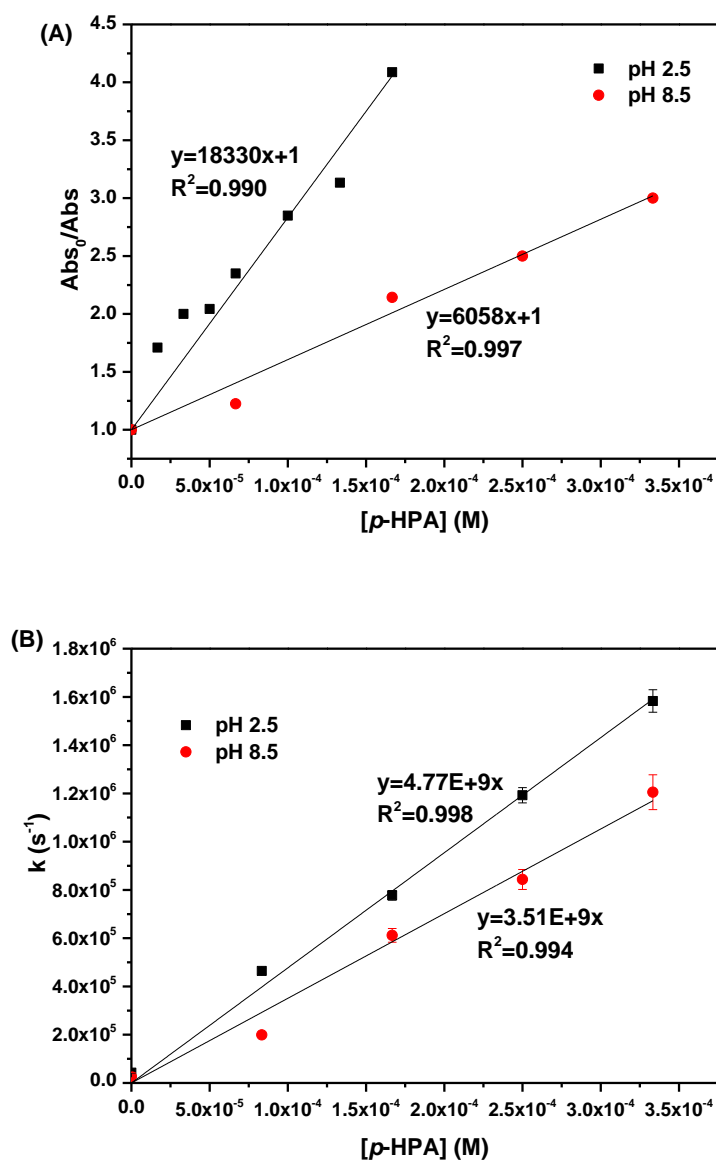
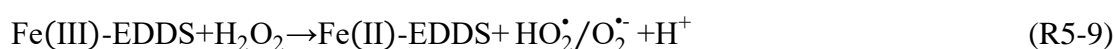
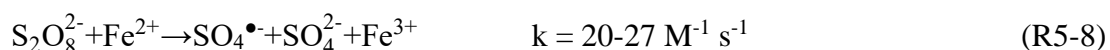
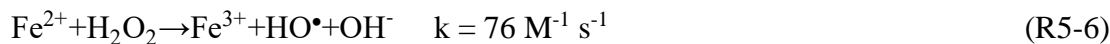


Figure 5-2: (A) Ratio of absorption of transient at 475 nm in the absence (Abs_0) and presence (Abs) of *p*-HPA used for determination of second order rate constant between hydroxyl radical and *p*-HPA. (B) Pseudo-first order rate constant of $SO_4^{\bullet-}$ decay as function of different concentrated *p*-HPA.

5.3 Effect of UV and Fe(III)-EDDS complex

In the dark, *p*-HPA is stable in aqueous solution even in the presence of Fe(III)-EDDS solution. Moreover, *p*-HPA is not degraded under UV, because it cannot

absorb the wavelengths longer than 300 nm, no photolysis process is observed in our experimental conditions. As a contrary, under UV irradiation used in this study, H₂O₂ and Na₂S₂O₈ can produce HO• (R5-1) and SO₄•⁻ (R5-5).



However, *p*-HPA has a relatively low degradation rate in the presence of H₂O₂ (1 mM) or Na₂S₂O₈ (1 mM) alone under UV irradiation, achieving 10% and 30% remove respectively, after 120 min of irradiation (**Fig. 5-3** and **5-4**). In fact, in our irradiation conditions (300 to 500 nm), the quantum yield of HO• formation is very low and so the kinetic of *p*-HPA degradation. In terms of pH effect, faster *p*-HPA degradation is observed at pH 3.0 or 4.5 than at pH 9.4 in agreement with the evaluated second order rate constants as a function of pH (**Table 5-1**).

Fig.5-5A shows the degradation of *p*-HPA with Fe(III)-EDDS (100 μM) at two different H₂O₂ concentrations (100 and 500 μM) with and without UV. The disappearance of *p*-HPA is much faster in Photo-Fenton (Fe(III)-EDDS/H₂O₂/UV) system than in Fenton-like process (R5-7, $k_{\text{Fe(III),H}_2\text{O}_2} = 0.02 \text{ M}^{-1} \text{ s}^{-1}$)¹¹¹. According to the Fenton reaction (R5-6), the production of HO• is correlated with the formation of Fe(II) (R5-9 and R5-10)^{96, 111} and so with the efficiency of pollutant oxidation. Under irradiation, UV increases and contributes a lot to the generation of Fe(II), inducing the fast decomposition of *p*-HPA in the first 10 min through the Fenton process (R5-6)^{95, 96}. At higher H₂O₂ concentration (500 μM) added into the solution, *p*-HPA can be removed completely in 60 min in Fenton-like process and in 10 min in photo-Fenton system. At lower concentration of H₂O₂ (100 μM) *p*-HPA is not removed completely of the solution with or without UV irradiation. These results indicate that H₂O₂

concentration is a crucial and a limiting parameter in the oxidation process.

For the experiments with $\text{Na}_2\text{S}_2\text{O}_8$, pH and the different concentrations are kept the same compared with systems using H_2O_2 . The different degradation kinetics are shown in **Fig.5-5B**. Although some previous papers have reported that Fe(III) can activate persulfate to produce $\text{SO}_4^{\bullet-}$ in the dark, it was not the case in our system. In fact, much higher concentration of Fe(III) species and persulfate seem needed to do this activation²⁰⁷. Under irradiation, Fe(III)-EDDS/ $\text{Na}_2\text{S}_2\text{O}_8$ system shows a good efficiency for *p*-HPA degradation but much lower compared to the system with H_2O_2 . Different reasons can explain the lower efficiency in the presence of $\text{Na}_2\text{S}_2\text{O}_8$. First of all, it is important to mention that the formation of Fe(II) *via* reaction R5-10 is one of the crucial step to active $\text{S}_2\text{O}_8^{2-}$ or H_2O_2 to produce oxidative species through reactions R5-6 and R5-8, which are identified and evaluated in terms of relative importance in the following part of this paper. The lower efficiency can be due to the fact that the second order rate constant of the activation of $\text{S}_2\text{O}_8^{2-}$ ($k_{\text{Na}_2\text{S}_2\text{O}_8 \cdot \text{Fe(II)}} = 20\text{-}27 \text{ M}^{-1} \text{ s}^{-1}$) is more than three times smaller than the one with H_2O_2 ($k_{\text{H}_2\text{O}_2 \cdot \text{Fe(II)}} = 76 \text{ M}^{-1} \text{ s}^{-1}$). In addition, the lower efficiency of $\text{Na}_2\text{S}_2\text{O}_8$ can be also due to the second order rate constants between *p*-HPA with HO^{\bullet} or $\text{SO}_4^{\bullet-}$, $k_{p\text{-HPA}, \text{HO}^{\bullet}}$ is four times higher than $k_{p\text{-HPA}, \text{SO}_4^{\bullet-}}$ in acidic solutions (**Table 5-1**). As a contrary, the photolysis of H_2O_2 and $\text{Na}_2\text{S}_2\text{O}_8$ were not responsible of this effect. Indeed, with the concentration and light irradiation used this process of photolysis is negligible and moreover is more efficient with $\text{Na}_2\text{S}_2\text{O}_8$ than H_2O_2 .

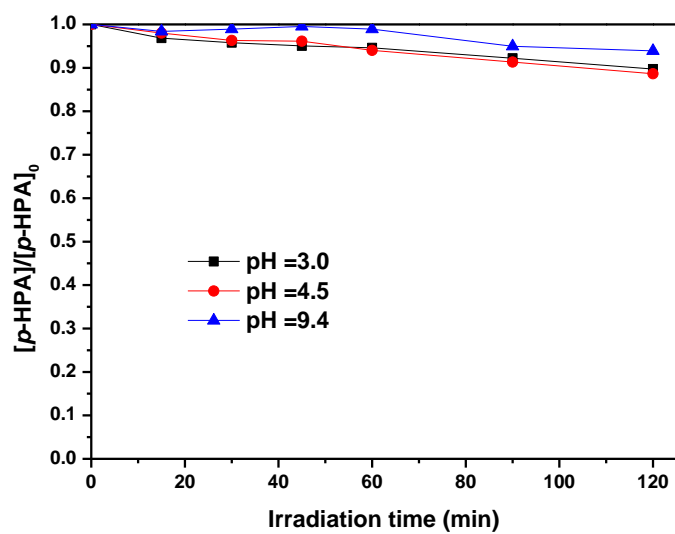


Fig.5-3 Degradation of *p*-HPA (50 μM) in the UV/ H_2O_2 (1 mM) system

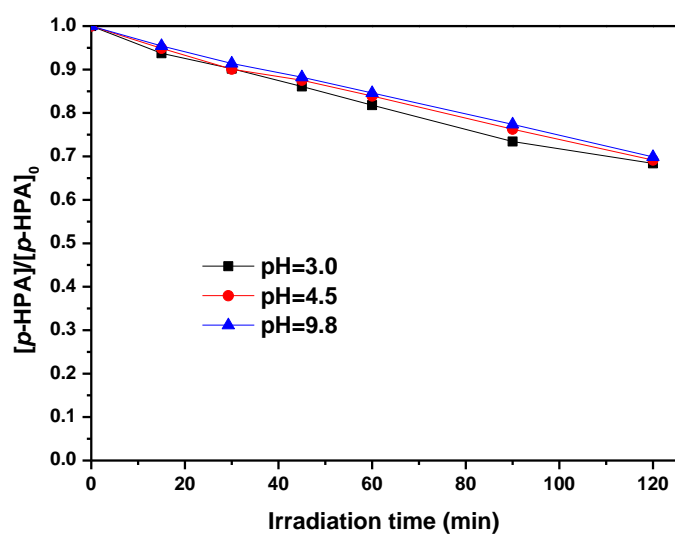


Fig.5-4 Degradation of *p*-HPA (50 μM) in the UV/ $\text{Na}_2\text{S}_2\text{O}_8$ (1 mM) system

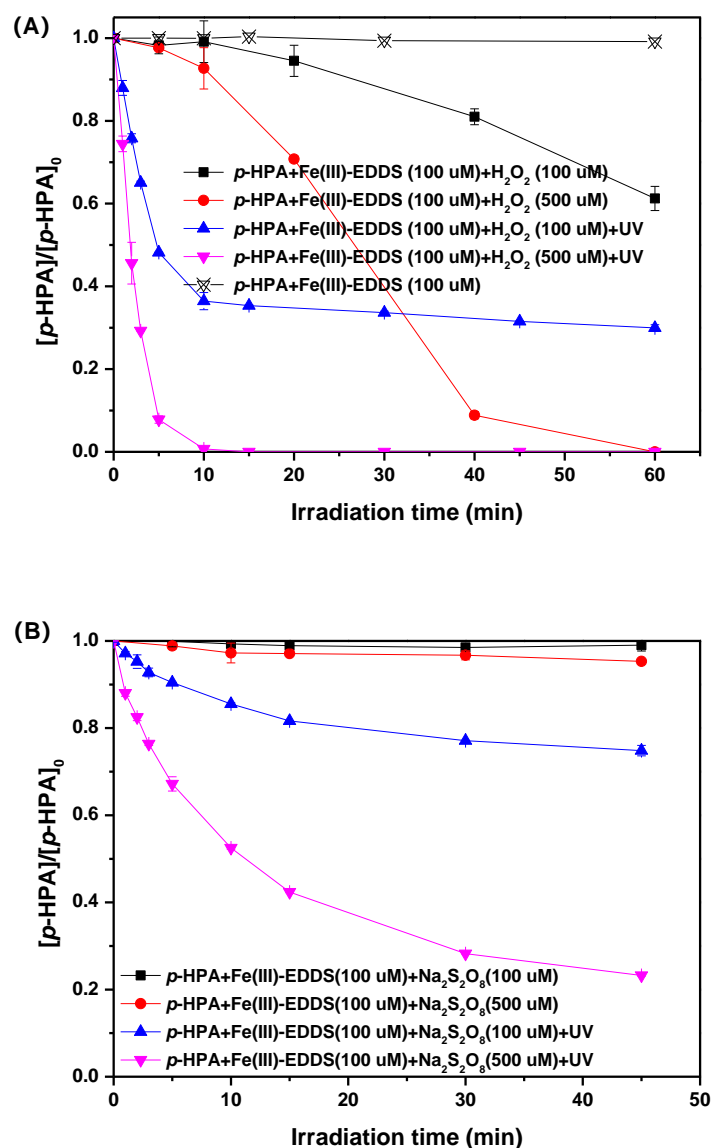


Fig.5-5 (A) The concentration change of *p*-HPA in the Fenton and photo-Fenton systems with different amount of H₂O₂ added, (B) The degradation of *p*-HPA with different Na₂S₂O₈ concentration with and without UV. $[p\text{-HPA}] = 50 \mu\text{M}$, $[\text{Fe(III)-EDDS}] = 100 \mu\text{M}$, pH = 3.9.

5.4 Effects of H₂O₂ and Na₂S₂O₈ concentrations

Initial degradation rate of *p*-HPA ($R_{p\text{-HPA}}$) is adopted to evaluate the degradation efficiency of the reaction process. $R_{p\text{-HPA}}$ is evaluated from the first 5 min of

irradiation, because during this period pH of the solution kept stable, and the degradation can be well fitted by pseudo first order kinetics. **Fig.5-6A** shows the initial degradation rate of *p*-HPA with different H₂O₂ concentrations in photo-Fenton process. R_{*p*-HPA} increases from 1.50×10⁻⁷ to 3.80×10⁻⁷ M s⁻¹ when H₂O₂ concentrations increases from 50 μM to 1 mM. The observed increase of *p*-HPA degradation when the concentration of H₂O₂ increased is not a surprise considering that H₂O₂ is one of the two compounds generating HO• in the Fenton process and as described in **Fig.5-5A**, H₂O₂ concentration was the limiting parameter. However, H₂O₂ is also a scavenger of HO• (k_{H₂O₂·HO•} = 2.7×10⁷ M⁻¹ s⁻¹) and so too high concentration of H₂O₂ will lead to a decrease of the organic compound degradation rate⁹⁵. Due to the much higher rate constant of HO• reaction on *p*-HPA (k_{*p*-HPA·HO•} = 2.2×10¹⁰ M⁻¹s⁻¹) the decrease of the *p*-HPA degradation is not observed in our experimental condition; at our highest H₂O₂ concentration used (1 mM) 90% of HO• is still consumed by *p*-HPA. So it was only observed that the increase rate slowed down when H₂O₂ increased from 250 μM to 1 mM. Moreover, at this concentration the photolysis of H₂O₂ is still negligible (**Fig. 5-3**) and do not strongly interact in the *p*-HPA degradation.

The effect of Na₂S₂O₈ concentration is shown in **Fig.5-6B**. Similar to H₂O₂, the degradation rate is always increasing when Na₂S₂O₈ concentration increases. In fact S₂O₈²⁻ is the source of radical species and the negative effect of Na₂S₂O₈, in terms of radical species scavenger probably SO₄^{•-} in this case (k_{Na₂S₂O₈2-,SO₄•-} = 6.1×10⁵ M⁻¹ s⁻¹)¹⁰⁹, is much slower than in the case with H₂O₂ (k_{H₂O₂·HO•} = 2.7×10⁷ M⁻¹ s⁻¹). So in our experimental conditions ([Na₂S₂O₈²⁻] ≤ 1 mM) a constant increase of the degradation rate of *p*-HPA with the increase of persulfate concentration is observed.

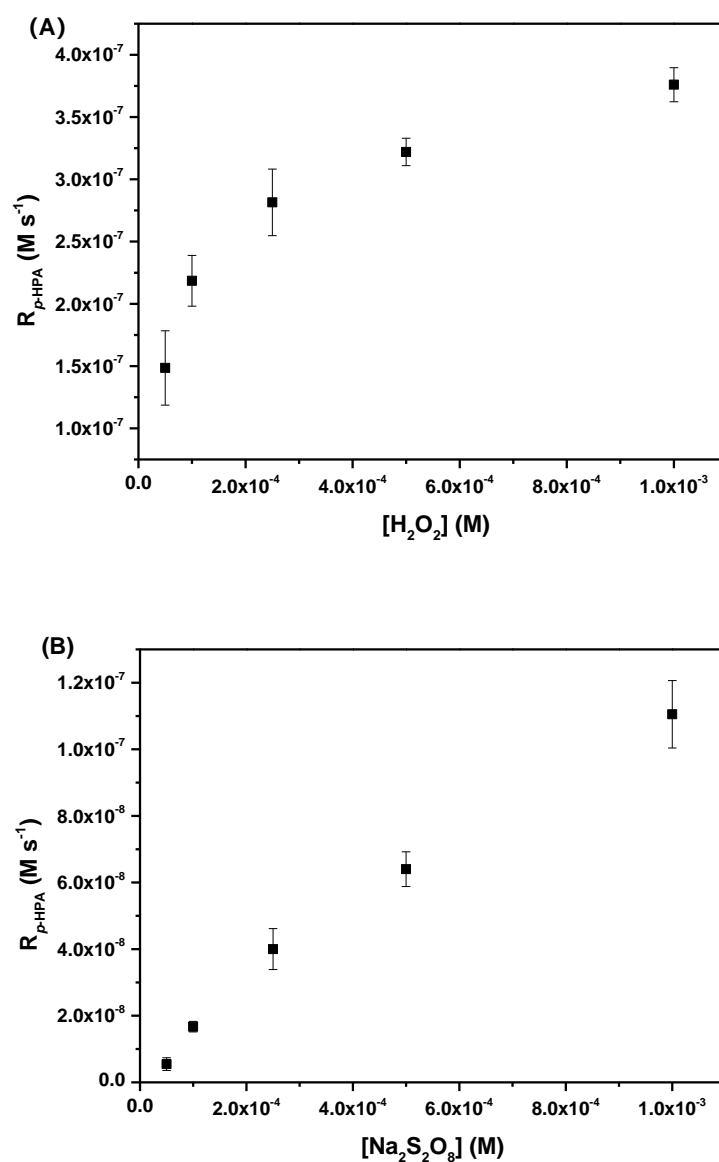


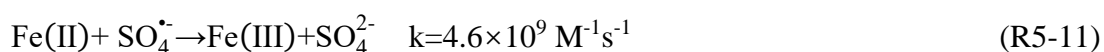
Fig.5-6 (A) The H_2O_2 concentration effect on the initial degradation rate of *p*-HPA in photo-Fenton system at pH = 7.5, (B) The $\text{Na}_2\text{S}_2\text{O}_8$ concentration effect on the initial degradation rate of *p*-HPA in Fe(III)-EDDS/ $\text{Na}_2\text{S}_2\text{O}_8$ /UV system at pH = 3.9 . [*p*-HPA] = 50 μM , [Fe(III)-EDDS] = 100 μM , irradiation time considered to evaluate the degradation rate = 5 min.

5.5. Effects of Fe(III)-EDDS concentrations

Fig.5-7A shows the removal percentage of *p*-HPA with different Fe(III)-EDDS

concentrations after 5 min of irradiation in the presence of 100 μM of H_2O_2 . The removal percentage of *p*-HPA increases when Fe(III)-EDDS concentration increases from 50 to 250 μM . Then, it decreases at higher Fe(III)-EDDS concentration up to 1 mM. Higher concentration of Fe(III)-EDDS produces under irradiation larger amount of Fe(II) followed with higher concentration of HO^\bullet through Fenton process. However, EDDS is one kind of organic matter and is able to interact in the process. Compared with H_2O_2 , EDDS has an almost 100 times higher second order rate constant with HO^\bullet ($k_{\text{EDDS},\text{HO}^\bullet}=2.48\pm 0.43\times 10^9 \text{ M}^{-1} \text{ s}^{-1} \gg k_{\text{H}_2\text{O}_2,\text{HO}^\bullet}=2.7\times 10^7 \text{ M}^{-1} \text{ s}^{-1}$)²⁴². So, EDDS and its photo-induced by-products can compete more strongly with *p*-HPA molecules. Moreover, another reason can explain the inhibition at higher Fe(III)-EDDS concentration. In fact, Fe(III)-EDDS is decomposed very fast under irradiation^{217, 218}, and the high concentration of Fe(II) produced is oxidized by different ways and the formed Fe(III) species are spontaneously precipitated at the used pH (7.5). Thus the formed colloid or precipitation can be responsible for the inhibition of the penetration of photons in the solution.

In Fe(III)-EDDS/ $\text{Na}_2\text{S}_2\text{O}_8$ /UV system, $\text{Na}_2\text{S}_2\text{O}_8$ is set as 500 μM , because at lower concentration (100 μM), it is difficult to differentiate the effect of Fe(III)-EDDS concentration due to relatively low degradation percentages. From **Fig.5-7B**, a similar trend can be observed than with H_2O_2 , so EDDS and its by-product also function as scavengers of $\text{SO}_4^{\bullet-}$ radical ($k_{\text{EDDS},\text{SO}_4^{\bullet-}}=6.21\times 10^9 \text{ M}^{-1}\text{s}^{-1}$)⁶⁷. Moreover, higher concentration of Fe(III)-EDDS can produce high concentration of Fe(II) in solution at the initial stage, while too much Fe(II) also can compete reacting with $\text{SO}_4^{\bullet-}$ with high rate constant (R5-11).¹¹⁰



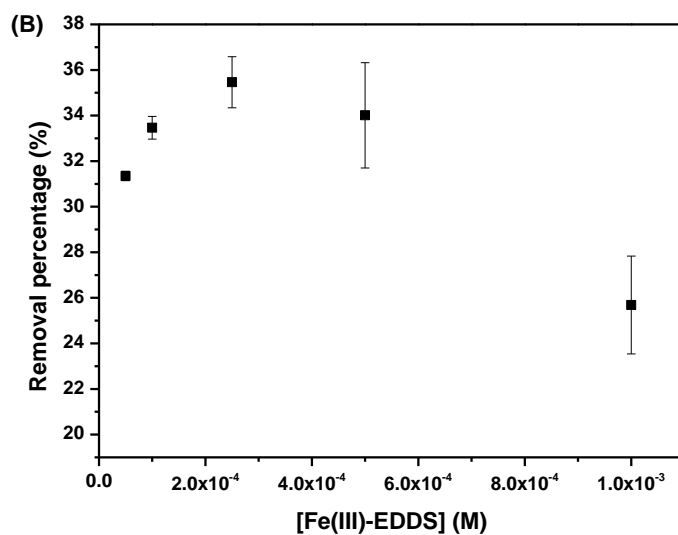
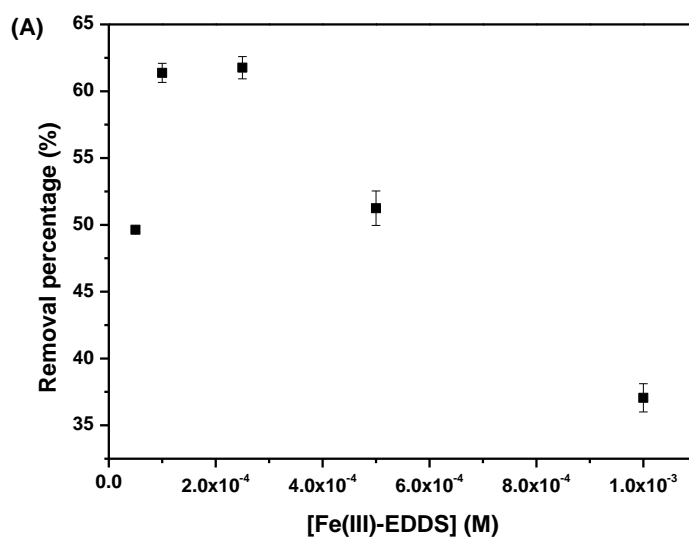


Fig.5-7 (A) Fe(III)-EDDS concentration effect on the removal percentage of *p*-HPA in photo-Fenton system after 5 min of irradiation. [*p*-HPA] = 50 μ M, [H₂O₂] = 100 μ M, pH = 7.5

(B) Fe(III)-EDDS concentration effect on the removal percentage of *p*-HPA in Fe(III)-EDDS/Na₂S₂O₈/UV system after 5 min of irradiation. [*p*-HPA] = 50 μ M, [Na₂S₂O₈] = 500 μ M, pH = 3.9.

5.6. Effects of pH

In the Fe(III) (photo)-induced activation reactions, pH always plays a significant role during the whole process. Firstly, in the *p*-HPA/Fe(III)-EDDS/UV system, pH effects are investigated, as shown in **Fig.5-8**. Under irradiation ($\lambda > 300$ nm), Fe(III)-EDDS can produce HO• through a series of reactions as it is described in Abida et al. (2006)²⁴³ and as it is proved in different studies like in the paper of Li et al. (2010)²¹⁸. However, if we compare with photo-Fenton process, the photo-production of HO• is very limited without H₂O₂ and so the removal of *p*-HPA is much slower (**Fig.5-5**)

When pH increases from 3.0 to 4.7, the removal efficiency increases very fast, while with pH further increase up to 9.4, degradation percentage continues to increase but much more slowly. The constant increase of the percentage of *p*-HPA removal with the increase of pH is due to the higher HO• formation quantum yield when the pH increases as it is demonstrated in the paper of Li et al. (2010)²¹⁸. The slower increase observed at pH higher than 4.7, can be attributed to the lower reactivity (three times lower) of HO• on the mono-anionic form of *p*-HPA. The rate constants have been evaluated for the first time during this study and are presented in **Table 5-1**.

The pH effect on the Fe(III)-EDDS/H₂O₂/UV and Fe(III)-EDDS/Na₂S₂O₈/UV processes during the initial stage (5 min of irradiation) are shown in **Fig.5-9**. The trend of pH effects is different from Fe(III)-EDDS/UV system and moreover the trend in **Fig.5-9A** and **Fig.5-9B** are also quite different although the experimental conditions are similar but the oxidation species used (H₂O₂ and Na₂S₂O₈) are different. So, the activation mechanisms of these two different processes are not exactly the same.

In Fe(III)-EDDS/H₂O₂/UV reaction, *p*-HPA degradation efficiency increases fast from pH 2.5 to 7.5, then it begin to decrease when pH increases to 9.0. As explained with the system Fe(III)-EDDS/UV (**Fig.5-8**), in general, the increase of efficiency with the increase of pH is mainly due to the increased HO• formation quantum yield. However, in the photo-Fenton process HO• generation is mainly due to the Fenton

process and so to the photo-generation of Fe(II) which is correlated with the first photochemical step, the photoredox process from the complex Fe(III)-EDDS leading to the formation EDDS• and Fe(II). To compare and understand well this mechanism, Fe³⁺ is introduced instead of Fe(III)-EDDS, see **Fig.5-10A**. In order to keep Fe³⁺ soluble in the solution, a very acidic pH is selected (pH = 2.0). Fe(III)-EDDS shows faster degradation efficiency than Fe³⁺ in the initial stage, ascribing to the higher photochemical activity of the complex Fe(III)-EDDS than the ion Fe³⁺. Like for Fe(III)-EDDS the degradation is also very fast in the first 10 minutes and after slows down. In Fe³⁺/H₂O₂/UV system, the degradation nearly stopped after about 30 minutes of irradiation. This important slow down and then complete stop of the reaction is due to the almost total consumption of H₂O₂. The higher final removal percentage observed with Fe³⁺ than with Fe(III)-EDDS is due to the presence of EDDS which can consume also HO• and so decrease the reactivity efficiency on *p*-HPA.

As a contrary of this rapid initial degradation observed with H₂O₂, in the Fe(III)-EDDS/Na₂S₂O₈/UV system, a gradual degradation during the irradiation process is observed (**Fig.5-5**). Fe(III)-EDDS is decomposed fast almost in the first 10 min by photoredox process, into Fe(II) and EDDS•, whatever the species present in the solution^{67, 217}. In the Fe(III)-EDDS/Na₂S₂O₈/UV system R_{*p*-HPA} slightly increases until pH 4.0 and then decreases when the pH increases (**Fig 5-9B**). The pH effect is not exactly the same than with H₂O₂ (increase is observed until around pH 8.0). This difference of pH effect could be due to the interaction of S₂O₈²⁻ in the radical chemistry processes. Indeed, S₂O₈²⁻ can react with the first radical generated by the photoredox process on EDDS (R5-12) and then avoid the reaction with O₂ leading to the formation of HO₂•/O₂•⁻. This hypothesis was deduced from the literature (Miralles-Cuevas et al. 2014)⁹⁹, EDDS• can react with anions in aqueous solution like hydroxyl to form related radicals. Furthermore, the existence of S₂O₈²⁻ can consume electrons and O₂•⁻ to form sulfate radicals (R5-13-R5-14)^{240, 244}. While it's well known that HO₂•/O₂•⁻ radicals are particularly important because they can accelerate the Fe(III)/Fe(II) cycle and so the reactivity as it is described in the paper

of Huang et al.¹¹¹ Moreover, as it is demonstrated in the paper of Wu et al. (2014)³⁰ the degradation efficiency is mainly affected by the photochemical activation abilities of different formed of Fe(III)-EDDS complex and the soluble Fe(III) concentrations in solution²¹⁷. With pH increase, Fe(III)-EDDS is less efficient photochemically, and the precipitation of Fe(III) in aqueous solution is stronger. Comparison between Fe³⁺ and Fe(III)-EDDS also was conducted, as shown in **Fig.5-10B**. At pH 2.0, Fe³⁺/Na₂S₂O₈ (500 μM)/UV system shows a fast and gradual degradation of *p*-HPA, and *p*-HPA can be removed completely in 45 min.

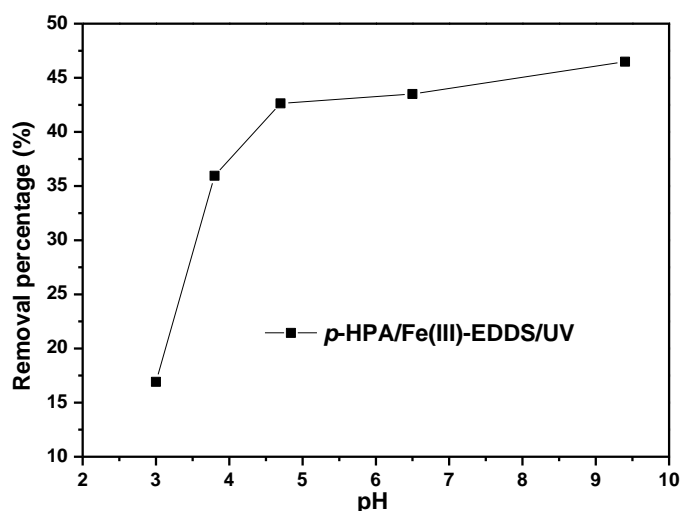


Fig.5-8 Removal percentage of *p*-HPA in Fe(III)-EDDS/UV system after 120 min of irradiation at different pH. [Fe(III)-EDDS] = 100 μM, [*p*-HPA] = 50 μM.

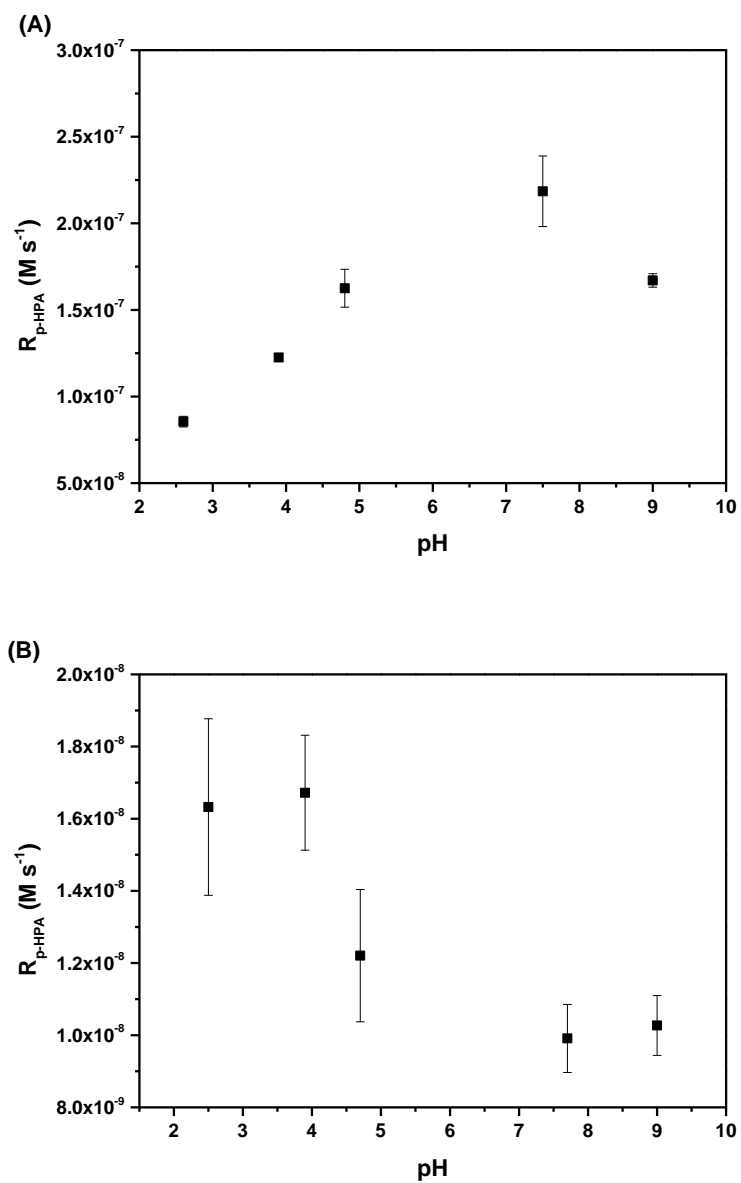


Fig.5-9 (A) pH effect on the initial degradation rate of *p*-HPA in photo-Fenton system and (B) in Fe(III)-EDDS/Na₂S₂O₈/UV system.

[*p*-HPA] = 50 μM , [Fe(III)-EDDS] = 100 μM , [H₂O₂] = 100 μM , [Na₂S₂O₈] = 100 μM , irradiation time considered to evaluate the degradation rate = 5min.

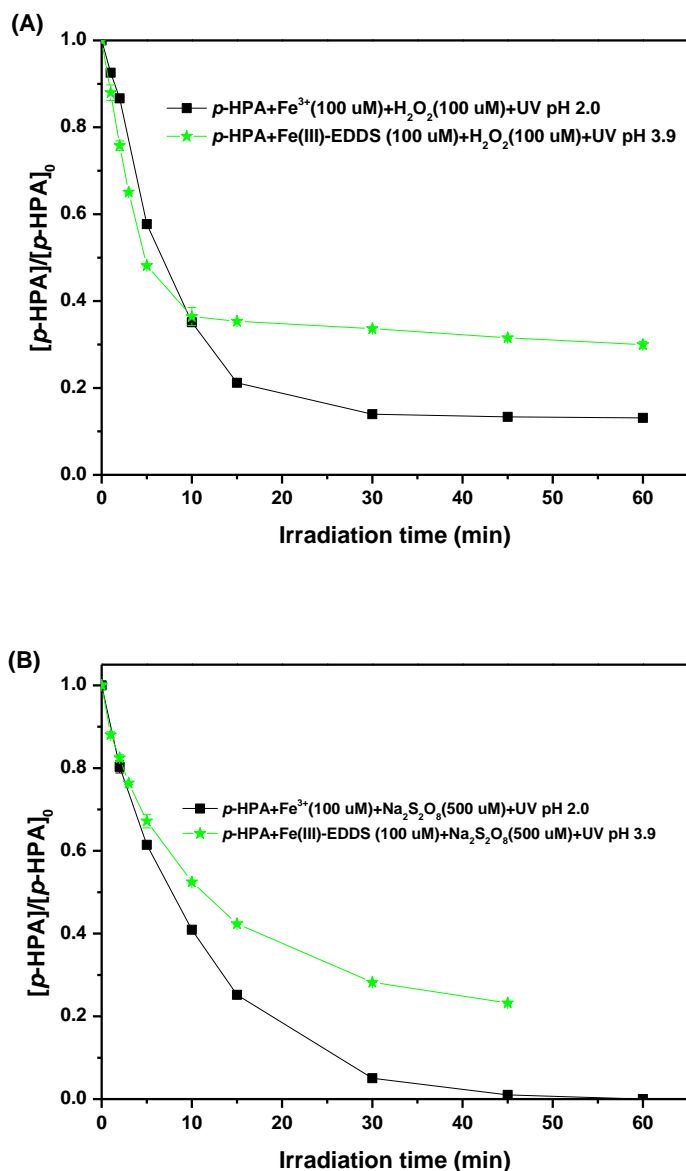


Fig.5-10 Comparison of Fe(III)-EDDS and Fe^{3+} in (A) photo-Fenton process and (B) in ferric ions / $\text{Na}_2\text{S}_2\text{O}_8$ /UV process. $[p\text{-HPA}] = 50 \mu\text{M}$, $[\text{Fe(III)-EDDS}]$ or $[\text{Fe}^{3+}] = 100 \mu\text{M}$, $[\text{H}_2\text{O}_2] = 100 \mu\text{M}$, $[\text{Na}_2\text{S}_2\text{O}_8] = 500 \mu\text{M}$.

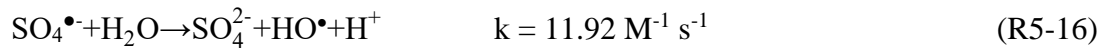
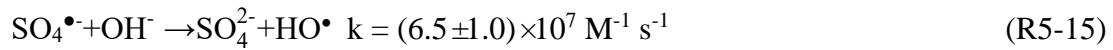
5.7. Identification of active species at pH 3.9

In order to determine the radicals involved in the degradation of p-HPA in the different processes, IPA and TBA are used as scavengers of radicals and so added in the solution (**Fig.5-11**). In fact, at adopted concentrations, IPA (10 or 20 mM) was

considered to quench efficiently both generated $\text{SO}_4^{\bullet-}$ and HO^\bullet , considering the second order rate constants of $k_{\text{IPA},\text{SO}_4^{\bullet-}} = 7.42 \times 10^7 \text{ M}^{-1}\text{s}^{-1}$ and $k_{\text{IPA},\text{HO}^\bullet} = 1.9 \times 10^9 \text{ M}^{-1}\text{s}^{-1}$, while TBA (1 or 2 mM) can be considered to be more selective toward HO^\bullet ($k_{\text{TBA},\text{HO}^\bullet} = 6.0 \times 10^8 \text{ M}^{-1}\text{s}^{-1}$) than with $\text{SO}_4^{\bullet-}$ ($k_{\text{TBA},\text{SO}_4^{\bullet-}} = 8.31 \times 10^5 \text{ M}^{-1}\text{s}^{-1}$)²⁰⁷.

From **Fig.5-11A**, 20 mM of IPA can almost completely inhibit the degradation of *p*-HPA. At this concentration, 97 % of HO^\bullet is consumed by IPA and only 3% was consumed by *p*-HPA. At lower concentration of IPA (1 mM) only 63% of HO^\bullet can react with IPA and so a degradation of *p*-HPA was still observed and correspond to almost 30% of removal. So, HO^\bullet radical is identified as the active species responsible of *p*-HPA transformation in the system with H_2O_2 .

In the presence of persulfate (500 μM), 20 mM of IPA can react with 86% $\text{SO}_4^{\bullet-}$ when *p*-HPA is present at 50 μM , so higher concentrated IPA is needed if $\text{SO}_4^{\bullet-}$ want to be completely inhibited. HO^\bullet radical is mainly generated from two routes. Firstly, it is generated from the photolysis of Fe(III)-EDDS complex. Secondly, $\text{SO}_4^{\bullet-}$ can also react with hydroxyl anion or water molecule to produce HO^\bullet (R15-16)^{109, 112, 245}. To evaluate the relative significance of the two radicals (sulfate and hydroxyl) in this system, experiments are also performed with TBA acting specifically as a trap for hydroxyl radical. When the concentration of TBA increases from 1 to 2 mM the decrease of *p*-HPA concentration near 60% is the same (**Fig.5-11B**). So, from **Fig.5-11B**, it is possible to conclude both radicals are involved in the system Fe(III)-EDDS/ $\text{Na}_2\text{S}_2\text{O}_8$ /UV with a specific percentage respectively near 20% for HO^\bullet and 80% for $\text{SO}_4^{\bullet-}$.



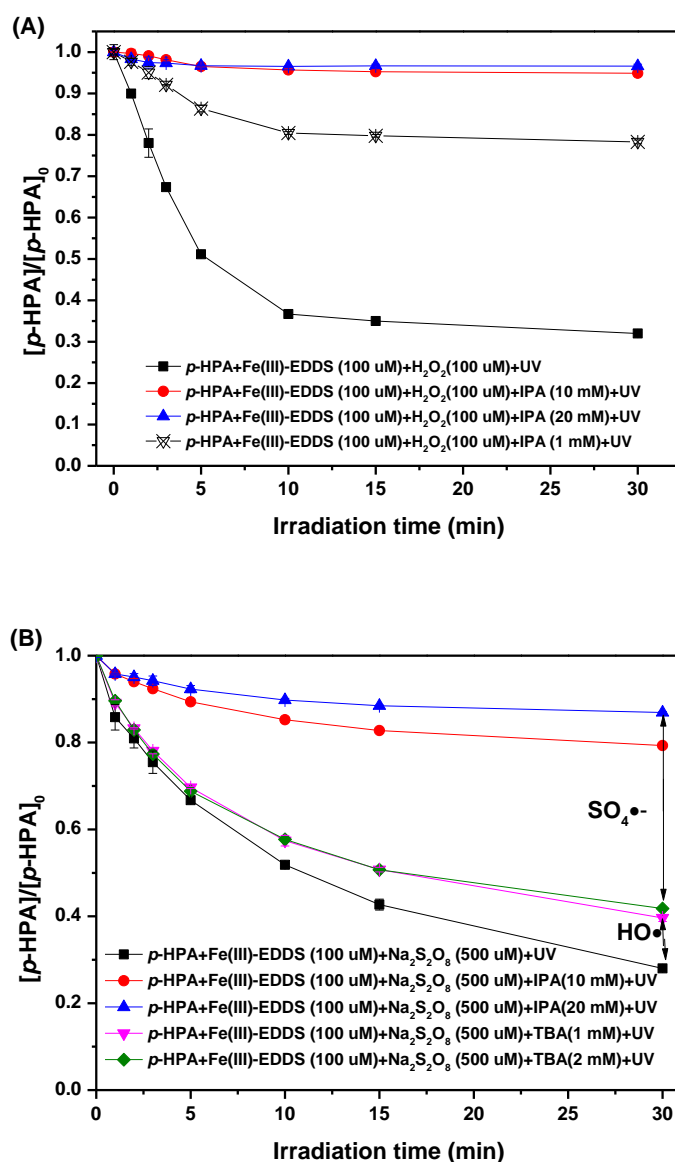


Fig.5-11 (A) Kinetic of *p*-HPA concentration when different concentrations of isopropanol were added to the photo-Fenton process

$[p\text{-HPA}] = 50 \mu\text{M}$, $[\text{H}_2\text{O}_2] = 100 \mu\text{M}$, $[\text{Fe(III)-EDDS}] = 100 \mu\text{M}$, $\text{pH} = 3.9$ under UV

(B) Kinetic of *p*-HPA concentration when different concentrations of isopropanol or tert-butyl alcohol were added to the Fe(III)-EDDS/ $\text{Na}_2\text{S}_2\text{O}_8$ /UV process

$[p\text{-HPA}] = 50 \mu\text{M}$, $[\text{Na}_2\text{S}_2\text{O}_8] = 500 \mu\text{M}$, $[\text{Fe(III)-EDDS}] = 100 \mu\text{M}$, $\text{pH} = 3.9$ under

UV

5.8. Conclusion: comparison of H₂O₂ and S₂O₈²⁻ efficiency

In general, the *p*-HPA degradation efficiency is much higher with Fe(III)-EDDS/H₂O₂/UV system than with Fe(III)-EDDS/Na₂S₂O₈/UV system whatever the solution pH's. Firstly, this difference can be explain by taking into account the second order rate constants $k_{p\text{-HPA},\text{HO}\cdot}$ and $k_{p\text{-HPA},\text{SO}_4\cdot-}$ into consideration (**Table5-1**). The value of $k_{p\text{-HPA},\text{HO}\cdot}$ is higher than $k_{p\text{-HPA},\text{SO}_4\cdot-}$ both at pH 2.5 (4.6 times) and 8.5 (2 times). Secondly the rate constants of the key reactions generating the radical species is more than 3 times higher for the Fenton process (R5-6) than for the activation of persulfate with Fe(II) (R5-8). However, at pH 2.5, the ratio of the rate constants between radical species and *p*-HPA $k_{p\text{-HPA},\text{HO}\cdot}/k_{p\text{-HPA},\text{SO}_4\cdot-}$ equal to 4.6 and the ratio of *p*-HPA disappearance rate in the two systems $R_{p\text{-HPA}}(\text{H}_2\text{O}_2)/R_{p\text{-HPA}}(\text{Na}_2\text{S}_2\text{O}_8)$ equal to 5.2 are similar. It is slightly higher for the *p*-HPA disappearance rate which is coherent with the two reasons mentioned at the beginning of this paragraph. As a contrary the difference between these two ratios is much higher at pH 8.5, $R_{p\text{-HPA}}(\text{H}_2\text{O}_2)/R_{p\text{-HPA}}(\text{Na}_2\text{S}_2\text{O}_8)$ equal to 16.7 is eight times higher than $k_{p\text{-HPA},\text{HO}\cdot}/k_{p\text{-HPA},\text{SO}_4\cdot-}$ equal to 2.1. So, as we demonstrated in the paper of Huang et al.¹¹¹, the Fenton process, involving Fe(III)-EDDS complex, is higher near neutral pH than in acidic pH. This significant result in terms of environmental aquatic compartments seems not present for the activation of persulfate to generate $\text{SO}_4^{\bullet-}$ radical. Indeed, in this case a dramatic decrease of the efficiency is observed. So, in this particular study, with *p*-HPA used as organic pollutant and UV/Fe(III)EDDS as source of Fe(II), we clearly demonstrated that the Fenton process is more efficient than activation of persulfate process and more particularly at environmentally closed pH values.

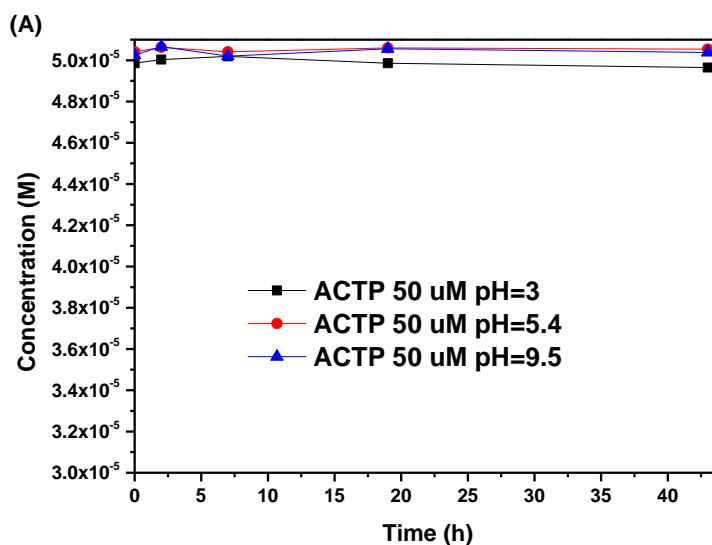
6. Degradation of Acetaminophen by UV-induced advanced oxidation processes (AOPs): different degradation abilities of HO•, SO₄•⁻ and HO₂•/O₂•⁻

As one of the most important pain killer mainly sold as over the counter drugs, acetaminophen (ACTP) is heavily used all over the world, ranking as one of the top three drugs in England²⁴⁶. Different researches based on advanced oxidation processes such as UV/H₂O₂⁵⁸, Fenton⁶⁰, electron Fenton⁵⁹ and electrochemical degradation^{115, 247, 248} of ACTP are present in literature. Furthermore, heterogeneous photocatalytic degradation efficiency and mechanism of ACTP by TiO₂ was also widely used^{246, 249, 250}. In TiO₂ photocatalytic system, HO• is always the predominant active species²⁴⁹. As described in Chapter 4, BiOCl_{0.75}I_{0.25} possessed the greatest surface area and most suitable band-gap, showing excellent adsorption and photocatalytic degradation abilities in removing ACTP from water under simulated solar and visible light. In this system, O₂•⁻ was the main radical determined by indirect scavenging experiments. In this work, three different oxidation species HO•, SO₄•⁻ and HO₂•/O₂•⁻ produced by UV/H₂O₂, UV/Na₂S₂O₈, UV/H₂O₂/Fe(III)-EDDS, UV/Na₂S₂O₈/Fe(III)-EDDS and UV/BiOCl_{0.75}I_{0.25} respectively were studied. Under simulated solar irradiation (300 nm < λ < 500 nm) their efficiency on the degradation of ACTP was compared for the first time. ACTP degradation in UV/H₂O₂, UV/Na₂S₂O₈ and UV/BiOCl_{0.75}I_{0.25} under different pH was studied, and influence of halide ions (Cl⁻ and I⁻) were investigated at the same time. Interfacial mechanism, mineralization and efficiency of this degradation will be explained in detail. Furthermore, Second order constant between ACTP with HO• and SO₄•⁻ radicals was determined by laser flash photolysis (LFP) or chemical competition reactions.

6.1. Blank experiment of ACTP mixed with H₂O₂ and Na₂S₂O₈ in the dark

To explore ACTP degradation with H₂O₂ and Na₂S₂O₈ under UV irradiation, blank experiments must be conducted in the dark firstly to check its stability, as shown in

Fig.6-1. From **Fig.6-1A**, it can be seen that ACTP solution was stable between pH 3.0 and 9.5 within 40 hours. Moreover, when ACTP was mixed with H₂O₂ and Na₂S₂O₈ (**Fig.6-1B** and **Fig.6-1C**), no significant degradation was observed when the initial pH of the solution was lower than 10. At pH 11.5 a degradation in the first 2 hours was observed (the pK_a of ACTP was 9.38⁵⁶). It was well known that H₂O₂ (E⁰=1.77 V) and Na₂S₂O₈ (E⁰=2.01 V) are two common oxidants. So it can be deduced that ACTP was easily to be oxidized in the ionized form. Su et al.⁶¹ evaluated ACTP removal in Fenton process, H₂O₂ (50 mM) alone has negligible effects on ACTP degradation at pH 3. Zhang et al.²⁵¹ also studied the ACTP degradation in the presence of persulfate anion, and results showed that 35% of degradation was achieved with the initial concentration of PS set at 0.6 g L⁻¹ at pH 6.5 within 40 min. In this study, control experiments on ACTP degradation was highly related to the solution pH.



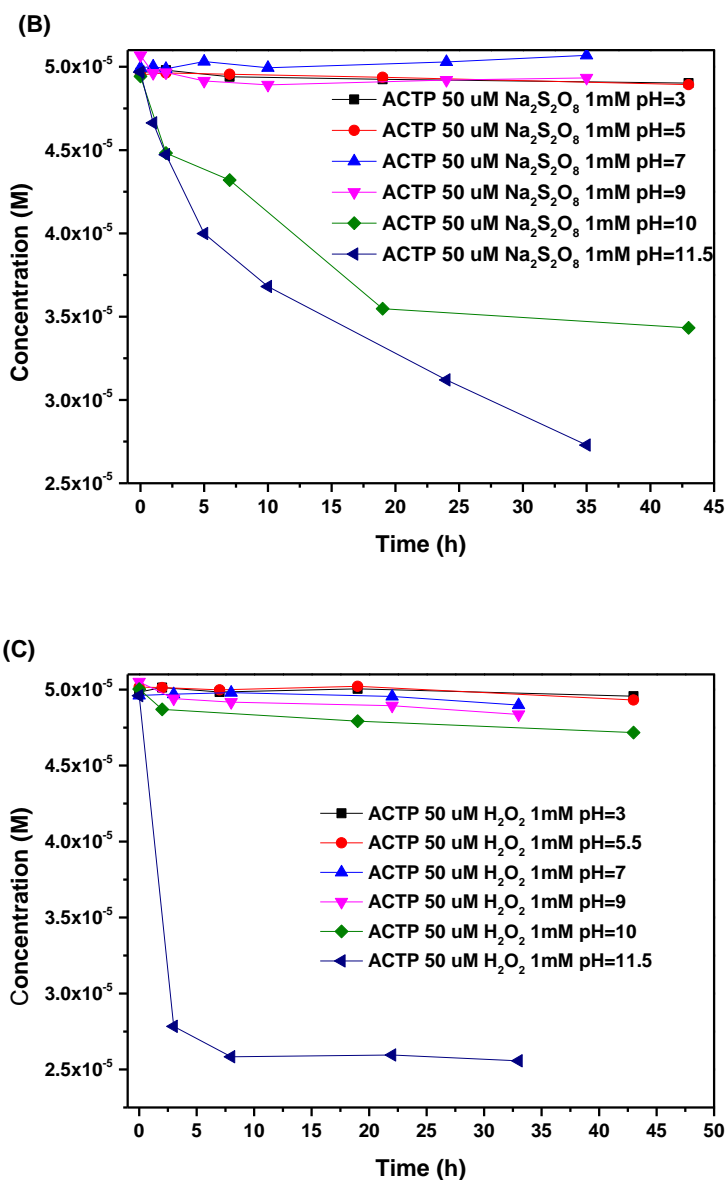
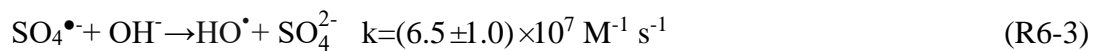


Fig.6-1 (A) 50 μM ACTP concentration as a function of time at different pH in the dark, (B) with $\text{Na}_2\text{S}_2\text{O}_8$ (1 mM), (C) with H_2O_2 (1 mM).

6.2. ACTP degradation in UV/ H_2O_2 and UV/ $\text{Na}_2\text{S}_2\text{O}_8$ systems under different pH values

The time evolution of Acetaminophen concentration in the presence of H_2O_2 and $\text{Na}_2\text{S}_2\text{O}_8$ was shown in **Fig.6-2**, and degradation profiles followed pseudo first order reaction kinetics. Firstly, direct photolysis of ACTP could be neglected (**Fig.6-2a**). UV-vis spectrum of ACTP at different pH was shown in **Fig.6-3**, in which can be seen

that, at pH 3 and 6.5, it showed same spectrum with the highest adsorption at 244 nm. While when increased the solution pH to 11.2 a red shift with a maximum at 256 nm can be observed. In our photochemical reactor in which the emission spectrum is between 300 and 500 nm, ACTP has almost no adsorption. With H₂O₂ and Na₂S₂O₈ addition, ACTP showed different degradation kinetics under various pH. Results of quenching experiments demonstrated that HO• and SO₄•⁻ were the premoninant radicals involved in the UV/H₂O₂ and UV/Na₂S₂O₈ system (Eq.1-2) at pH 5 respectively by taking IPA and EtOH as HO• (k_{IPA, HO•}=1.9×10⁹ M⁻¹ s⁻¹)²⁰⁷ and SO₄•⁻ (k_{EtOH, SO₄•⁻}=1.6-7.7×10⁷ M⁻¹ s⁻¹)⁵⁶ scavengers respectively. In UV/H₂O₂ system, at neutral pH the maximum removal percentage is observed. As contrast, in UV/Na₂S₂O₈ system, degradation rate increased with increasing of pH (Fig.6-2b). At least two reasons were involved simultaneously to account for this phenomenon. As reported in Fig.6-3, ACTP under anion form was easier to be oxidized. Furthermore, in alkaline solution the generation of HO• from SO₄•⁻ is favoured (Eq.3-4)¹⁰⁹. So, alkaline solution can provide a suitable environment to support the oxidation of ACTP by HO• and SO₄•⁻ radicals, as in the UV/Na₂S₂O₈ system. However, at very high pH values (>11) hydrogen peroxide (pKa = 11.7) is present as hydroperoxide anion (HO₂⁻). This form also showed like a scavenger of hydroxyl radicals and cause decomposition of H₂O₂. It was reported that the reaction of hydroxyl radicals with hydroperoxide anions is approximately 100 times faster than its reaction with H₂O₂²⁵². In addition, too basic solution make H₂O₂ unstable and accelerate its self decomposition⁵⁶. (Eq.5-7) Furthermore, it has been reported that the standard redox potential of HO• in acidic pH is about 2.4-2.7 eV which is higher than that in alkaline pH (1.9-2.0 eV)²⁵³. However, persulfate radical redox potential does not depend on the pH²⁴⁵.



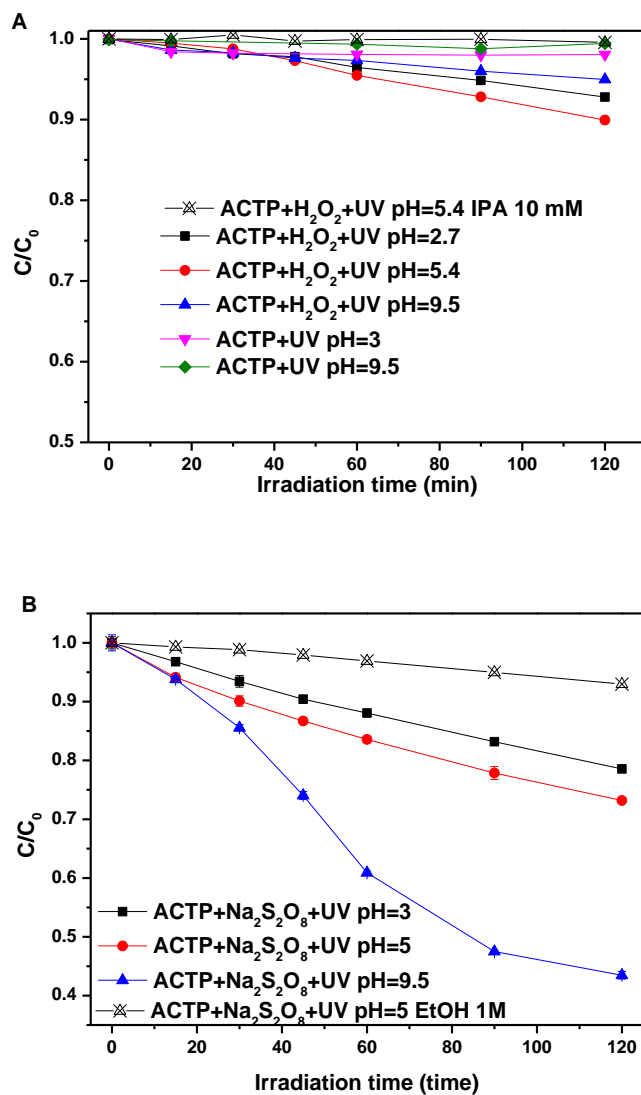


Fig.6-2 Direct photolysis and degradations of ACTP (50 μM) in the UV/H₂O₂ (1 mM) (A) UV/ Na₂S₂O₈ (1 mM) (B) systems under different pH.

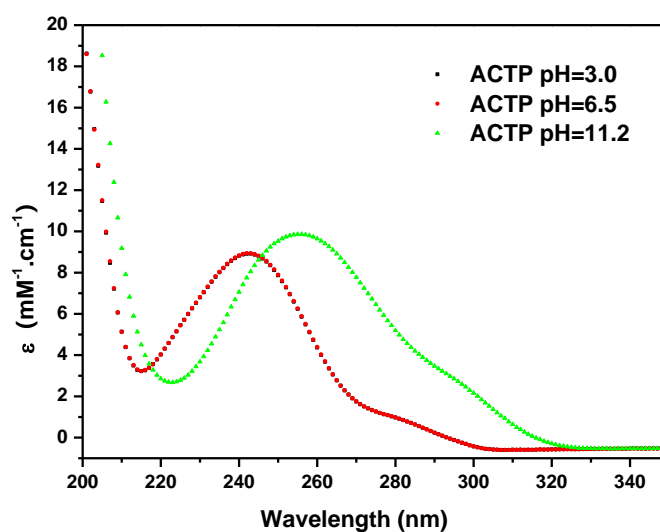


Fig.6-3 UV-Vis spectrum of ACTP at different pH

6.3. Halide ions (chloride and iodide) effects on ACTP degradation in UV/H₂O₂ and UV/Na₂S₂O₈ systems

Effects of halide ions were widely studied in previous articles, especially chloride and bromide^{73, 254}. While comparison of Cl⁻ and I⁻, which were commonly detected in coastal seawater, saline water or industrial wastewater discharges, were investigated for the first time by taking different concentrations in UV/H₂O₂ and UV/Na₂S₂O₈ systems, respectively. Firstly, ACTP concentration kept unchanged when NaCl, H₂O₂ or Na₂S₂O₈ are mixed under dark conditions (see **Fig.6-4**). Under irradiation, the effects of Cl⁻ are shown in **Table 6-1**, in which can be seen that in UV/H₂O₂ system, when 10 mM of NaCl are added, degradation rate slightly increased, while no differences can be observed using lower NaCl concentration was used in agreement with results obtained by Li et al.⁷³. In UV/Na₂S₂O₈ system, Cl⁻ always exhibited negligible effects at various concentrations. In previous works, Cl⁻ plays a role of radical scavengers leading to the formation of chloride reactive species (Cl[•], Cl₂^{•-} or ClHO[•]) in the presence of HO[•] or SO₄^{•-}^{255, 56, 82, 252}.

When iodide ions were added to the solution, degradation rate was significantly affected as shown in **Fig.6-5**. In the dark, the addition of KI (260 μM-5 mM)

accelerate the degradation of ACTP in the presence of H₂O₂ or Na₂S₂O₈ at pH 5.4, and H₂O₂ showed higher oxidation rates than Na₂S₂O₈. Similar to HOCl, HOI was supposed to be generated from iodine ions by H₂O₂ and Na₂S₂O₈ (Eq.8-11). It's well known that HOI is a very strong and unstable oxidant, and it can react with ACTP molecules²⁵². Under As shown in Fig.6-6, under UV irradiation, no degradation of ACTP was observed in the presence of KI. However, when H₂O₂ or Na₂S₂O₈ were added into the solution at same time, the degradation was highly enhanced. Except for the existence of HOI, reactive halogenated species can be generated from HO• or SO₄•⁻ as shown in Eq.12-14²⁵⁶. Different from chloride radicals, iodide induced radicals (I•, HOI• and I₂•⁻) showed higher degradation reactivities with organic molecules. Tamtam et al.²⁵⁴ have demonstrated that reactive halogenated species reacted more selectively than hydroxyl radicals with electron-rich organic pollutants in agreement with Li et al.⁷³. As acetaminophen contains hydroxyl and acetamido groups, which are electron donors to the aromatic rings, it's hypothesized in this research that these electron-rich moieties may selectively react with these iodide related radical reactive species. Using much higher concentrations of iodide ions a decrease of rate was observed due to the self quenching effects as reported in Eq.14.



Table 6-1 Cl⁻ concentration effects on the degradation of ACTP in UV/H₂O₂ and UV/Na₂S₂O₈ systems

system	k (s ⁻¹)	error	system	k (s ⁻¹)	error
UV/H ₂ O ₂ /NaCl 0 mM	-1.539E-5	9.195E-7	UV/Na ₂ S ₂ O ₈ /NaCl 0 mM	-3.729E-5	1.968E-6
UV/H ₂ O ₂ /NaCl 1 mM	-1.530E-5	9.390E-7	UV/Na ₂ S ₂ O ₈ /NaCl 1 mM	-3.560E-5	1.001E-6
UV/H ₂ O ₂ /NaCl 2 mM	-1.563E-5	6.764E-7	UV/Na ₂ S ₂ O ₈ /NaCl 2 mM	-3.622E-5	6.830E-7
UV/H ₂ O ₂ /NaCl 10 mM	-2.046E-5	6.020E-7	UV/Na ₂ S ₂ O ₈ /NaCl 10 mM	-3.512E-5	1.287E-6

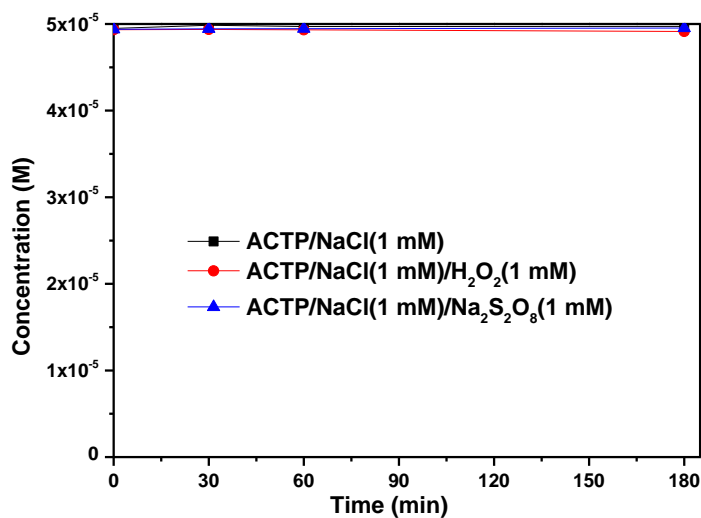


Fig.6-4 ACTP concentration change when mixed with NaCl (1 mM) in the dark at pH

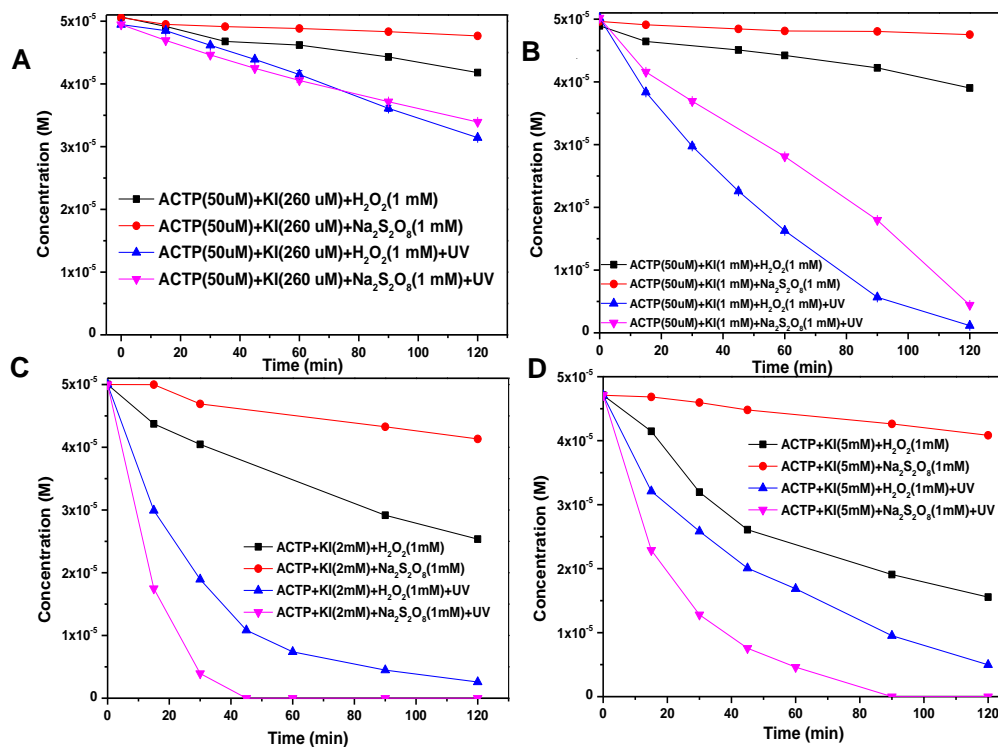


Fig.6-5 Effects of KI concentration on the degradation of ACTP (50 μM) in the UV/ H_2O_2 (1 mM) system and UV/ $\text{Na}_2\text{S}_2\text{O}_8$ (1 mM) system at pH 5.4

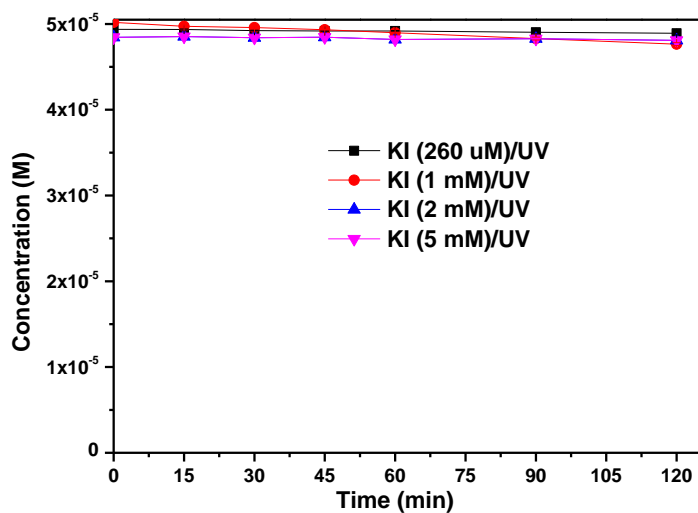


Fig.6-6 ACTP concentration change with different concentrated KI under UV at pH 6

6.4. Photo-degradation of ACTP in UV/H₂O₂/Fe(III)-EDDS and UV/Na₂S₂O₈/Fe(III)-EDDS system

As shown in **Fig.6-2**, only UV/H₂O₂ and UV/Na₂S₂O₈ showed a low degradation rate of ACTP, especially in UV/H₂O₂ where about 10% of ACTP was removed in 2 hours. Fe(III)-EDDS is a potential iron complex in activating H₂O₂ and Na₂S₂O₈, as explained in Chapter 5. So Fe(III)-EDDS mediated degradation of ACTP was discussed in this section, as shown in **Fig.6-7**. With a lower concentration of H₂O₂ and Na₂S₂O₈ (500 μ M), ACTP showed a fast degradation in these two systems and was completely removed in 15 min in UV/H₂O₂/Fe(III)-EDDS while 80% was removed in 30 min in UV/Na₂S₂O₈/Fe(III)-EDDS. Compared to the direct photolysis of H₂O₂ and Na₂S₂O₈, the addition of iron enhances the formation of HO \cdot and SO₄ \cdot^- , followed with a series oxidation reaction. With *p*-HPA, H₂O₂ showed faster degradation rate than Na₂S₂O₈ because of the faster activation rate by Fe(II).

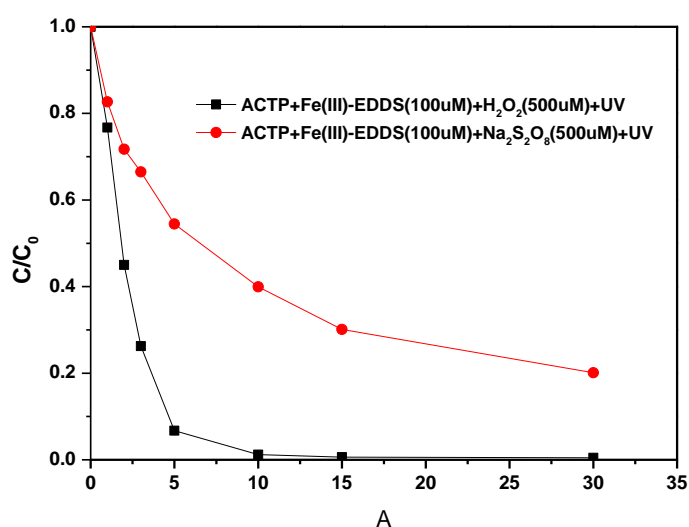


Fig.6-7 Degradation of ACTP in the UV/H₂O₂/Fe(III)-EDDS and UV/Na₂S₂O₈/Fe(III)-EDDS

Conditions: [ACTP] = 50 μ M, [Fe(III)-EDDS] = 100 μ M, [H₂O₂] = [Na₂S₂O₈] = 500 μ M, pH = 3.9

6.5. pH effects in UV/H₂O₂/Fe(III)-EDDS and UV/Na₂S₂O₈/Fe(III)-EDDS system

Fig.6-8 showed the pH effect on the degradation rate of ACTP (R_{ACTP}) in UV/H₂O₂/Fe(III)-EDDS. Similar to *p*-HPA, R_{ACTP} increased with pH increase from 2.5 to 7.5, then it decrease when further increase to pH 9.0. Several reasons can be accounted for this phenomenon; firstly the concentration of soluble Fe(II) was the limited step in the whole reaction, while HO₂[•]/O₂^{•-} was essential in the transformation of Fe(III)/Fe(II) and O₂^{•-} showed a faster transformation rate from Fe(III) to Fe(II). However, when pH further increased beyond 7.5, a less photoactive form Fe(III)(OH)-EDDS²⁻ prevailed⁶⁷. So it obtained the maximum R_{ACTP} at pH 7.5, then it began to decrease with the help of Fe(III) precipitation in higher pH.

pH effect on the initial degradation rate of ACTP in Fe(III)-EDDS/Na₂S₂O₈/UV system was shown in **Fig.6-9**. Different to **Fig.6-8**, R_{ACTP} increased from 2.0 to 3.5, decreases for higher pH values. Similar reasons can be taken into consideration as **Fig.5-8B**.

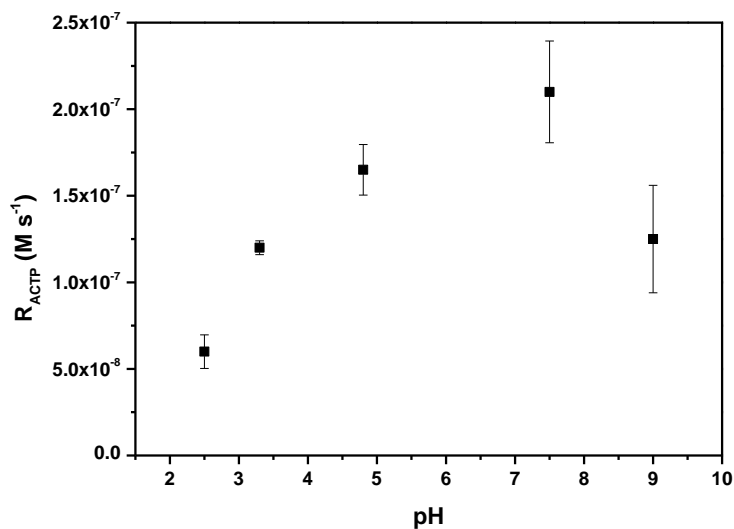


Fig.6-8 pH effect on the initial degradation rate of ACTP in photo-Fenton system
[ACTP] = 50 μ M, [Fe(III)-EDDS] = 100 μ M, [H₂O₂] = 100 μ M, irradiation time considered to evaluate the degradation rate = 5min.

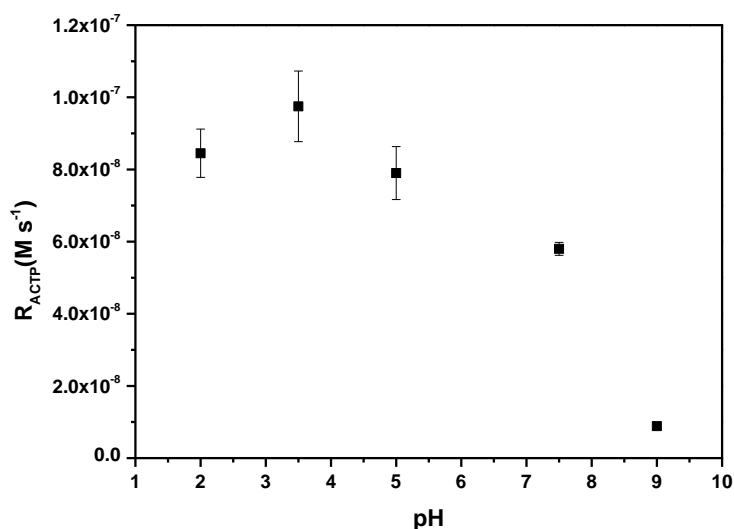


Fig.6-9 pH effect on the initial degradation rate of ACTP in Fe(III)-EDDS/Na₂S₂O₈/UV system.

[ACTP] = 50 μ M, [Fe(III)-EDDS] = 100 μ M, [Na₂S₂O₈] = 500 μ M, irradiation time considered to evaluate the degradation rate = 5min.

6.6. Photo-catalytic degradation of ACTP by BiOCl_{0.75}I_{0.25} catalyst under different pH

Heterogeneous photocatalytic degradation of ACTP involved semiconductors such as TiO₂ has attracted numerous attentions recently^{57, 77, 80, 250}. Photo-induced holes and hydroxy radicals always were justified as main reactive species and various degradation pathways have been proposed for transformation and mineralization. Up to now, seldom studies are investigating the degradation of ACTP predominantly by superoxide radicals. In our previous studies²²⁶, BiOCl_{0.75}I_{0.25} catalyst has been synthesized by mixed solvent precipitation method, and it has been characterized seriously as shown in chapter 4.1. It showed excellent photocatalytic degradation abilities under simulated solar and visible irradiations. Through the quenching experiments, HO₂[•]/O₂^{•-} was justified as the main radical species by taking benzoquinone as scavengers and purging nitrogen (see **Fig.6-10**). The present work is an attempt to investigate the reaction activities between ACTP and HO₂[•]/O₂^{•-}

produced by $\text{BiOCl}_{0.75}\text{I}_{0.25}$ catalyst under UV irradiation, and then make comparison with HO^\bullet or $\text{SO}_4^{\bullet-}$. Firstly, photocatalytic degradation of ACTP under pH was investigated as shown in **Fig.6-11**. In the dark, ACTP has less than 10% percentage adsorption on the surface of catalyst at different pH. Considering that the pKa is 9.38, ACTP showed the same molecular form within the pH of this experiment, and the zero point charge of $\text{BiOCl}_{0.75}\text{I}_{0.25}$ catalyst located at pH 1.6. However, under UV irradiation for 120 min, all the degradation followed pseudo first order reaction kinetics and the removal efficiency differed a lot as function of pH. In acidic solution (pH=3) the fastest degradation rate was observed, consistent with previous reports about BiOX related photocatalytic degradation researches^{172, 233}. Zeta-potential of $\text{BiOCl}_{0.75}\text{I}_{0.25}$ was more negative with pH increased, so less photo-induced electrons can transferred to the surface of the catalyst. While, as discussed above, electrons were crucial to form $\text{HO}_2^\bullet/\text{O}_2^{\bullet-}$, which were main active species involved in the degradation processes.

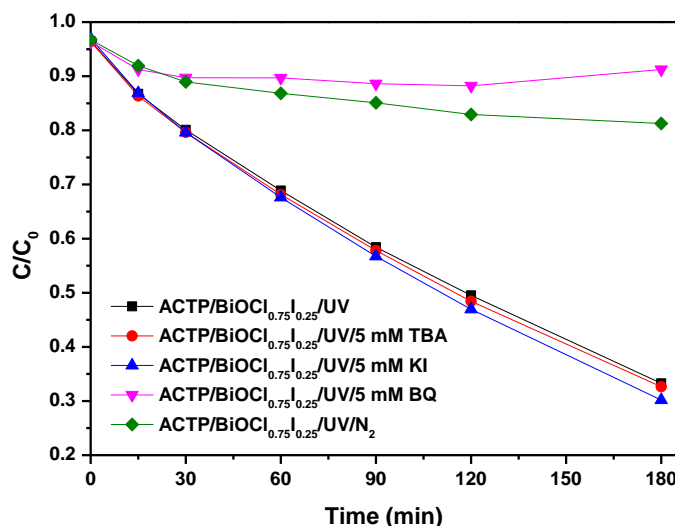


Fig.6-10 Concentration change of ACTP with different scavengers added

Conditions: $[\text{ACTP}] = 50 \mu\text{M}$, $[\text{catalyst}] = 0.3\text{g/L}$, under UV, pH=6

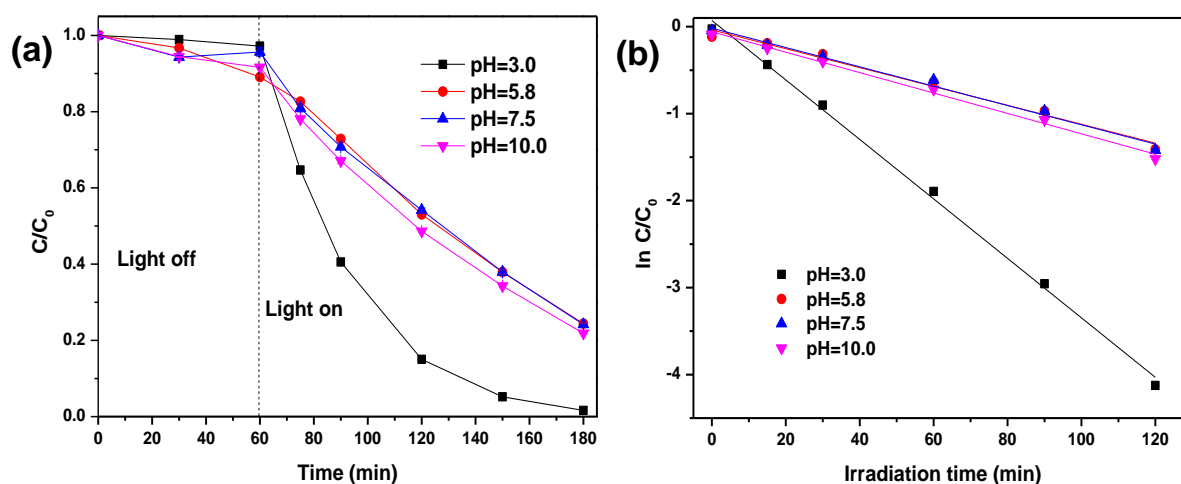


Fig.6-11 The photocatalytic degradation of ACTP at different pH (a) and the pseudo first order reaction (b)

Conditions: [ACTP]= 50 μ M, [catalyst]= 0.3g/L, under UV

6.7. Heterogeneous reaction mechanism

For heterogeneous photocatalytic degradation, interfacial mechanism was investigated to confirm if the reaction mechanism occurs in the solution or on the surface of catalyst. To clarify this point, $\text{NaH}_2\text{PO}_4 \cdot \text{H}_2\text{O}$ has been proved to be a good desorbing molecule in our experiment. Because NaH_2PO_4 can occupy almost all the adsorption site on the surface of catalyst, and the surface was tightly surrounded by NaH_2PO_4 molecules instead of ACTP. While after the addition of NaH_2PO_4 , the degradation rate and removal percentage also decreased as shown in **Fig. 6-12**. Due to shielding effect, the number of active sites decreased and the penetration of light irradiation reduced¹⁷². As we discussed above, the main active species $\text{HO}_2^\bullet/\text{O}_2^{\bullet-}$ came from the combination of dissolved oxygen in water and valence band induced electrons. The very short half-life time of $\text{HO}_2^\bullet/\text{O}_2^{\bullet-}$ indicated it would subsequently undergo easy disproportionation to produce other reactive oxygen species (ROS)²³³. The fast and direct contact of pollutant and catalyst surface was necessary for the reaction. So in this photocatalytic degradation system, degradation in the solution must be occurred on the surface or very close to the surface of the catalyst.

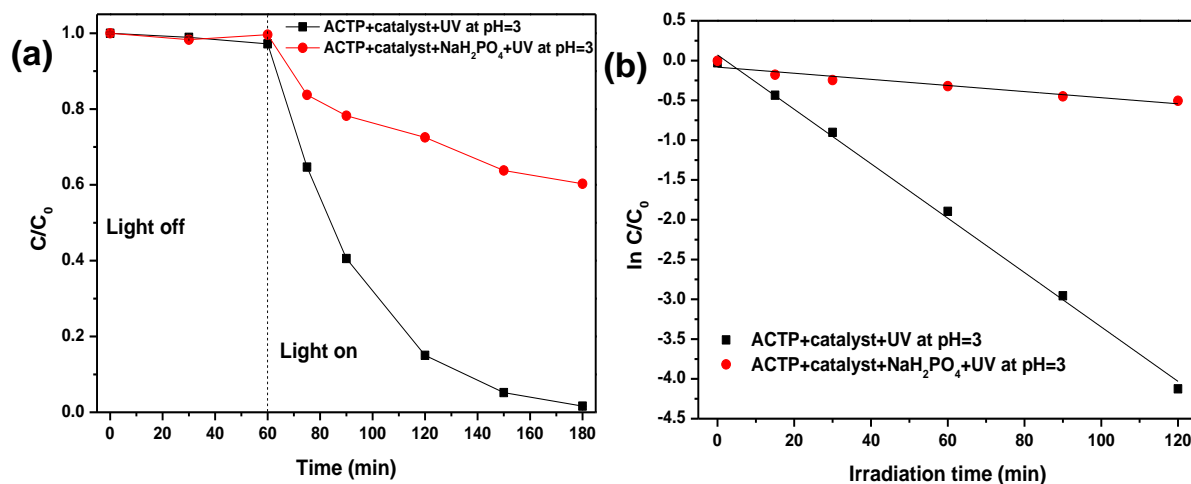


Fig.6-12 The effects of adsorption and photocatalytic degradation of ACTP after the addition of NaH₂PO₄•H₂O (a) and pseudo first order kinetics (b)

Conditions: [ACTP]= 50 μ M, [NaH₂PO₄•H₂O]= 2 mM, [catalyst]= 0.3 g/L, pH=3

6.8. Second order reaction constant between ACTP and HO•, SO₄•⁻ radicals

To determine the second order constant between ACTP and HO• at pH 5.4, laser flash photolysis was adopted and the method was shown in section 3.6. Under 266 nm laser excitation of ACTP alone, there is no detected transition species in the solution between 300-600 nm (Δ 20 nm). The determination of $k_{ACTP,HO\cdot}$ was based on the Eq.15-18, and obtained by following the absorbance of SCN• at 475 nm with different concentration of ACTP added. The absorbance decreased from 0.021 to 0.006 when ACTP concentration increased from 0 to 2.33×10^{-4} M, because ACTP competes with SCN⁻ for the reaction of HO•. The slope “a” can be obtained from the linear regression of Abs₀/Abs versus different ACTP concentrations (see Fig.6-13), and it was 11276. Thus the second order constant $k_{ACTP,HO\cdot}$ can be evaluated from the product of “a”, concentration of SCN⁻ (1×10^{-4} M) and $k_{HO\cdot,SCN^-} = 1.2 \times 10^{10} \text{ s}^{-1}$, finally it was calculated to be $1.35 \times 10^{10} \text{ M}^{-1} \text{ s}^{-1}$.





A chemical competition method was adopted to determine the second order constant between ACTP and sulfate radical, and bisphenol A (BPA) was used as the reference compound (see Fig.6-14), $k_{\text{SO}_4\cdot-, \text{BPA}} = 1.5 \times 10^9 \text{ M}^{-1} \text{ s}^{-1}$ has been determined in previous studies^{74, 257, 258}. For this experiment, the initial concentration of BPA was 50 μM in the presence of 50 μM ACTP and 1 mM $\text{Na}_2\text{S}_2\text{O}_8$ under UV irradiation at pH 5.4 for 240 min. At this pH conditions, sulfate radical was the predominant radicals, and there was negligible hydroxyl radical formation¹¹². Then the concentration of BPA and ACTP were obtained at different treatment time intervals and the degradation rate constants of ACTP with sulfate radical were calculated using the above degradation rate constant of BPA and the following equation. Finally, $k_{\text{SO}_4\cdot-, \text{ACTP}} = (1.94 \pm 0.1) \times 10^9 \text{ M}^{-1} \text{ s}^{-1}$ was determined.

$$k_{\text{ACTP}, \text{SO}_4\cdot-} = k_{\text{BPA}, \text{SO}_4\cdot-} \times \left[\frac{\text{Ln}\left(\frac{[\text{ACTP}]_t}{[\text{ACTP}]_0}\right)}{\text{Ln}\left(\frac{[\text{BPA}]_t}{[\text{BPA}]_0}\right)} \right] \quad (\text{R6-19})$$

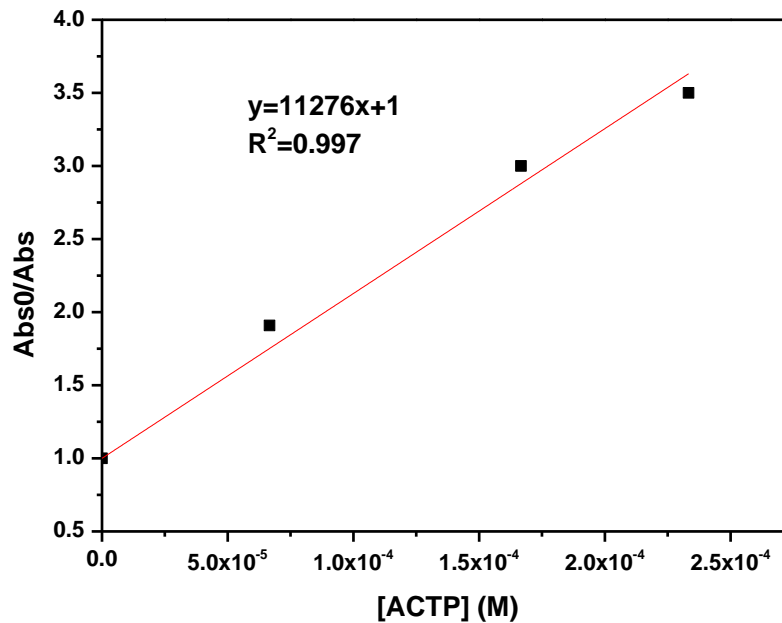


Fig.6-13 Linear regression of Abs₀/Abs versus different ACTP concentrations

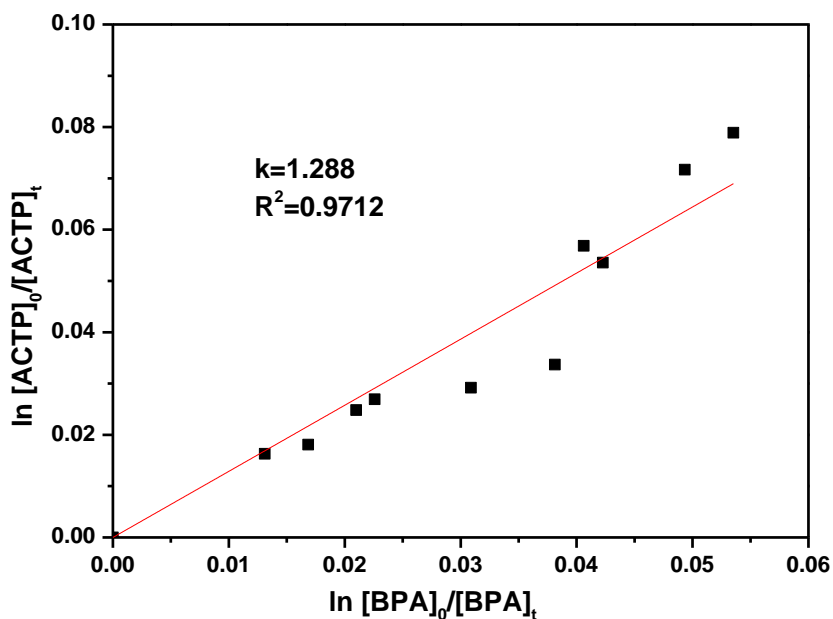


Fig.6-14 The second order constant between ACTP with $\text{SO}_4^{\bullet-}$ decided by competition with BPA

Conditions: $[\text{ACTP}] = [\text{BPA}] = 50 \mu\text{M}$ $[\text{Na}_2\text{S}_2\text{O}_8] = 1 \text{ mM}$, $\text{pH} = 5.2$, under UV

6.9. Conclusion

In this work, different homogeneous and heterogeneous AOPs were adopted to the degradation of ACTP, which were all based on the UV irradiation. Firstly, ACTP was stable alone in solution, while it showed a rapid oxidation when mixed with H_2O_2 and $\text{Na}_2\text{S}_2\text{O}_8$ when pH exceeded 10, indicating easily reacts with ionic form. Faster degradation rate was observed at pH 5.4 in UV/ H_2O_2 and at pH 9.5 in UV/ $\text{Na}_2\text{S}_2\text{O}_8$. The addition of chloride ions (10 mM) had negligible effects on these two systems, while low concentrated iodide ions can accelerate the degradation. This trend was attributed to the fact that reactive halogenated species reacted more selectively than hydroxyl radicals with electron-rich organic pollutants such as ACTP. The addition of Fe(III)-EDDS greatly increased the degradation rate in a short time due to the fast activation between Fe(II) with H_2O_2 and $\text{Na}_2\text{S}_2\text{O}_8$. ACTP showed fastest removal rate at pH 7.5 in UV/ H_2O_2 /Fe(III)-EDDS and at pH 3.2 in UV/ $\text{Na}_2\text{S}_2\text{O}_8$ /Fe(III)-EDDS,

which can be attributed to the photochemical properties of Fe(III)-EDDS under different pH. Secondly, in the heterogeneous photocatalytic degradation of ACTP, $\text{BiOCl}_{0.75}\text{I}_{0.25}$ was taken as a semiconductor catalyst we synthesized before. ACTP showed the fastest removal at pH 3, because acidic solution favored the transformation of electrons to the surface of catalyst, followed with closed to the surface. $k_{\text{ACTP},\text{HO}\cdot}$ was determined by LFP to be $1.35 \times 10^{10} \text{ M}^{-1} \text{ s}^{-1}$, and $k_{\text{SO}_4^{\cdot-},\text{ACTP}}$ was determined to be $(1.94 \pm 0.1) \times 10^9 \text{ M}^{-1} \text{ s}^{-1}$ when competing with BPA.

7. Conclusion

In my PhD work, different homogenous and heterogeneous AOPs efficiency were investigated using representative pharmaceutical pollutants: ACTP and *p*-HPA. The interfacial mechanism was proposed in the BiOCl_{0.75}I_{0.25} based photocatalytic degradation. In the Fe(III)-EDDS activated photo-Fenton and PS reactions, the different degradation efficiencies were evaluated under same conditions.

Firstly, BiOCl_{0.75}I_{0.25} has been prepared by precipitation method in EG-H₂O mixed solvent. The as-prepared samples showed 3D flower-like morphology, possessing great surface area 34.93 m² g⁻¹ and narrow band-gap 2.12 eV. Furthermore, adsorption and photocatalytic degradation of *p*-HPA by BiOCl_{0.75}I_{0.25} in water have been investigated. Interfacial mechanism experiments reveal that photocatalytic degradation of *p*-HPA occurred mainly on the catalyst surface. pH strongly affects the adsorption percentage and degradation rate through changing the surface charge of catalyst and molecular form of *p*-HPA. *p*-HPA showed the maximum adsorption at pH 4.5 (Natural pH) which can be ascribed to the electrostatic attraction occurred between the positively charged *p*-HPA and negatively charged BiOCl_{0.75}I_{0.25}. While, *p*-HPA exhibited the fastest degradation rate at pH 3. Dissolved oxygen concentration is determined to be a key parameter necessary to generate HO₂[•]/O₂^{•-}, the main active species responsible for the pollutant degradation, which was identified by quenching experiment. Na₂S₂O₈ showed synergistic effect with BiOCl_{0.75}I_{0.25} under UV irradiation by supplying SO₄^{•-} radicals. BiOCl_{0.75}I_{0.25} shows promising *p*-HPA removal abilities but some photo-generated by-products still adsorbed on the surface of catalyst, seems not degraded. This photocatalyst, generating mainly HO₂[•]/O₂^{•-}, is very promising and can have strong implication in the treatment of polluted media in which hydroxyl radical should be strongly scavenged by organic matter or inorganic constituents. Furthermore, the problem of recycle use needs to be solved in the future.

Secondly, the different activation efficiency of H₂O₂ and persulfate (PS) by Fe(III)-EDDS under irradiation to produce HO[•] and SO₄^{•-} under same conditions

were investigated in detail. Firstly, second order constant $k_{p\text{-HPA},\text{HO}\cdot}$ and $k_{p\text{-HPA},\text{SO}_4\cdot^-}$ were determined by LFP at different pH. Result showed that both $k_{p\text{-HPA},\text{HO}\cdot}$ and $k_{p\text{-HPA},\text{SO}_4\cdot^-}$ are higher at pH 2.5 than pH 8.5. Photo-Fenton (Fe(III)-EDDS/H₂O₂/UV) reaction was much faster than Fenton-like (Fe(III)-EDDS/H₂O₂, $k_{\text{Fe(III),H}_2\text{O}_2}=0.02 \text{ M}^{-1}\text{s}^{-1}$) ascribing to the fast formation of Fe(II) under irradiation. Under same conditions, Fe(III)-EDDS possessed lower activating efficiency of Na₂S₂O₈ compared with H₂O₂ which can be due to the fact that the $k_{\text{Na}_2\text{S}_2\text{O}_8\cdot\text{Fe(II)}}= 20\text{-}27 \text{ M}^{-1} \text{ s}^{-1}$ is more than three times smaller than $k_{\text{H}_2\text{O}_2\cdot\text{Fe(II)}}=76 \text{ M}^{-1} \text{ s}^{-1}$. In addition, the lower efficiency of Na₂S₂O₈ can also be due to the second order rate constants between *p*-HPA with HO[•] or SO₄^{•-}, $k_{p\text{-HPA},\text{HO}\cdot}$ was higher than $k_{p\text{-HPA},\text{SO}_4\cdot^-}$ at both acidic and alkaline solutions. The initial degradation rate of *p*-HPA ($R_{p\text{-HPA}}$) increased from $1.49\times 10^{-7} \text{ M s}^{-1}$ to $3.76\times 10^{-7} \text{ M s}^{-1}$ when H₂O₂ concentrations were ranging from 50 μM to 1 mM, indicating that H₂O₂ dosage was the limiting parameter. The effect of Na₂S₂O₈ concentrations was similar to H₂O₂, the degradation rate was always increasing, and the increase rate seemed unchanged between these concentrations. Using the same H₂O₂ and Na₂S₂O₈ concentrations, the removal percentage of *p*-HPA increased when Fe(III)-EDDS concentration increased from 50 to 250 μM. Then it decreased when further increased Fe(III)-EDDS concentration to 1 mM due to the scavenging effects of EDDS. The pH influence on the Fe(III)-EDDS/H₂O₂/UV and Fe(III)-EDDS/Na₂S₂O₈/UV processes during the initial stage are evidently different. In Fe(III)-EDDS/H₂O₂/UV reaction, *p*-HPA degradation efficiency increased fast from pH 2.5 to 7.5, then it began to decrease when pH increased to 9.0. While $R_{p\text{-HPA}}$ began to decrease when pH increased to 3.9 in Fe(III)-EDDS/Na₂S₂O₈/UV. HO[•] was the main active species in photo-Fenton process, and both SO₄^{•-} and HO[•] were responsible for the degradation in Fe(III)-EDDS/Na₂S₂O₈/UV system. In general, Fe(III)-EDDS/H₂O₂/UV always showed higher degradation efficiency than Fe(III)-EDDS/Na₂S₂O₈/UV in different pH solutions, especially in neutral and basic solution. Fe(III)-EDDS was a promising iron complex in practical wastewater treatment in natural conditions.

Finally, different homogeneous and heterogeneous AOPs based on the UV

irradiation were investigated to archive the degradation of ACTP. Firstly, blank experiments in dark showed that ACTP was stable alone in solution, while it can be rapidly oxidized when mixed with H_2O_2 and $\text{Na}_2\text{S}_2\text{O}_8$ when pH exceeded 10, indicating that it was easily destroyed in ionic form. Under UV irradiation, it showed fastest degradation rate at pH 5.4 in UV/ H_2O_2 and at pH 9.5 in UV/ $\text{Na}_2\text{S}_2\text{O}_8$. The addition of chloride ions (10 mM) had negligible effects on these two systems. While low concentrated iodide ions can accelerate the degradation efficiencies, which can be ascribed to the fact that reactive halogenated species reacted more selectively than hydroxyl radicals with electron-rich organic pollutants like ACTP. The addition of Fe(III)-EDDS greatly increased the degradation rate in a short time due to the fast activation between Fe(II) with H_2O_2 and $\text{Na}_2\text{S}_2\text{O}_8$. ACTP showed fastest removal rate at pH 7.5 in UV/ H_2O_2 /Fe(III)-EDDS and at pH 3.2 in UV/ $\text{Na}_2\text{S}_2\text{O}_8$ /Fe(III)-EDDS, which can be attributed to the special photochemical properties of Fe(III)-EDDS under different pH. Secondly, in the heterogeneous photocatalytic degradation of ACTP, $\text{BiOCl}_{0.75}\text{I}_{0.25}$ was taken as a semiconductor catalyst we synthesized before. ACTP had the fastest removal rate at pH 3, because acidic solution favored the transformation of electrons to the surface of catalyst, followed with the formation of $\text{HO}_2^\bullet/\text{O}_2^{\bullet-}$, which was the main active species prevailed. Interfacial mechanism research indicated that the degradation occurred mainly on the surface of catalyst or in the bulk solution that closed to the surface. $k_{\text{ACTP},\text{HO}^\bullet}$ was determined by LFP to be $1.35 \times 10^{10} \text{ M}^{-1} \text{ s}^{-1}$, and $k_{\text{SO}_4^{2-},\text{ACTP}}$ was determined to be $(1.94 \pm 0.1) \times 10^9 \text{ M}^{-1} \text{ s}^{-1}$ when competing with BPA. Homogeneous AOPs than involved Fe(III)-EDDS and heterogeneous AOPs that used $\text{BiOCl}_{0.75}\text{I}_{0.25}$ both had good response to simulated solar light, and can remove ACTP effectively. Fe(III)-EDDS induced degradation was fast, efficient and effective, while it has the risk to expose some ions like Fe(III) or SO_4^{2-} to water. $\text{BiOCl}_{0.75}\text{I}_{0.25}$ induced heterogeneous degradation was relatively mild and clean, however, recycling problem need to be solved before its practical application.

Reference

1. Zhang, X.; Zhao, H. X.; Du, J.; Qu, Y. X.; Shen, C.; Tan, F.; Chen, J. W.; Quan, X., Occurrence, removal, and risk assessment of antibiotics in 12 wastewater treatment plants from Dalian, China. *Environ. Sci. Pollut. Res.* **2017**, *24*, (19), 16478-16487.
2. Fram, M. S.; Belitz, K., Occurrence and concentrations of pharmaceutical compounds in groundwater used for public drinking-water supply in California. *Sci. Total Environ.* **2011**, *409*, (18), 3409-3417.
3. Gibs, J.; Heckathorn, H. A.; Meyer, M. T.; Klapinski, F. R.; Alebus, M.; Lippincott, R. L., Occurrence and partitioning of antibiotic compounds found in the water column and bottom sediments from a stream receiving two wastewater treatment plant effluents in Northern New Jersey, 2008. *Sci. Total Environ.* **2013**, *458*, 107-116.
4. Zhang, R. F.; Eggleston, K.; Rotimi, V.; Zeckhauser, R. J., Antibiotic resistance as a global threat: Evidence from China, Kuwait and the United States. *Globalization and Health* **2006**, *2*.
5. Zhou, P.; Su, C. Y.; Li, B. W.; Yi, Q., Treatment of high-strength pharmaceutical wastewater and removal of antibiotics in anaerobic and aerobic biological treatment processes. *Journal of Environmental Engineering-Asce* **2006**, *132*, (1), 129-136.
6. Zuccato, E.; Calamari, D.; Natangelo, M.; Fanelli, R., Presence of therapeutic drugs in the environment. *The Lancet* **2000**, *355*, (9217), 1789-1790.
7. Terzic, S.; Senta, I.; Ahel, M.; Gros, M.; Petrovic, M.; Barcelo, D.; Muller, J.; Knepper, T.; Marti, I.; Ventura, F.; Jovancic, P.; Jabucar, D., Occurrence and fate of emerging wastewater contaminants in Western Balkan Region. *Sci. Total Environ.* **2008**, *399*, (1-3), 66-77.
8. Jelic, A.; Gros, M.; Ginebreda, A.; Cespedes-Sánchez, R.; Ventura, F.; Petrovic, M.; Barcelo, D., Occurrence, partition and removal of pharmaceuticals in sewage water and sludge during wastewater treatment. *Water Res.* **2011**, *45*, (3), 1165-1176.
9. Radjenović, J.; Petrović, M.; Barceló, D.; Petrović, M., Advanced mass spectrometric methods applied to the study of fate and removal of pharmaceuticals in wastewater treatment. *TrAC Trends in Analytical Chemistry* **2007**, *26*, (11), 1132-1144.
10. Radjenovic, J.; Petrovic, M.; Barcelo, D., Fate and distribution of pharmaceuticals in wastewater and sewage sludge of the conventional activated sludge (CAS) and

- advanced membrane bioreactor (MBR) treatment. *Water Res* **2009**, *43*, (3), 831-41.
11. Gibson, R.; Duran-Alvarez, J. C.; Estrada, K. L.; Chavez, A.; Cisneros, B. J., Accumulation and leaching potential of some pharmaceuticals and potential endocrine disruptors in soils irrigated with wastewater in the Tula Valley, Mexico. *Chemosphere* **2010**, *81*, (11), 1437-1445.
12. Chen, F.; Ying, G. G.; Kong, L. X.; Wang, L.; Zhao, J. L.; Zhou, L. J.; Zhang, L. J., Distribution and accumulation of endocrine-disrupting chemicals and pharmaceuticals in wastewater irrigated soils in Hebei, China. *Environ Pollut* **2011**, *159*, (6), 1490-1498.
13. Kinney, C. A.; Furlong, E. T.; Kolpin, D. W.; Burkhardt, M. R.; Zaugg, S. D.; Werner, S. L.; Bossio, J. P.; Benotti, M. J., Bioaccumulation of Pharmaceuticals and Other Anthropogenic Waste Indicators in Earthworms from Agricultural Soil Amended With Biosolid or Swine Manure. *Environ. Sci. Technol.* **2008**, *42*, (6), 1863-1870.
14. Wu, C. X.; Spongberg, A. L.; Witter, J. D.; Fang, M.; Czajkowski, K. P., Uptake of Pharmaceutical and Personal Care Products by Soybean Plants from Soils Applied with Biosolids and Irrigated with Contaminated Water. *Environ. Sci. Technol.* **2010**, *44*, (16), 6157-6161.
15. Ho, Y. B.; Zakaria, M. P.; Latif, P. A.; Saari, N., Simultaneous determination of veterinary antibiotics and hormone in broiler manure, soil and manure compost by liquid chromatography-tandem mass spectrometry. *Journal of Chromatography A* **2012**, *1262*, 160-168.
16. Gurr, C. J.; Reinhard, M., Harnessing natural attenuation of pharmaceuticals and hormones in rivers. *Environ. Sci. Technol.* **2006**, *40*, (9), 2872-2876.
17. Phan, T. P. H.; Managaki, S.; Nakada, N.; Takada, H.; Shimizu, A.; Anh, D. H.; Viet, P. H.; Suzuki, S., Antibiotic contamination and occurrence of antibiotic-resistant bacteria in aquatic environments of northern Vietnam. *Sci. Total Environ.* **2011**, *409*, (15), 2894-2901.
18. Brown, K. D.; Kulis, J.; Thomson, B.; Chapman, T. H.; Mawhinney, D. B., Occurrence of antibiotics in hospital, residential, and dairy, effluent, municipal wastewater, and the Rio Grande in New Mexico. *Sci. Total Environ.* **2006**, *366*, (2-3), 772-783.
19. Kleywegt, S.; Pileggi, V.; Yang, P.; Hao, C.; Zhao, X.; Rocks, C.; Thach, S.; Cheung, P.; Whitehead, B., Pharmaceuticals, hormones and bisphenol A in untreated

- source and finished drinking water in Ontario, Canada — Occurrence and treatment efficiency. *Sci. Total Environ.* **2011**, *409*, (8), 1481-1488.
20. Van Stempvoort, D. R.; Roy, J. W.; Grabuski, J.; Brown, S. J.; Bickerton, G.; Sverko, E., An artificial sweetener and pharmaceutical compounds as co-tracers of urban wastewater in groundwater. *Sci. Total Environ.* **2013**, *461*, 348-359.
21. Martin, J.; Camacho-Munoz, D.; Santos, J. L.; Aparicio, I.; Alonso, E., Occurrence of pharmaceutical compounds in wastewater and sludge from wastewater treatment plants: Removal and ecotoxicological impact of wastewater discharges and sludge disposal. *J. Hazard. Mater.* **2012**, *239*, 40-47.
22. Al Aukidy, M.; Verlicchi, P.; Jelic, A.; Petrovic, M.; Barcelo, D., Monitoring release of pharmaceutical compounds: Occurrence and environmental risk assessment of two WWTP effluents and their receiving bodies in the Po Valley, Italy. *Sci. Total Environ.* **2012**, *438*, 15-25.
23. Calderon-Preciado, D.; Matamoros, V.; Bayona, J. M., Occurrence and potential crop uptake of emerging contaminants and related compounds in an agricultural irrigation network. *Sci. Total Environ.* **2011**, *412*, 14-19.
24. Lopez-Serna, R.; Petrovic, M.; Barcelo, D., Occurrence and distribution of multi-class pharmaceuticals and their active metabolites and transformation products in the Ebro River basin (NE Spain). *Sci. Total Environ.* **2012**, *440*, 280-289.
25. Loos, R.; Locoro, G.; Comero, S.; Contini, S.; Schwesig, D.; Werres, F.; Balsaa, P.; Gans, O.; Weiss, S.; Blaha, L.; Bolchi, M.; Gawlik, B. M., Pan-European survey on the occurrence of selected polar organic persistent pollutants in ground water. *Water Res.* **2010**, *44*, (14), 4115-4126.
26. Sim, W. J.; Lee, J. W.; Lee, E. S.; Shin, S. K.; Hwang, S. R.; Oh, J. E., Occurrence and distribution of pharmaceuticals in wastewater from households, livestock farms, hospitals and pharmaceutical manufactures. *Chemosphere* **2011**, *82*, (2), 179-186.
27. Fang, T. H.; Nan, F. H.; Chin, T. S.; Feng, H. M., The occurrence and distribution of pharmaceutical compounds in the effluents of a major sewage treatment plant in Northern Taiwan and the receiving coastal waters. *Marine Pollution Bulletin* **2012**, *64*, (7), 1435-1444.
28. Zhang, J. C.; Giorno, L.; Drioli, E., Study of a hybrid process combining PACs and membrane operations for antibiotic wastewater treatment. *Desalination* **2006**, *194*, (1-3), 101-107.
29. Chen, Z.; Ren, N.; Wang, A.; Zhang, Z. P.; Shi, Y., A novel application of

TPAD-MBR system to the pilot treatment of chemical synthesis-based pharmaceutical wastewater. *Water Res.* **2008**, *42*, (13), 3385-3392.

30. Ng, K. K.; Shi, X.; Tang, M. K. Y.; Ng, H. Y., A novel application of anaerobic bio-entrapped membrane reactor for the treatment of chemical synthesis-based pharmaceutical wastewater. *Sep. Purif. Technol.* **2014**, *132*, 634-643.

31. Mendez-Arriaga, F.; Esplugas, S.; Gimenez, J., Photocatalytic degradation of non-steroidal anti-inflammatory drugs with TiO₂ and simulated solar irradiation. *Water Res.* **2008**, *42*, (3), 585-594.

32. Taheran, M.; Naghdi, M.; Brar, S. K.; Knystautas, E. J.; Verma, M.; Surampalli, R. Y., Degradation of chlortetracycline using immobilized laccase on Polyacrylonitrile-biochar composite nanofibrous membrane. *Sci. Total Environ.* **2017**, *605*, 315-321.

33. Wu, F.; Huang, H. W.; Xu, T. F.; Lu, W. Y.; Li, N.; Chen, W. X., Visible-light-assisted peroxymonosulfate activation and mechanism for the degradation of pharmaceuticals over pyridyl-functionalized graphitic carbon nitride coordinated with iron phthalocyanine. *Appl. Catal. B* **2017**, *218*, 230-239.

34. Zhang, Y.; Hu, S. Q.; Zhang, H. C.; Shen, G. X.; Yuan, Z. J.; Zhang, W., Degradation kinetics and mechanism of sulfadiazine and sulfamethoxazole in an agricultural soil system with manure application. *Sci. Total Environ.* **2017**, *607*, 1348-1356.

35. Adityosulindro, S.; Barthe, L.; Gonzalez-Labrada, K.; Haza, U. J. J.; Delmas, H.; Julcour, C., Sonolysis and sono-Fenton oxidation for removal of ibuprofen in (waste) water. *Ultrasonics Sonochemistry* **2017**, *39*, 889-896.

36. Ben, W. W.; Shi, Y. W.; Li, W. W.; Zhang, Y.; Qiang, Z. M., Oxidation of sulfonamide antibiotics by chlorine dioxide in water: Kinetics and reaction pathways. *Chem. Eng. J.* **2017**, *327*, 743-750.

37. Deng, F.; Zhong, F.; Zhao, L. N.; Luo, X. B.; Luo, S. L.; Dionysiou, D. D., One-step in situ hydrothermal fabrication of octahedral CdS/SnIn₄S₈ nano-heterojunction for highly efficient photocatalytic treatment of nitrophenol and real pharmaceutical wastewater. *J. Hazard. Mater.* **2017**, *340*, 85-95.

38. Nomura, Y.; Fukahori, S.; Fukada, H.; Fujiwara, T., Removal behaviors of sulfamonomethoxine and its degradation intermediates in fresh aquaculture wastewater using zeolite/TiO₂ composites. *J. Hazard. Mater.* **2017**, *340*, 427-434.

39. Savun-Hekimoglu, B.; Ince, N. H., Decomposition of PPCPs by

- ultrasound-assisted advanced Fenton reaction: A case study with salicylic acid. *Ultrasonics Sonochemistry* **2017**, *39*, 243-249.
40. Daoud, F.; Pelzer, D.; Zuehlke, S.; Spitteller, M.; Kayser, O., Ozone pretreatment of process waste water generated in course of fluoroquinolone production. *Chemosphere* **2017**, *185*, 953-963.
41. Hussain, S.; Steter, J. R.; Gul, S.; Motheo, A. J., Photo-assisted electrochemical degradation of sulfamethoxazole using a Ti/Ru_{0.3}Ti_{0.7}O₂ anode: Mechanistic and kinetic features of the process. *Journal of Environmental Management* **2017**, *201*, 153-162.
42. Li, S. Y.; Tang, Y. M.; Chen, W. R.; Hu, Z.; Li, X. K.; Li, L. S., Heterogeneous catalytic ozonation of clofibric acid using Ce/MCM-48: Preparation, reaction mechanism, comparison with Ce/MCM-41. *Journal of Colloid and Interface Science* **2017**, *504*, 238-246.
43. Serna-Galvis, E. A.; Ferraro, F.; Silva-Agredo, J.; Torres-Palma, R. A., Degradation of highly consumed fluoroquinolones, penicillins and cephalosporins in distilled water and simulated hospital wastewater by UV254 and UV254/persulfate processes. *Water Res.* **2017**, *122*, 128-138.
44. Hofman-Caris, C. H. M.; Siegers, W. G.; van de Merlen, K.; de Man, A. W. A.; Hofman, J., Removal of pharmaceuticals from WWTP effluent: Removal of EfOM followed by advanced oxidation. *Chem. Eng. J.* **2017**, *327*, 514-521.
45. Radjenovic, J.; Petrovic, M.; Barcelo, D., Analysis of pharmaceuticals in wastewater and removal using a membrane bioreactor. *Analytical and bioanalytical chemistry* **2007**, *387*, (4), 1365-77.
46. Yamamoto, T.; Toyoda, N., In-situ Adsorption of Polymer Particles on Multi-wall Carbon Nanotubes Using Colloidal Techniques. *Colloid and Interface Science Communications* **2017**, *20*, (Supplement C), 1-4.
47. Bahamon, D.; Carro, L.; Guri, S.; Vega, L. F., Computational study of ibuprofen removal from water by adsorption in realistic activated carbons. *Journal of Colloid and Interface Science* **2017**, *498*, (Supplement C), 323-334.
48. Álvarez-Torrellas, S.; Peres, J. A.; Gil-Álvarez, V.; Ovejero, G.; García, J., Effective adsorption of non-biodegradable pharmaceuticals from hospital wastewater with different carbon materials. *Chem. Eng. J.* **2017**, *320*, (Supplement C), 319-329.
49. Benitez, F. J.; Acero, J. L.; Real, F. J.; Rubio, F. J.; Leal, A. I., The role of hydroxyl radicals for the decomposition of p-hydroxy phenylacetic acid in aqueous

- solutions. *Water Res.* **2001**, *35*, (5), 1338-1343.
50. Miranda, M. A.; Marín, M. a. L.; Amat, A. M.; Arques, A.; Seguí, S., Pyrylium salt-photosensitized degradation of phenolic contaminants present in olive oil wastewater with solar light: Part III. Tyrosol and p-hydroxyphenylacetic acid. *Appl. Catal., B* **2002**, *35*, (3), 167-174.
51. Sanchez, I.; Stüber, F.; Fabregat, A.; Font, J.; Fortuny, A.; Bengoa, C., Degradation of model olive mill contaminants of OMW catalysed by zero-valent iron enhanced with a chelant. *J. Hazard. Mater.* **2012**, *199–200*, 328-335.
52. Minh, D. P.; Aubert, G.; Gallezot, P.; Besson, M., Degradation of olive oil mill effluents by catalytic wet air oxidation: 2-Oxidation of p-hydroxyphenylacetic and p-hydroxybenzoic acids over Pt and Ru supported catalysts. *Appl. Catal. B* **2007**, *73*, (3-4), 236-246.
53. Flores, N.; Sirés, I.; Rodríguez, R. M.; Centellas, F.; Cabot, P. L.; Garrido, J. A.; Brillas, E., Removal of 4-hydroxyphenylacetic acid from aqueous medium by electrochemical oxidation with a BDD anode: Mineralization, kinetics and oxidation products. *Journal of Electroanalytical Chemistry* **2016**.
54. Flores, N.; Cabot, P. L.; Centellas, F.; Garrido, J. A.; Rodríguez, R. M.; Brillas, E.; Sires, I., 4-Hydroxyphenylacetic acid oxidation in sulfate and real olive oil mill wastewater by electrochemical advanced processes with a boron-doped diamond anode. *J Hazard Mater* **2017**, *321*, 566-575.
55. Kim, Y.; Choi, K.; Jung, J.; Park, S.; Kim, P.-G.; Park, J., Aquatic toxicity of acetaminophen, carbamazepine, cimetidine, diltiazem and six major sulfonamides, and their potential ecological risks in Korea. *Environment International* **2007**, *33*, (3), 370-375.
56. Tan, C.; Gao, N.; Zhou, S.; Xiao, Y.; Zhuang, Z., Kinetic study of acetaminophen degradation by UV-based advanced oxidation processes. *Chem. Eng. J.* **2014**, *253*, 229-236.
57. Zhang, X.; Wu, F.; Wu, X.; Chen, P.; Deng, N., Photodegradation of acetaminophen in TiO₂ suspended solution. *J Hazard Mater* **2008**, *157*, (2-3), 300-7.
58. Andreozzi, R.; Caprio, V.; Marotta, R.; Vogna, D., Paracetamol oxidation from aqueous solutions by means of ozonation and H₂O₂/UV system. *Water Res.* **2003**, *37*, (5), 993-1004.
59. de Luna, M. D. G.; Veciana, M. L.; Su, C.-C.; Lu, M.-C., Acetaminophen

- degradation by electro-Fenton and photoelectro-Fenton using a double cathode electrochemical cell. *J. Hazard. Mater.* **2012**, *217*, 200-207.
60. de Luna, M. D. G.; Briones, R. M.; Su, C.-C.; Lu, M.-C., Kinetics of acetaminophen degradation by Fenton oxidation in a fluidized-bed reactor. *Chemosphere* **2013**, *90*, (4), 1444-1448.
61. Su, C.-C.; Bellotindos, L. M.; Chang, A.-T.; Lu, M.-C., Degradation of acetaminophen in an aerated Fenton reactor. *Journal of the Taiwan Institute of Chemical Engineers* **2013**, *44*, (2), 310-316.
62. Trovo, A. G.; Pupo Nogueira, R. F.; Aguera, A.; Fernandez-Alba, A. R.; Malato, S., Paracetamol degradation intermediates and toxicity during photo-Fenton treatment using different iron species. *Water Res* **2012**, *46*, (16), 5374-80.
63. Yang, Y.; Zhang, G.; Yu, S.; Shen, X., Efficient removal of organic contaminants by a visible light driven photocatalyst Sr₆Bi₂O₉. *Chem. Eng. J.* **2010**, *162*, (1), 171-177.
64. Pignatello, J. J.; Oliveros, E.; MacKay, A., Advanced oxidation processes for organic contaminant destruction based on the Fenton reaction and related chemistry. *Crit. Rev. Env. Sci. Tec.* **2006**, *36*, (1), 1-84.
65. Sherwood, M. K.; Cassidy, D. P., Modified Fenton oxidation of diesel fuel in arctic soils rich in organic matter and iron. *Chemosphere* **2014**, *113*, 56-61.
66. Giannakis, S.; Liu, S.; Carratalà, A.; Rtimi, S.; Bensimon, M.; Pulgarin, C., Effect of Fe(II)/Fe(III) species, pH, irradiance and bacterial presence on viral inactivation in wastewater by the photo-Fenton process: Kinetic modeling and mechanistic interpretation. *Appl. Catal. B* **2017**, *204*, 156-166.
67. Wu, Y.; Bianco, A.; Brigante, M.; Dong, W.; de Sainte-Claire, P.; Hanna, K.; Mailhot, G., Sulfate Radical Photogeneration Using Fe-EDDS: Influence of Critical Parameters and Naturally Occurring Scavengers. *Environ Sci Technol* **2015**, *49*, (24), 14343-9.
68. Parsons, S., Advanced oxidation processes for water and wastewater treatment. *Water Intelligence Online* **2005**, *4*, 9781780403076.
69. Nie, M.; Yan, C.; Li, M.; Wang, X.; Bi, W.; Dong, W., Degradation of chloramphenicol by persulfate activated by Fe²⁺ and zerovalent iron. *Chem. Eng. J.* **2015**, *279*, 507-515.
70. Nie, M.; Yang, Y.; Zhang, Z.; Yan, C.; Wang, X.; Li, H.; Dong, W., Degradation of chloramphenicol by thermally activated persulfate in aqueous solution. *Chem. Eng. J.*

2014, 246, 373-382.

71. Brillas, E.; Sires, I.; Oturan, M. A., Electro-Fenton Process and Related Electrochemical Technologies Based on Fenton's Reaction Chemistry. *Chemical Reviews* **2009**, 109, (12), 6570-6631.

72. Huang, D.; Hu, C.; Zeng, G.; Cheng, M.; Xu, P.; Gong, X.; Wang, R.; Xue, W., Combination of Fenton processes and biotreatment for wastewater treatment and soil remediation. *Sci. Total Environ.* **2017**, 574, 1599-1610.

73. Li, Y.; Song, W.; Fu, W.; Tsang, D. C. W.; Yang, X., The roles of halides in the acetaminophen degradation by UV/H₂O₂ treatment: Kinetics, mechanisms, and products analysis. *Chem. Eng. J.* **2015**, 271, 214-222.

74. Sanchez-Polo, M.; Abdel daiem, M. M.; Ocampo-Perez, R.; Rivera-Utrilla, J.; Mota, A. J., Comparative study of the photodegradation of bisphenol A by HO(•), SO₄(•-) and CO₃(•-)/HCO₃ radicals in aqueous phase. *Sci Total Environ* **2013**, 463-464, 423-31.

75. Andreozzi, R.; Caprio, V.; Marotta, R.; Radovnikovic, A., Ozonation and H₂O₂/UV treatment of clofibric acid in water: a kinetic investigation. *J. Hazard. Mater.* **2003**, 103, (3), 233-246.

76. Hua, W.; Bennett, E. R.; Letcher, R. J., Ozone treatment and the depletion of detectable pharmaceuticals and atrazine herbicide in drinking water sourced from the upper Detroit River, Ontario, Canada. *Water Res.* **2006**, 40, (12), 2259-2266.

77. Xiong, P.; Hu, J., Degradation of acetaminophen by UVA/LED/TiO₂ process. *Sep. Purif. Technol.* **2012**, 91, 89-95.

78. Doll, T. E.; Frimmel, F. H., Photocatalytic degradation of carbamazepine, clofibric acid and iomeprol with P25 and Hombikat UV100 in the presence of natural organic matter (NOM) and other organic water constituents. *Water Res.* **2005**, 39, (2-3), 403-411.

79. Perez-Estrada, L. A.; Maldonado, M. I.; Gernjak, W.; Aguera, A.; Fernandez-Alba, A. R.; Ballesteros, M. M.; Malato, S., Decomposition of diclofenac by solar driven photocatalysis at pilot plant scale. *Cata. Today* **2005**, 101, (3-4), 219-226.

80. Arredondo Valdez, H. C.; Garc ía Jim énez, G.; Guti érez Granados, S.; Ponce de Le ón, C., Degradation of paracetamol by advance oxidation processes using modified reticulated vitreous carbon electrodes with TiO₂ and CuO/TiO₂/Al₂O₃. *Chemosphere* **2012**, 89, (10), 1195-1201.

81. Ghasemian, S.; Nasuhoglu, D.; Omanovic, S.; Yargeau, V., Photoelectrocatalytic degradation of pharmaceutical carbamazepine using Sb-doped Sn80%-W20%-oxide electrodes. *Sep. Purif. Technol.* **2017**, *188*, (Supplement C), 52-59.
82. Zhang, W.; Xiao, X.; An, T.; Song, Z.; Fu, J.; Sheng, G.; Cui, M., Kinetics, degradation pathway and reaction mechanism of advanced oxidation of 4-nitrophenol in water by a UV/H₂O₂ process. *Journal of Chemical Technology & Biotechnology* **2003**, *78*, (7), 788-794.
83. Fujishima, A.; Zhang, X. T.; Tryk, D. A., TiO₂ photocatalysis and related surface phenomena. *Surface Science Reports* **2008**, *63*, (12), 515-582.
84. Sangchay, W.; Sikong, L.; Kooptarnond, K., Comparison of photocatalytic reaction of commercial P25 and synthetic TiO₂-AgCl nanoparticles. *Procedia Engineering* **2012**, *32*, (Supplement C), 590-596.
85. Wang, C.; Hu, B., Photoelectric properties of ZnS/Au/ZnS transparent conductive tri-layer films. *Optics & Laser Technology* **2017**, *94*, (Supplement C), 217-220.
86. Yan, Z.-g.; Lars T. Andersson*, S., Catalytic oxidation of toluene over V₂O₅-WO₃ catalysts. *Applied Catalysis* **1990**, *66*, (1), 149-165.
87. Li, G.; Qin, F.; Wang, R.; Xiao, S.; Sun, H.; Chen, R., BiOX (X=Cl, Br, I) nanostructures: mannitol-mediated microwave synthesis, visible light photocatalytic performance, and Cr(VI) removal capacity. *J Colloid Interface Sci* **2013**, *409*, 43-51.
88. Hernández Castillo, R.; Acosta, M.; Riech, I.; Santana-Rodríguez, G.; Mendez-Gamboa, J.; Acosta, C.; Zambrano, M., Study of ZnS/CdS structures for solar cells applications. *Optik - International Journal for Light and Electron Optics* **2017**.
89. Jung, Y.; Shin, Y. J.; Pyo, Y. D.; Cho, C. P.; Jang, J.; Kim, G., NO_x and N₂O emissions over a Urea-SCR system containing both V₂O₅-WO₃/TiO₂ and Cu-zeolite catalysts in a diesel engine. *Chem. Eng. J.* **2017**, *326*, (Supplement C), 853-862.
90. Mehraj, O.; Mir, N. A.; Pirzada, B. M.; Sabir, S., Fabrication of novel Ag₃PO₄/BiOBr heterojunction with high stability and enhanced visible-light-driven photocatalytic activity. *Appl. Surf. Sci.* **2015**, *332*, 419-429.
91. Wang, Y.; Li, X.; Wang, Y.; Fan, C., Novel visible-light AgBr/Ag₃PO₄ hybrids photocatalysts with surface plasma resonance effects. *Journal of Solid State Chemistry* **2013**, *202*, 51-56.
92. Shayegan, Z.; Lee, C.-S.; Haghghat, F., TiO₂ photocatalyst for removal of volatile organic compounds in gas phase – A review. *Chem. Eng. J.* **2017**.
93. Fang, W.; Xing, M.; Zhang, J., Modifications on reduced titanium dioxide

photocatalysts: A review. *Journal of Photochemistry and Photobiology C: Photochemistry Reviews* **2017**, *32*, (Supplement C), 21-39.

94. Huang, W.; Brigante, M.; Wu, F.; Hanna, K.; Mailhot, G., Effect of ethylenediamine-N,N'-disuccinic acid on Fenton and photo-Fenton processes using goethite as an iron source: optimization of parameters for bisphenol A degradation. *Environ Sci Pollut Res Int* **2013**, *20*, (1), 39-50.

95. Huang, W.; Brigante, M.; Wu, F.; Hanna, K.; Mailhot, G., Development of a new homogenous photo-Fenton process using Fe(III)-EDDS complexes. *J. Photoch. Photobio. A* **2012**, *239*, 17-23.

96. Wu, Y.; Passananti, M.; Brigante, M.; Dong, W.; Mailhot, G., Fe(III)-EDDS complex in Fenton and photo-Fenton processes: from the radical formation to the degradation of a target compound. *Environ Sci Pollut Res Int* **2014**, *21*, (21), 12154-62.

97. Santos-Juanes, L.; Garc á Einschlag, F. S.; Amat, A. M.; Arques, A., Combining ZVI reduction with photo-Fenton process for the removal of persistent pollutants. *Chem. Eng. J.* **2017**, *310*, Part 2, 484-490.

98. Wu, Y.; Yuan, H.; Wei, G.; Zhang, S.; Li, H.; Dong, W., Photodegradation of 4-tert octylphenol in aqueous solution promoted by Fe(III). *Environ Sci Pollut Res Int* **2013**, *20*, (1), 3-9.

99. Miralles-Cuevas, S.; Audino, F.; Oller, I.; S á nchez-Moreno, R.; S á nchez P é rez, J. A.; Malato, S., Pharmaceuticals removal from natural water by nanofiltration combined with advanced tertiary treatments (solar photo-Fenton, photo-Fenton-like Fe(III)-EDDS complex and ozonation). *Sep. Purif. Technol.* **2014**, *122*, 515-522.

100. Rastogi, A.; Al-Abed, S. R.; Dionysiou, D. D., Effect of inorganic, synthetic and naturally occurring chelating agents on Fe(II) mediated advanced oxidation of chlorophenols. *Water Res* **2009**, *43*, (3), 684-94.

101. Park, J.-H.; Wang, J. J.; Xiao, R.; Tafti, N.; DeLaune, R. D.; Seo, D.-C., Degradation of Orange G by Fenton-like reaction with Fe-impregnated biochar catalyst. *Bioresource Technology* **2018**, *249*, 368-376.

102. Babaei, A. A.; Kakavandi, B.; Rafiee, M.; Kalantarhormizi, F.; Purkaram, I.; Ahmadi, E.; Esmaeili, S., Comparative treatment of textile wastewater by adsorption, Fenton, UV-Fenton and US-Fenton using magnetic nanoparticles-functionalized carbon (MNPs@C). *Journal of Industrial and Engineering Chemistry* **2017**, *56*, 163-174.

103. Rott, E.; Minke, R.; Bali, U.; Steinmetz, H., Removal of phosphonates from industrial wastewater with UV/FeII, Fenton and UV/Fenton treatment. *Water Res.* **2017**, *122*, 345-354.
104. Gümüş, D.; Akbal, F., Comparison of Fenton and electro-Fenton processes for oxidation of phenol. *Process Safety and Environmental Protection* **2016**, *103*, 252-258.
105. Polli, F.; Zingaretti, D.; Crognale, S.; Pesciaroli, L.; D'Annibale, A.; Petruccioli, M.; Baciocchi, R., Impact of the Fenton-like treatment on the microbial community of a diesel-contaminated soil. *Chemosphere* **2018**, *191*, 580-588.
106. Expósito, A. J.; Monteagudo, J. M.; Durán, A.; San Martín, I.; González, L., Study of the intensification of solar photo-Fenton degradation of carbamazepine with ferrioxalate complexes and ultrasound. *J. Hazard. Mater.* **2018**, *342*, 597-605.
107. Vilardi, G.; Sebastiani, D.; Miliziano, S.; Verdone, N.; Di Palma, L., Heterogeneous nZVI-induced Fenton oxidation process to enhance biodegradability of excavation by-products. *Chem. Eng. J.* **2018**, *335*, 309-320.
108. Quadrado, R. F. N.; Fajardo, A. R., Fast decolorization of azo methyl orange via heterogeneous Fenton and Fenton-like reactions using alginate-Fe²⁺/Fe³⁺ films as catalysts. *Carbohydrate Polymers* **2017**, *177*, 443-450.
109. Ji, Y.; Ferronato, C.; Salvador, A.; Yang, X.; Chovelon, J.-M., Degradation of ciprofloxacin and sulfamethoxazole by ferrous-activated persulfate: Implications for remediation of groundwater contaminated by antibiotics. *Sci. Total Environ.* **2014**, *472*, 800-808.
110. Han, D.; Wan, J.; Ma, Y.; Wang, Y.; Li, Y.; Li, D.; Guan, Z., New insights into the role of organic chelating agents in Fe(II) activated persulfate processes. *Chem. Eng. J.* **2015**, *269*, 425-433.
111. Huang, W.; Brigante, M.; Wu, F.; Mousty, C.; Hanna, K.; Mailhot, G., Assessment of the Fe(III)-EDDS complex in Fenton-like processes: from the radical formation to the degradation of bisphenol A. *Environ Sci Technol* **2013**, *47*, (4), 1952-9.
112. Fang, G.-D.; Dionysiou, D. D.; Zhou, D.-M.; Wang, Y.; Zhu, X.-D.; Fan, J.-X.; Cang, L.; Wang, Y.-J., Transformation of polychlorinated biphenyls by persulfate at ambient temperature. *Chemosphere* **2013**, *90*, (5), 1573-1580.
113. Esplugas, S.; Gimenez, J.; Contreras, S.; Pascual, E.; Rodríguez, M., Comparison of different advanced oxidation processes for phenol degradation. *Water Res.* **2002**, *36*,

(4), 1034-1042.

114. Andreozzi, R.; Caprio, V.; Insola, A.; Marotta, R., Advanced oxidation processes (AOP) for water purification and recovery. *Cata. Today* **1999**, *53*, (1), 51-59.

115. Oturan, N.; Van Hullebusch, E. D.; Zhang, H.; Mazeas, L.; Budzinski, H.; Le Menach, K.; Oturan, M. A., Occurrence and removal of organic micropollutants in landfill leachates treated by electrochemical advanced oxidation processes. *Environ. Sci. Technol.* **2015**, *49*, (20), 12187-12196.

116. Pera-Titus, M.; Garcia-Molina, V.; Baños, M. A.; Giménez, J.; Esplugas, S., Degradation of chlorophenols by means of advanced oxidation processes: a general review. *Appl. Catal. B* **2004**, *47*, (4), 219-256.

117. Rosenfeldt, E. J.; Linden, K. G., Degradation of endocrine disrupting chemicals bisphenol A, ethinyl estradiol, and estradiol during UV photolysis and advanced oxidation processes. *Environ. Sci. Technol.* **2004**, *38*, (20), 5476-5483.

118. Huber, M. M.; Canonica, S.; Park, G.-Y.; Von Gunten, U., Oxidation of pharmaceuticals during ozonation and advanced oxidation processes. *Environ. Sci. Technol.* **2003**, *37*, (5), 1016-1024.

119. Abdelmelek, S. B.; Greaves, J.; Ishida, K. P.; Cooper, W. J.; Song, W., Removal of pharmaceutical and personal care products from reverse osmosis retentate using advanced oxidation processes. *Environ. Sci. Technol.* **2011**, *45*, (8), 3665-3671.

120. Neyens, E.; Baeyens, J., A review of classic Fenton's peroxidation as an advanced oxidation technique. *J. Hazard. Mater.* **2003**, *98*, (1), 33-50.

121. Huang, W.; Brigante, M.; Wu, F.; Mousty, C.; Hanna, K.; Mailhot, G., Assessment of the Fe (III)-EDDS complex in Fenton-like processes: from the radical formation to the degradation of bisphenol A. *Environ. Sci. Technol.* **2013**, *47*, (4), 1952-1959.

122. Wu, Y.; Brigante, M.; Dong, W.; de Sainte-Claire, P.; Mailhot, G., Toward a better understanding of Fe (III)-EDDS photochemistry: Theoretical stability calculation and experimental investigation of 4-tert-butylphenol degradation. *The Journal of Physical Chemistry A* **2014**, *118*, (2), 396-403.

123. Wu, Y.; Bianco, A.; Brigante, M.; Dong, W.; de Sainte-Claire, P.; Hanna, K.; Mailhot, G., Sulfate radical photogeneration using Fe-EDDS: Influence of critical parameters and naturally occurring scavengers. *Environ. Sci. Technol.* **2015**, *49*, (24), 14343-14349.

124. Shaban, Y. A.; El Sayed, M. A.; El Maradny, A. A.; Al Farawati, R. K.; Al Zobidi,

M. I., Photocatalytic degradation of phenol in natural seawater using visible light active carbon modified (CM)-n-TiO₂ nanoparticles under UV light and natural sunlight illuminations. *Chemosphere* **2013**, *91*, (3), 307-313.

125. Tekin, H.; Bilkay, O.; Ataberk, S. S.; Balta, T. H.; Ceribasi, I. H.; Sanin, F. D.; Dilek, F. B.; Yetis, U., Use of Fenton oxidation to improve the biodegradability of a pharmaceutical wastewater. *J Hazard Mater* **2006**, *136*, (2), 258-65.

126. Karpinska, A.; Sokół, A.; Karpinska, J., Studies on the kinetics of carbamazepine degradation in aqueous matrix in the course of modified Fenton's reactions. *Journal of Pharmaceutical and Biomedical Analysis* **2015**, *106*, (Supplement C), 46-51.

127. Chen, H.; Wang, X.; Bi, W.; Wu, Y.; Dong, W., Photodegradation of carbamazepine with BiOCl/Fe₃O₄ catalyst under simulated solar light irradiation. *J Colloid Interface Sci* **2017**, *502*, 89-99.

128. Stapleton, D. R.; Emery, R. J.; Mantzavinos, D.; Papadaki, M., Photolytic destruction of halogenated pyridines in wastewaters. *Process Safety and Environmental Protection* **2006**, *84*, (B4), 313-316.

129. Stapleton, D. R.; Konstantinou, I. K.; Mantzavinos, D.; Hela, D.; Papadaki, M., On the kinetics and mechanisms of photolytic/TiO₂-photocatalytic degradation of substituted pyridines in aqueous solutions. *Appl. Catal. B* **2010**, *95*, (1-2), 100-109.

130. Shemer, H.; Kunukcu, Y. K.; Linden, K. G., Degradation of the pharmaceutical metronidazole via UV, Fenton and photo-Fenton processes. *Chemosphere* **2006**, *63*, (2), 269-76.

131. Calza, P.; Sakkas, V.; Medana, C.; Baiocchi, C.; Dimou, A.; Pelizzetti, E.; Albanis, T., Photocatalytic degradation study of diclofenac over aqueous TiO₂ suspensions. *Appl. Catal. B* **2006**, *67*, (3-4), 197-205.

132. Hartmann, J.; Bartels, P.; Mau, U.; Witter, M.; Tumpling, W. V.; Hofmann, J.; Nietzsche, E., Degradation of the drug diclofenac in water by sonolysis in presence of catalysts. *Chemosphere* **2008**, *70*, (3), 453-61.

133. Pereira, V. J.; Linden, K. G.; Weinberg, H. S., Evaluation of UV irradiation for photolytic and oxidative degradation of pharmaceutical compounds in water. *Water Res.* **2007**, *41*, (19), 4413-4423.

134. Abellán, M. N.; Bayarri, B.; Giménez, J.; Costa, J., Photocatalytic degradation of sulfamethoxazole in aqueous suspension of TiO₂. *Appl. Catal. B* **2007**, *74*, (3-4), 233-241.

135. Gonzalez, O.; Sans, C.; Esplugas, S., Sulfamethoxazole abatement by

- photo-Fenton Toxicity, inhibition and biodegradability assessment of intermediates. *J. Hazard. Mater.* **2007**, *146*, (3), 459-464.
136. Dantas, R. F.; Contreras, S.; Sans, C.; Esplugas, S., Sulfamethoxazole abatement by means of ozonation. *J. Hazard. Mater.* **2008**, *150*, (3), 790-794.
137. Molinari, R.; Pirillo, F.; Loddo, V.; Palmisano, L., Heterogeneous photocatalytic degradation of pharmaceuticals in water by using polycrystalline TiO₂ and a nanofiltration membrane reactor. *Cata. Today* **2006**, *118*, (1-2), 205-213.
138. Coleman, H. M.; Abdullah, M. I.; Eggins, B. R.; Palmer, F. L., Photocatalytic degradation of 17 β -oestradiol, oestriol and 17 α -ethynylestradiol in water monitored using fluorescence spectroscopy. *Appl. Catal. B* **2005**, *55*, (1), 23-30.
139. Murugananthan, M.; Yoshihara, S.; Rakuma, T.; Uehara, N.; Shirakashi, T., Electrochemical degradation of 17 β -estradiol (E2) at boron-doped diamond (Si/BDD) thin film electrode. *Electrochimica Acta* **2007**, *52*, (9), 3242-3249.
140. Bora, L. V.; Mewada, R. K., Visible/solar light active photocatalysts for organic effluent treatment: Fundamentals, mechanisms and parametric review. *Renewable and Sustainable Energy Reviews* **2017**, *76*, (Supplement C), 1393-1421.
141. Shi, Y. Y.; Luo, L. J.; Zhang, Y. F.; Chen, Y.; Wang, S.; Li, L. X.; Long, Y. J.; Jiang, F. Z., Synthesis and characterization of alpha/beta-Bi₂O₃ with enhanced photocatalytic activity for 17 alpha-ethynylestradiol. *Ceramics International* **2017**, *43*, (10), 7627-7635.
142. Lopes, O. F.; Carvalho, K. T. G.; Avansi, W.; Ribeiro, C., Growth of BiVO₄ Nanoparticles on a Bi₂O₃ Surface: Effect of Heterojunction Formation on Visible Irradiation-Driven Catalytic Performance. *Journal of Physical Chemistry C* **2017**, *121*, (25), 13747-13756.
143. Cheng, H.; Huang, B.; Dai, Y., Engineering BiOX (X = Cl, Br, I) nanostructures for highly efficient photocatalytic applications. *Nanoscale* **2014**, *6*, (4), 2009-26.
144. Zhang, X.; Guo, T.; Wang, X.; Wang, Y.; Fan, C.; Zhang, H., Facile composition-controlled preparation and photocatalytic application of BiOCl/Bi₂O₂CO₃ nanosheets. *Appl. Catal. B* **2014**, *150-151*, 486-495.
145. Xiao, Z.; Zhang, J. W.; Xia, Y.; Zhu, L. Z.; Lei, L.; Xu, S. Q., Nanoplates-assembled Bi₂WO₆ microcoins with hierarchical porous structure as efficient visible-light-active photocatalysts. *Materials Research Bulletin* **2017**, *94*, 322-327.
146. Tien, L. C.; Shen, I. C., Facile synthesis of Bi₂₅VO₄₀ nanowires for

- visible-light-driven photocatalysts. *Materials Letters* **2017**, *202*, 73-77.
147. Sudrajat, H.; Sujaridworakun, P., Low-temperature synthesis of delta-Bi₂O₃ hierarchical nanostructures composed of ultrathin nanosheets for efficient photocatalysis. *Materials & Design* **2017**, *130*, 501-511.
148. Zhang, X.; Ai, Z. H.; Jia, F. L.; Zhang, L. Z., Generalized one-pot synthesis, characterization, and photocatalytic activity of hierarchical BiOX (X = Cl, Br, I) nanoplate microspheres. *Journal of Physical Chemistry C* **2008**, *112*, (3), 747-753.
149. Xiao, X.; Zhang, W.-D., Facile synthesis of nanostructured BiOI microspheres with high visible light-induced photocatalytic activity. *Journal of Materials Chemistry* **2010**, *20*, (28), 5866.
150. Pare, B.; Sarwan, B.; Jonnalagadda, S. B., The characteristics and photocatalytic activities of BiOCl as highly efficient photocatalyst. *Journal of Molecular Structure* **2012**, *1007*, 196-202.
151. Chang, X.; Huang, J.; Cheng, C.; Sui, Q.; Sha, W.; Ji, G.; Deng, S.; Yu, G., BiOX (X=Cl, Br, I) photocatalysts prepared using NaBiO₃ as the Bi source: Characterization and catalytic performance. *Catalysis Communications* **2010**, *11*, (5), 460-464.
152. Li, K.; Tang, Y.; Xu, Y.; Wang, Y.; Huo, Y.; Li, H.; Jia, J., A BiOCl film synthesis from Bi₂O₃ film and its UV and visible light photocatalytic activity. *Appl. Catal. B* **2013**, *140-141*, 179-188.
153. Zhang, X.; Wang, X. B.; Wang, L. W.; Wang, W. K.; Long, L. L.; Li, W. W.; Yu, H. Q., Synthesis of a highly efficient BiOCl single-crystal nanodisk photocatalyst with exposing {001} facets. *ACS Appl Mater Interfaces* **2014**, *6*, (10), 7766-72.
154. Xiong, J.; Cheng, G.; Qin, F.; Wang, R.; Sun, H.; Chen, R., Tunable BiOCl hierarchical nanostructures for high-efficient photocatalysis under visible light irradiation. *Chem. Eng. J.* **2013**, *220*, 228-236.
155. Gao, X.; Zhang, X.; Wang, Y.; Peng, S.; Yue, B.; Fan, C., Rapid synthesis of hierarchical BiOCl microspheres for efficient photocatalytic degradation of carbamazepine under simulated solar irradiation. *Chem. Eng. J.* **2015**, *263*, 419-426.
156. Xu, J.; Meng, W.; Zhang, Y.; Li, L.; Guo, C., Photocatalytic degradation of tetrabromobisphenol A by mesoporous BiOBr: Efficacy, products and pathway. *Appl. Catal. B* **2011**, *107*, (3-4), 355-362.
157. Zhang, D.; Li, J.; Wang, Q.; Wu, Q., High {001} facets dominated BiOBr lamellas: facile hydrolysis preparation and selective visible-light photocatalytic activity. *Journal of Materials Chemistry A* **2013**, *1*, (30), 8622.

158. Hu, J.; Fan, W.; Ye, W.; Huang, C.; Qiu, X., Insights into the photosensitivity activity of BiOCl under visible light irradiation. *Appl. Catal. B* **2014**, *158-159*, 182-189.
159. Dong, F.; Sun, Y.; Fu, M.; Wu, Z.; Lee, S. C., Room temperature synthesis and highly enhanced visible light photocatalytic activity of porous BiOI/BiOCl composites nanoplates microflowers. *J Hazard Mater* **2012**, *219-220*, 26-34.
160. Wang, P.; Wu, Y.; Shi, J.; Liu, D.; Dong, W., Preparation of carbon-supported Bi/Ti composites and its catalytic activity under solar irradiation. *Appl. Surf. Sci.* **2014**, *292*, 1077-1082.
161. Zhang, K.; Liu, C.; Huang, F.; Zheng, C.; Wang, W., Study of the electronic structure and photocatalytic activity of the BiOCl photocatalyst. *Appl. Catal. B* **2006**, *68*, (3-4), 125-129.
162. Wang, X.; Chen, H.; Li, H.; Mailhot, G.; Dong, W., Preparation and formation mechanism of BiOCl_{0.75}I_{0.25} nanospheres by precipitation method in alcohol–water mixed solvents. *Journal of Colloid and Interface Science* **2016**.
163. Liu, Q. C.; Ma, D. K.; Hu, Y. Y.; Zeng, Y. W.; Huang, S. M., Various bismuth oxyiodide hierarchical architectures: alcohothermal-controlled synthesis, photocatalytic activities, and adsorption capabilities for phosphate in water. *ACS Appl Mater Interfaces* **2013**, *5*, (22), 11927-34.
164. Shi, X.; Chen, X.; Chen, X.; Zhou, S.; Lou, S., Solvothermal synthesis of BiOI hierarchical spheres with homogeneous sizes and their high photocatalytic performance. *Materials Letters* **2012**, *68*, 296-299.
165. Yu, J.; Wei, B.; Zhu, L.; Gao, H.; Sun, W.; Xu, L., Flowerlike C-doped BiOCl nanostructures: Facile wet chemical fabrication and enhanced UV photocatalytic properties. *Appl. Surf. Sci.* **2013**, *284*, 497-502.
166. Huo, Y.; Zhang, J.; Miao, M.; Jin, Y., Solvothermal synthesis of flower-like BiOBr microspheres with highly visible-light photocatalytic performances. *Appl. Catal. B* **2012**, *111-112*, 334-341.
167. Tian, H.; Li, J.; Ge, M.; Zhao, Y.; Liu, L., Removal of bisphenol A by mesoporous BiOBr under simulated solar light irradiation. *Catalysis Science & Technology* **2012**, *2*, (11), 2351.
168. Zhang, K.-L.; Liu, C.-M.; Huang, F.-Q.; Zheng, C.; Wang, W.-D., Study of the electronic structure and photocatalytic activity of the BiOCl photocatalyst. *Appl. Catal. B* **2006**, *68*, (3), 125-129.

169. Yuan, R. S.; Lin, C.; Wu, B. C.; Fu, X. Z., Synthesis of SnO₂, Fe₂O₃, and BiOCl Fibers from Inorganic Salts by a Templating Route. *Eur. J. Inorg. Chem.* **2009**, (24), 3537-3540.
170. Wang, D. H.; Gao, G. Q.; Zhang, Y. W.; Zhou, L. S.; Xu, A. W.; Chen, W., Nanosheet-constructed porous BiOCl with dominant {001} facets for superior photosensitized degradation. *Nanoscale* **2012**, *4*, (24), 7780-5.
171. Kim, W. J.; Pradhan, D.; Min, B.-K.; Sohn, Y., Adsorption/photocatalytic activity and fundamental natures of BiOCl and BiOCl_{1-x}I_{1-x} prepared in water and ethylene glycol environments, and Ag and Au-doping effects. *Appl. Catal. B* **2014**, *147*, 711-725.
172. Gao, X.; Zhang, X.; Wang, Y.; Peng, S.; Yue, B.; Fan, C., Photocatalytic degradation of carbamazepine using hierarchical BiOCl microspheres: Some key operating parameters, degradation intermediates and reaction pathway. *Chem. Eng. J.* **2015**, *273*, 156-165.
173. Zhang, K.; Liang, J.; Wang, S.; Liu, J.; Ren, K.; Zheng, X.; Luo, H.; Peng, Y.; Zou, X.; Bo, X.; Li, J.; Yu, X., BiOCl Sub-Microcrystals Induced by Citric Acid and Their High Photocatalytic Activities. *Crystal Growth & Design* **2012**, *12*, (2), 793-803.
174. Xiong, J.; Cheng, G.; Li, G.; Qin, F.; Chen, R., Well-crystallized square-like 2D BiOCl nanoplates: mannitol-assisted hydrothermal synthesis and improved visible-light-driven photocatalytic performance. *RSC Advances* **2011**, *1*, (8), 1542.
175. Tian, Y.; Guo, C. F.; Guo, Y.; Wang, Q.; Liu, Q., BiOCl nanowire with hierarchical structure and its Raman features. *Appl. Surf. Sci.* **2012**, *258*, (6), 1949-1954.
176. Zhang, D.; Wen, M.; Jiang, B.; Li, G.; Yu, J. C., Ionothermal synthesis of hierarchical BiOBr microspheres for water treatment. *J Hazard Mater* **2012**, *211-212*, 104-11.
177. Feng, Y.; Li, L.; Li, J.; Wang, J.; Liu, L., Synthesis of mesoporous BiOBr 3D microspheres and their photodecomposition for toluene. *J Hazard Mater* **2011**, *192*, (2), 538-44.
178. Shang, M.; Wang, W.; Zhang, L., Preparation of BiOBr lamellar structure with high photocatalytic activity by CTAB as Br source and template. *J. Hazard. Mater.* **2009**, *167*, (1-3), 803-809.
179. Li, Y.; Wang, J.; Yao, H.; Dang, L.; Li, Z., Efficient decomposition of organic

compounds and reaction mechanism with BiOI photocatalyst under visible light irradiation. *Journal of Molecular Catalysis A: Chemical* **2011**, *334*, (1-2), 116-122.

180. Xia, J.; Yin, S.; Li, H.; Xu, H.; Yan, Y.; Zhang, Q., Self-assembly and enhanced photocatalytic properties of BiOI hollow microspheres via a reactable ionic liquid. *Langmuir : the ACS journal of surfaces and colloids* **2011**, *27*, (3), 1200-6.

181. Lei, Y.; Wang, G.; Song, S.; Fan, W.; Pang, M.; Tang, J.; Zhang, H., Room temperature, template-free synthesis of BiOI hierarchical structures: Visible-light photocatalytic and electrochemical hydrogen storage properties. *Dalton Transactions* **2010**, *39*, (13), 3273.

182. Hao, R.; Xiao, X.; Zuo, X.; Nan, J.; Zhang, W., Efficient adsorption and visible-light photocatalytic degradation of tetracycline hydrochloride using mesoporous BiOI microspheres. *J. Hazard. Mater.* **2012**, *209-210*, 137-145.

183. Jia, X.; Cao, J.; Lin, H.; Zhang, M.; Guo, X.; Chen, S., Transforming type-I to type-II heterostructure photocatalyst via energy band engineering: A case study of I-BiOCl/I-BiOBr. *Appl. Catal. B* **2017**, *204*, 505-514.

184. Reddy, K. H.; Martha, S.; Parida, K. M., Fabrication of novel p-BiOI/n-ZnTiO₃ heterojunction for degradation of rhodamine 6G under visible light irradiation. *Inorg Chem* **2013**, *52*, (11), 6390-401.

185. Xiao, X.; Hao, R.; Liang, M.; Zuo, X.; Nan, J.; Li, L.; Zhang, W., One-pot solvothermal synthesis of three-dimensional (3D) BiOI/BiOCl composites with enhanced visible-light photocatalytic activities for the degradation of bisphenol-A. *J Hazard Mater* **2012**, *233-234*, 122-30.

186. Wang, W.; Huang, F.; Lin, X., xBiOI-(1-x)BiOCl as efficient visible-light-driven photocatalysts. *Scripta Materialia* **2007**, *56*, (8), 669-672.

187. Chai, S. Y.; Kim, Y. J.; Jung, M. H.; Chakraborty, A. K.; Jung, D.; Lee, W. I., Heterojunctioned BiOCl/Bi₂O₃, a new visible light photocatalyst. *Journal of Catalysis* **2009**, *262*, (1), 144-149.

188. Li, Y.; Wang, J.; Yao, H.; Dang, L.; Li, Z., Chemical etching preparation of BiOI/Bi₂O₃ heterostructures with enhanced photocatalytic activities. *Catalysis Communications* **2011**, *12*, (7), 660-664.

189. Li, L.; Zhang, M.; Liu, Y.; Zhang, X., Hierarchical assembly of BiOCl nanosheets onto bicrystalline TiO₂ nanofiber: enhanced photocatalytic activity based on photoinduced interfacial charge transfer. *J Colloid Interface Sci* **2014**, *435*, 26-33.

190. Duo, F.; Wang, Y.; Fan, C.; Mao, X.; Zhang, X.; Wang, Y.; Liu, J., Low

temperature one-step synthesis of rutile TiO₂/BiOCl composites with enhanced photocatalytic activity. *Materials Characterization* **2015**, *99*, 8-16.

191. Jiang, S.; Zhou, K.; Shi, Y.; Lo, S.; Xu, H.; Hu, Y.; Gui, Z., In situ synthesis of hierarchical flower-like Bi₂S₃/BiOCl composite with enhanced visible light photocatalytic activity. *Appl. Surf. Sci.* **2014**, *290*, 313-319.

192. Cao, J.; Xu, B.; Lin, H.; Luo, B.; Chen, S., Novel heterostructured Bi₂S₃/BiOI photocatalyst: facile preparation, characterization and visible light photocatalytic performance. *Dalton Trans* **2012**, *41*, (37), 11482-90.

193. Yu, L.; Zhang, X.; Li, G.; Cao, Y.; Shao, Y.; Li, D., Highly efficient Bi₂O₂CO₃/BiOCl photocatalyst based on heterojunction with enhanced dye-sensitization under visible light. *Appl. Catal. B* **2016**, *187*, 301-309.

194. Li, X.; Niu, C.; Huang, D.; Wang, X.; Zhang, X.; Zeng, G.; Niu, Q., Preparation of magnetically separable Fe₃O₄/BiOI nanocomposites and its visible photocatalytic activity. *Appl. Surf. Sci.* **2013**, *286*, 40-46.

195. Xu, X.; Shen, X.; Zhu, G.; Jing, L.; Liu, X.; Chen, K., Magnetically recoverable Bi₂WO₆-Fe₃O₄ composite photocatalysts: Fabrication and photocatalytic activity. *Chem. Eng. J.* **2012**, *200-202*, 521-531.

196. Lv, Y.; Liu, H.; Zhang, W.; Ran, S.; Chi, F.; Yang, B.; Xia, A., Room-temperature synthesis and high visible-light-induced photocatalytic activity of AgI/BiOI composites. *Journal of Environmental Chemical Engineering* **2013**, *1*, (3), 526-533.

197. Cheng, H.; Wang, W.; Huang, B.; Wang, Z.; Zhan, J.; Qin, X.; Zhang, X.; Dai, Y., Tailoring AgI nanoparticles for the assembly of AgI/BiOI hierarchical hybrids with size-dependent photocatalytic activities. *Journal of Materials Chemistry A* **2013**, *1*, (24), 7131.

198. Cao, J.; Zhao, Y.; Lin, H.; Xu, B.; Chen, S., Facile synthesis of novel Ag/AgI/BiOI composites with highly enhanced visible light photocatalytic performances. *Journal of Solid State Chemistry* **2013**, *206*, 38-44.

199. Zhu, L.; He, C.; Huang, Y.; Chen, Z.; Xia, D.; Su, M.; Xiong, Y.; Li, S.; Shu, D., Enhanced photocatalytic disinfection of E. coli 8099 using Ag/BiOI composite under visible light irradiation. *Sep. Purif. Technol.* **2012**, *91*, 59-66.

200. Li, T.; Luo, S.; Yang, L., Microwave-assisted solvothermal synthesis of flower-like Ag/AgBr/BiOBr microspheres and their high efficient photocatalytic degradation for p-nitrophenol. *Journal of Solid State Chemistry* **2013**, *206*, 308-316.

201. Lu, L.; Kong, L.; Jiang, Z.; Lai, H. H. C.; Xiao, T.; Edwards, P. P.,

- Visible-Light-Driven Photodegradation of Rhodamine B on Ag-Modified BiOBr. *Catalysis Letters* **2012**, *142*, (6), 771-778.
202. Kong, L.; Jiang, Z.; Lai, H. H.; Nicholls, R. J.; Xiao, T.; Jones, M. O.; Edwards, P. P., Unusual reactivity of visible-light-responsive AgBr–BiOBr heterojunction photocatalysts. *Journal of Catalysis* **2012**, *293*, 116-125.
203. Cheng, H.; Huang, B.; Dai, Y.; Qin, X.; Zhang, X., One-step synthesis of the nanostructured AgI/BiOI composites with highly enhanced visible-light photocatalytic performances. *Langmuir : the ACS journal of surfaces and colloids* **2010**, *26*, (9), 6618-24.
204. Xiong, W.; Zhao, Q.; Li, X.; Zhang, D., One-step synthesis of flower-like Ag/AgCl/BiOCl composite with enhanced visible-light photocatalytic activity. *Catalysis Communications* **2011**, *16*, (1), 229-233.
205. Ao, Y.; Tang, H.; Wang, P.; Wang, C., Deposition of Ag@AgCl onto two dimensional square-like BiOCl nanoplates for high visible-light photocatalytic activity. *Materials Letters* **2014**, *131*, 74-77.
206. Benkelberg, H. J.; Warneck, P., PHOTODECOMPOSITION OF IRON(III) HYDROXO AND SULFATO COMPLEXES IN AQUEOUS-SOLUTION - WAVELENGTH DEPENDENCE OF OH AND SO₄⁻ QUANTUM YIELDS. *Journal of Physical Chemistry* **1995**, *99*, (14), 5214-5221.
207. Wu, Y.; Prulho, R.; Brigante, M.; Dong, W.; Hanna, K.; Mailhot, G., Activation of persulfate by Fe(III) species: Implications for 4-tert-butylphenol degradation. *J Hazard Mater* **2017**, *322*, (Pt B), 380-386.
208. Ylivainio, K., Effects of iron(III)chelates on the solubility of heavy metals in calcareous soils. *Environ Pollut* **2010**, *158*, (10), 3194-200.
209. Yan, D. Y.; Lo, I. M., Removal effectiveness and mechanisms of naphthalene and heavy metals from artificially contaminated soil by iron chelate-activated persulfate. *Environ Pollut* **2013**, *178*, 15-22.
210. Zhao, C.; Arroyo-Mora, L. E.; DeCaprio, A. P.; Sharma, V. K.; Dionysiou, D. D.; O'Shea, K. E., Reductive and oxidative degradation of iopamidol, iodinated X-ray contrast media, by Fe(III)-oxalate under UV and visible light treatment. *Water Res.* **2014**, *67*, 144-153.
211. Zhou, D.; Wu, F.; Deng, N. S., Fe(III)-oxalate complexes induced photooxidation of diethylstilbestrol in water. *Chemosphere* **2004**, *57*, (4), 283-291.
212. Hug, S. J.; Canonica, L.; Wegelin, M.; Gechter, D.; Von Gunten, U., Solar

- oxidation and removal of arsenic at circumneutral pH in iron containing waters. *Environ. Sci. Technol.* **2001**, *35*, (10), 2114-2121.
213. Tandy, S.; Ammann, A.; Schulin, R.; Nowack, B., Biodegradation and speciation of residual SS-ethylenediaminedisuccinic acid (EDDS) in soil solution left after soil washing. *Environ Pollut* **2006**, *142*, (2), 191-199.
214. Bretti, C.; Cigala, R. M.; De Stefano, C.; Lando, G.; Sammartano, S., Understanding the bioavailability and sequestration of different metal cations in the presence of a biodegradable chelant S,S-EDDS in biological fluids and natural waters. *Chemosphere* **2016**, *150*, 341-356.
215. Schowanek, D.; Feijtel, T. C. J.; Perkins, C. M.; Hartman, F. A.; Federle, T. W.; Larson, R. J., Biodegradation of [S,S], [R,R] and mixed stereoisomers of Ethylene Diamine Disuccinic Acid (EDDS), a transition metal chelator. *Chemosphere* **1997**, *34*, (11), 2375-2391.
216. Jaworska, J. S.; Schowanek, D.; Feijtel, T. C. J., Environmental risk assessment for trisodium [S,S]-ethylene diamine disuccinate, a biodegradable chelator used in detergent applications. *Chemosphere* **1999**, *38*, (15), 3597-3625.
217. Wu, Y.; Brigante, M.; Dong, W.; de Sainte-Claire, P.; Mailhot, G., Toward a better understanding of Fe(III)-EDDS photochemistry: theoretical stability calculation and experimental investigation of 4-tert-butylphenol degradation. *J Phys Chem A* **2014**, *118*, (2), 396-403.
218. Li, J.; Mailhot, G.; Wu, F.; Deng, N., Photochemical efficiency of Fe(III)-EDDS complex: OH radical production and 17 β -estradiol degradation. *J. Photoch. Photobio. A* **2010**, *212*, (1), 1-7.
219. Zhang, X.; Gu, X.; Lu, S.; Miao, Z.; Xu, M.; Fu, X.; Qiu, Z.; Sui, Q., Application of calcium peroxide activated with Fe(II)-EDDS complex in trichloroethylene degradation. *Chemosphere* **2016**, *160*, 1-6.
220. Papoutsakis, S.; Brites-Nóbrega, F. F.; Pulgarin, C.; Malato, S., Benefits and limitations of using Fe(III)-EDDS for the treatment of highly contaminated water at near-neutral pH. *J. Photoch. Photobio. A* **2015**, *303-304*, 1-7.
221. Cui, H.; Gu, X.; Lu, S.; Fu, X.; Zhang, X.; Fu, G. Y.; Qiu, Z.; Sui, Q., Degradation of ethylbenzene in aqueous solution by sodium percarbonate activated with EDDS–Fe(III) complex. *Chem. Eng. J.* **2017**, *309*, 80-88.
222. Han, D.; Wan, J.; Ma, Y.; Wang, Y.; Huang, M.; Chen, Y.; Li, D.; Guan, Z.; Li, Y., Enhanced decolorization of Orange G in a Fe(II)-EDDS activated persulfate process

- by accelerating the regeneration of ferrous iron with hydroxylamine. *Chem. Eng. J.* **2014**, *256*, 316-323.
223. Papoutsakis, S.; Miralles-Cuevas, S.; Oller, I.; Garcia Sanchez, J. L.; Pulgarin, C.; Malato, S., Microcontaminant degradation in municipal wastewater treatment plant secondary effluent by EDDS assisted photo-Fenton at near-neutral pH: An experimental design approach. *Cata. Today* **2015**, *252*, 61-69.
224. Dulin, D.; Mill, T., DEVELOPMENT AND EVALUATION OF SUNLIGHT ACTINOMETERS. *Environ. Sci. Technol.* **1982**, *16*, (11), 815-820.
225. Brigante, M.; Charbouillot, T.; Vione, D.; Mailhot, G., Photochemistry of 1-Nitronaphthalene: A Potential Source of Singlet Oxygen and Radical Species in Atmospheric Waters. *J. Phys. Chem. A* **2010**, *114*, (8), 2830-2836.
226. Wang, X.; Bi, W.; Zhai, P.; Wang, X.; Li, H.; Mailhot, G.; Dong, W., Adsorption and photocatalytic degradation of pharmaceuticals by BiOCl_xI_y nanospheres in aqueous solution. *Appl. Surf. Sci.* **2016**, *360*, 240-251.
227. Dong, F.; Sun, Y.; Fu, M.; Wu, Z.; Lee, S., Room temperature synthesis and highly enhanced visible light photocatalytic activity of porous BiOI/BiOCl composites nanoplates microflowers. *J. Hazard. Mater.* **2012**, *219*, 26-34.
228. Yang, C.; Li, F.; Zhang, M.; Li, T.; Cao, W., Preparation and first-principles study for electronic structures of BiOI/BiOCl composites with highly improved photocatalytic and adsorption performances. *Journal of Molecular Catalysis A: Chemical* **2016**, *423*, 1-11.
229. Xiao, X.; Hao, R.; Liang, M.; Zuo, X.; Nan, J.; Li, L.; Zhang, W., One-pot solvothermal synthesis of three-dimensional (3D) BiOI/BiOCl composites with enhanced visible-light photocatalytic activities for the degradation of bisphenol-A. *J. Hazard. Mater.* **2012**, *233*, 122-130.
230. Chang, X.; Gondal, M. A.; Al-Saadi, A. A.; Ali, M. A.; Shen, H.; Zhou, Q.; Zhang, J.; Du, M.; Liu, Y.; Ji, G., Photodegradation of Rhodamine B over unexcited semiconductor compounds of BiOCl and BiOBr. *J Colloid Interface Sci* **2012**, *377*, (1), 291-8.
231. Li, K.; Liang, Y.; Yang, J.; Gao, Q.; Zhu, Y.; Liu, S.; Xu, R.; Wu, X., Controllable synthesis of {001} facet dependent foursquare BiOCl nanosheets: A high efficiency photocatalyst for degradation of methyl orange. *Journal of Alloys and Compounds* **2017**, *695*, 238-249.
232. Park, Y.; Na, Y.; Pradhan, D.; Min, B.-K.; Sohn, Y., Adsorption and UV/Visible

- photocatalytic performance of BiOI for methyl orange, Rhodamine B and methylene blue: Ag and Ti-loading effects. *CrystEngComm* **2014**, *16*, (15), 3155.
233. Liang, J.; Shan, C.; Zhang, X.; Tong, M., Bactericidal mechanism of BiOI–AgI under visible light irradiation. *Chem. Eng. J.* **2015**, *279*, 277-285.
234. Buxton, G. V.; Greenstock, C. L.; Helman, W. P.; Ross, A. B., Critical review of rate constants for reactions of hydrated electrons, hydrogen atoms and hydroxyl radicals (OH/O⁻) in aqueous solution. *J. Phys. Chem. Ref. Data* **1988**, *17*, (2), 513-886.
235. Palominos, R.; Freer, J.; Mondaca, M. A.; Mansilla, H. D., Evidence for hole participation during the photocatalytic oxidation of the antibiotic flumequine. *J. Photochem. Photobiol., A* **2008**, *193*, (2), 139-145.
236. Willson, R. L., PULSE RADIOLYSIS STUDIES OF ELECTRON TRANSFER IN AQUEOUS QUINONE SOLUTIONS. *Transactions of the Faraday Society* **1971**, *67*, (586), 3020-&.
237. Lin, H.; Ye, H.; Li, X.; Cao, J.; Chen, S., Facile anion-exchange synthesis of BiOI/BiOBr composite with enhanced photoelectrochemical and photocatalytic properties. *Ceramics International* **2014**, *40*, (7), 9743-9750.
238. Maruthamuthu, P.; Neta, P., Phosphate radicals. Spectra, acid-base equilibria, and reactions with inorganic compounds. *J. Phys. Chem.* **1978**, *82*, (6), 710-713.
239. Sarwan, B.; Pare, B.; Acharya, A. D.; Jonnalagadda, S. B., Mineralization and toxicity reduction of textile dye neutral red in aqueous phase using BiOCl photocatalysis. *J. Photoch. Photobio. B* **2012**, *116*, 48-55.
240. Fang, G.-D.; Dionysiou, D. D.; Al-Abed, S. R.; Zhou, D.-M., Superoxide radical driving the activation of persulfate by magnetite nanoparticles: Implications for the degradation of PCBs. *Appl. Catal. B* **2013**, *129*, 325-332.
241. Motohashi, N.; Saito, Y., COMPETITIVE MEASUREMENT OF RATE CONSTANTS FOR HYDROXYL RADICAL REACTIONS USING RADIOLYTIC HYDROXYLATION OF BENZOATE. *Chem. Pharm. Bull.* **1993**, *41*, (10), 1842-1845.
242. Zhang, Y.; Klamerth, N.; Messele, S. A.; Chelme-Ayala, P.; Gamal El-Din, M., Kinetics study on the degradation of a model naphthenic acid by ethylenediamine-N,N'-disuccinic acid-modified Fenton process. *J Hazard Mater* **2016**, *318*, 371-8.
243. Abida, O.; Mailhot, G.; Litter, M.; Bolte, M., Impact of iron-complex

- (Fe(III)-NTA) on photoinduced degradation of 4-chlorophenol in aqueous solution. *Photochem. Photobiol. Sci.* **2006**, *5*, (4), 395-402.
244. Buxton, G. V.; Greenstock, C. L.; Helman, W. P.; Ross, A. B., CRITICAL-REVIEW OF RATE CONSTANTS FOR REACTIONS OF HYDRATED ELECTRONS, HYDROGEN-ATOMS AND HYDROXYL RADICALS (.OH/.O-) IN AQUEOUS-SOLUTION. *Journal of Physical and Chemical Reference Data* **1988**, *17*, (2), 513-886.
245. Neta, P.; Huie, R. E.; Ross, A. B., Rate constants for reactions of inorganic radicals in aqueous solution. *J. Phys. Chem. Ref. Data* **1988**, *17*, (3), 1027-1284.
246. Yang, L.; Liya, E. Y.; Ray, M. B., Degradation of paracetamol in aqueous solutions by TiO₂ photocatalysis. *Water Res.* **2008**, *42*, (13), 3480-3488.
247. Sirés, I.; Brillas, E., Remediation of water pollution caused by pharmaceutical residues based on electrochemical separation and degradation technologies: a review. *Environment international* **2012**, *40*, 212-229.
248. de Oliveira, Q.; Calora, M.; Tanaka, A. A.; de Vasconce los Lanza, M. R.; Del PilarTaboada Sotomayor, M., Studies of the Electrochemical Degradation of Acetaminophen Using a Real-Time Biomimetic Sensor. *Electroanalysis* **2011**, *23*, (11), 2616-2621.
249. Yang, L.; Yu, L. E.; Ray, M. B., Photocatalytic oxidation of paracetamol: dominant reactants, intermediates, and reaction mechanisms. *Environ. Sci. Technol.* **2008**, *43*, (2), 460-465.
250. Moctezuma, E.; Leyva, E.; Aguilar, C. A.; Luna, R. A.; Montalvo, C., Photocatalytic degradation of paracetamol: Intermediates and total reaction mechanism. *J. Hazard. Mater.* **2012**, *243*, 130-138.
251. Zhang, Y.; Zhang, Q.; Hong, J., Sulfate radical degradation of acetaminophen by novel iron–copper bimetallic oxidation catalyzed by persulfate: Mechanism and degradation pathways. *Appl. Surf. Sci.* **2017**, *422*, 443-451.
252. Deng, J.; Shao, Y.; Gao, N.; Xia, S.; Tan, C.; Zhou, S.; Hu, X., Degradation of the antiepileptic drug carbamazepine upon different UV-based advanced oxidation processes in water. *Chem. Eng. J.* **2013**, *222*, 150-158.
253. Wardman, P., Reduction potentials of one-electron couples involving free radicals in aqueous solution. *J. Phys. Chem. Ref. Data* **1989**, *18*, 1637-1755.
254. Tamtam, F.; Chiron, S., New insight into photo-bromination processes in saline surface waters: the case of salicylic acid. *Sci Total Environ* **2012**, *435-436*, 345-50.

255. Huang, W.; Bianco, A.; Brigante, M.; Mailhot, G., UVA-UVB activation of hydrogen peroxide and persulfate for advanced oxidation processes: Efficiency, mechanism and effect of various water constituents. *J. Hazard. Mater.* **2018**, *347*, 279-287.
256. Elliot, A. J., A PULSE-RADIOLYSIS STUDY OF THE REACTION OF OH WITH I₂ AND THE DECAY OF I₂. *Can. J. Chem.-Rev. Can. Chim.* **1992**, *70*, (6), 1658-1661.
257. Ji, Y.; Zhou, L.; Zhang, Y.; Ferronato, C.; Brigante, M.; Mailhot, G.; Yang, X.; Chovelon, J. M., Photochemical degradation of sunscreen agent 2-phenylbenzimidazole-5-sulfonic acid in different water matrices. *Water Res* **2013**, *47*, (15), 5865-75.
258. Ji, Y.; Zhou, L.; Ferronato, C.; Yang, X.; Salvador, A.; Zeng, C.; Chovelon, J.-M., Photocatalytic degradation of atenolol in aqueous titanium dioxide suspensions: Kinetics, intermediates and degradation pathways. *J. Photoch. Photobio. A* **2013**, *254*, 35-44.

Published papers

- [1] **Xiaoning Wang**, Marcello Brigante, Gilles Mailhot*, Wenbo Dong*, Bismuth catalyst mediated degradation of *p*-hydroxyphenylacetic acid: Photoactivation, interfacial mechanism, and influence of some critical parameters [J]. *Chemical Engineering Journal* Accepted in 2018. (IF=6.216)
- [2] **Xiaoning Wang**, Hongche Chen, Hongjing Li*, Gilles Mailhot, Wenbo Dong*, Preparation and formation mechanism of BiOCl_{0.75}I_{0.25} nanospheres by precipitation method in alcohol–water mixed solvents [J]. *Journal of Colloid and Interface Science* 478 (2016) 1–10. (IF = 4.233)
- [3] **Xiaoning Wang**, Wenlong Bi, Pingping Zhai, Xiaobing Wang, Hongjing Li*, Gilles Mailhot, Wenbo Dong*, Adsorption and photocatalytic degradation of pharmaceuticals by BiOCl_xI_y nanospheres in aqueous solution [J]. *Applied Surface Science* 360 (2016) 240–251. (IF = 3.387)
- [4] **Xiaoning Wang**, Zhijian Zhang, Yicen Xue, Minghua Nie, Hongjing Li*, Wenbo Dong*, Low crystallized BiOCl_{0.75}I_{0.25} synthesized in mixed solvent and its photocatalytic properties under simulated solar irradiation [J]. *Materials Letters* 136 (2014) 30-33. (IF = 2.437)
- [5] **Xiaoning Wang**, Hongjing Li, Wenbo Dong, Photodegradation of pharmaceuticals by BiOCl_xI_y under simulated solar and visible irradiation [M]. *The World Congress on Advances in Civil, Environmental, and Materials Research (ACEM 14)* Busan, Korea, August 24-28, 2014.
- [6] Zhijian Zhang, **Xiaoning Wang**, Yicen Xue, Hongjing Li*, Wenbo Dong*, Enhanced dechlorination of triclosan by hydrated electron reduction in aqueous solution [J]. *Chemical Engineering Journal* 263 (2015) 186-193. (IF = 5.309)
- [7] Hongche Chen, **Xiaoning Wang**, Wenlong Bi, Yanlin Wu*, Wenbo Dong*, Photodegradation of carbamazepine with BiOCl/Fe₃O₄ catalyst under simulated solar light irradiation [J]. *Journal of Colloid and Interface Science* 502 (2017) 89-99. (IF = 4.233)

- [8] Yicen Xue, Wenbo Dong*, **Xiaoning Wang**, Wenlong Bi, Pingping Zhai, Hongjing Li*, Minghua Nie, Degradation of sunscreen agent p-aminobenzoic acid using a combination system of UV irradiation, persulphate and iron(II) [J]. *Environment Science and Pollution Research* DOI 10.1007/s11356-015-5631-z. (IF= 2.759)
- [9] Wenlong Bi, Yanlin Wu, **Xiaoning Wang**, Pingping Zhai, Wenbo Dong*, Degradation of oxytetracycline with $\text{SO}_4^{\bullet-}$ under simulated solar light [J], *Chemical Engineering Journal* 302 (2016) 811-818. (IF= 6.216)

Acknowledgement

This project has been carried out within the cooperation program between Fudan University and Clermont Auvergne University. One part of my work was performed in the Department of Environmental Science and Engineering of Fudan University directed by Prof. Wenbo Dong and Dr. Hongjing Li, the other part was carried out in the Institut de Chimie de Clermont-Ferrand (ICCF) UMR 6296 led by Dr. Gilles MAILHOT and Marcello BRIGANTE. I would sincerely like to thank them for providing the good experimental conditions, supervision, and help.

I would like to express my thanks to Prof. Wenbo Dong and Dr. Hongjing Li in Fudan University during my whole study period. When I entered Fudan University in 2013 at the first time, I knew little about my profession knowledge. They showed me how to start scientific research, including searching literatures and doing experiments. They help me design my project plan, and discussed with me frequently. Their professional spirit gave me a lot of encouragement. Without them, I could not get this chance to study abroad in Clermont-Ferrand. They also paid special attention on my life and family.

I want to say thank you to Dr. Gilles MAILHOT and Dr. Marcello BRIGANTE who directed my experiments in France and help me to finish my papers and thesis. They gave me a lot of help in my study and life during my stay in France. Both of them always gave me helpful suggestion and idea for the whole study, their hard-working attitude and rich experience gave me deep impression and influenced me in my whole life.

I also want to thank sincerely Mr. Zhijian ZHANG, Miss Yanlin WU, Mr. Minghua NIE, Mr. Peng WANG, Miss Ping GONG, Miss Jin SHI, Miss Yicen XUE, Miss Pingping ZHAI, Miss Hongche CHEN, Miss Yahong SHI, Mr. Yankun LIU, Mr. Wenlong BI, Mr. Qi LIU, Mr. Shiyu LI, and Miss Juan ZAHO, who are my colleagues in the laboratory and friends in Fudan University. Particularly, I have to thank sincerely to Angelica, an Italian girl, my best friend in France. Furthermore, I want to

thank Wenyu HUANG, Lei ZHOU, Jinlong ZHA, Shengnan LI, Miao WANG, Jinpeng WANG, they gave me such a happy time during my stay in France.

Thanks for the fund support of China Scholarship Council (CSC) affiliated with the Ministry of Education of the P. R. China. Thanks also go to the Education Service of China Embassy in Paris.

Finally, I would thank my parents, they gave me a lot of care, support and encourage. I can't finish my Ph.D study without them. I thank my husband and my baby, they are my spiritual pillar during my whole life. I love you forever.